COMILLAS
UNIVERSIDAD PONTIFICIA

ICAI | ICADE | CIHS

Escuela Técnica Superior de Ingeniería - ICAI

Improving Modelling for Optimal Expansion Planning of Power Transmission Systems

Author: Erik F. Alvarez

Director: Prof. Dr. Andrés Ramos Galán

Prof. Dr. Luis Olmos Camacho

Madrid | November, 2024

To God, my beloved parents, Perú and Spain.

Abstract

The transition to a zero-carbon economy requires significant advances in the design and operation of power systems. As fossil fuel power plants are phased out in favour of renewable energy sources, the industry faces pressing challenges in maintaining grid stability and reliability while minimising environmental impacts and costs. Traditional transmission expansion planning methods, which often rely on decomposition techniques that barely represent the future operation of power systems, fail to capture the complex interdependencies between generation, transmission, and distribution infrastructure, resulting in less-than-ideal expansion strategies.

Rather than introducing a broad, large-scale model, this thesis delineates a nuanced approach to transmission expansion planning that aims to improve model performance and ensure its robustness and scalability while thoughtfully incorporating elements of local and utility-scale flexibility. The novelty of this work lies not only in the scope of local and utility-scale flexibility modeling, but also in the meticulous manner in which these components are woven into power transmission system expansion planning. The research is underpinned by three core objectives: the formulation of advanced optimisation methods designed to efficiently address complex issues across different system configurations and operational scenarios; the careful merging of the representation of local and utility-scale flexibility - highlighting the importance of distributed energy resources (DERs) and integrating utility-scale storage solutions into the transmission planning framework; and the creation of durable, scalable models that can serve as future-proof blueprints for system development.

By pursuing these goals, the thesis aims to contribute significantly to the development of more efficient, resilient, and sustainable power systems. Through careful modeling and analysis, it seeks to provide actionable insights and recommendations for optimising transmission system development amidst the low-carbon transition, underscoring the importance of targeted innovation in addressing the evolving challenges facing the sector.

Abstract (Spanish)

La transición a una economía sin emisiones de CO_2 exige avances significativos en el diseño y funcionamiento de los sistemas eléctricos. A medida que se van retirando las centrales eléctricas de combustibles fósiles en favor de las fuentes de energía renovables, el sector se enfrenta a retos acuciantes para mantener la estabilidad y la fiabilidad de la red y, al mismo tiempo, minimizar el impacto ambiental y los costes. Los métodos tradicionales de planificación de la expansión del transporte, que a menudo se basan en técnicas de descomposición que apenas representan el funcionamiento futuro de los sistemas eléctricos, no logran captar las complejas interdependencias entre las infraestructuras de generación, transmisión y distribución, lo que da lugar a estrategias de expansión poco idóneas.

En lugar de introducir un modelo amplio y a gran escala, esta tesis describe un enfoque refinado de la planificación de la expansión de la transmisión que pretende mejorar el rendimiento del modelo y garantizar su solidez y escalabilidad, al tiempo que incorpora cuidadosamente elementos de flexibilidad distribuida y centralizada. La novedad de este trabajo radica no sólo en el alcance del modelado de la flexibilidad, sino también en la forma meticulosa en que estos componentes se entretejen en la planificación de la expansión del sistema eléctrico. La investigación se basa en tres objetivos fundamentales: la formulación de métodos avanzados de optimización diseñados para abordar eficazmente cuestiones complejas en diferentes configuraciones del sistema y escenarios operativos; la cuidadosa integración de la flexibilidad distribuida y centralizada, destacando la importancia de los recursos energéticos distribuidos e integrando almacenamientos de gran tamaño en el marco de la planificación; y la creación de modelos duraderos y escalables que puedan servir como anteproyectos a prueba de futuro para el desarrollo del sistema.

Con estos objetivos, la tesis pretende contribuir de forma significativa al desarrollo de sistemas energéticos más eficientes, resistentes y sostenibles. A través de un modelado y un análisis minuciosos, se pretende ofrecer ideas y recomendaciones prácticas para optimizar el desarrollo de los sistemas de transporte en el marco de la transición hacia una economía con bajas emisiones de CO_2, subrayando la importancia de la innovación específica para abordar los retos cambiantes a los que se enfrenta el sector.

Acknowledgement

In this moment of profound reflection and joy, words falter to express my gratitude and myriad emotions fully. The completion of this journey marks not just an academic milestone but a collective achievement made possible by the unwavering support, guidance, and belief of those who have been pillars throughout this process.

First and foremost, I owe my deepest thanks to my parents, Eliana and Francisco, and my sister, Evenly. Your boundless love, sacrifices, and unwavering belief in me have been the foundation upon which I have built this journey. Your faith has been a constant source of strength, propelling me forward in moments of doubt. I also express my profound gratitude to God for the blessings of life, for guiding me, and for the lessons learned throughout this journey. To my family, thank you for being my anchor, for your unconditional support, and for inspiring me to keep pushing forward, always reaching for my dreams with resilience and grace.

To Kelly, who became a part of my life during the later years of my PhD, your support has been invaluable. You helped me to understand myself better and to learn many important lessons along the way. Your encouragement, patience and insight provided clarity in moments of uncertainty and your belief in me strengthened my resolve. I am grateful for the role you have played in helping me reach this milestone.

I am deeply grateful to my supervisors, Andrés Ramos Galán and Luis Olmos Camacho. Your mentorship, expertise, and encouragement have been invaluable. You have challenged me to think critically, inspired me to push boundaries, and provided the guidance necessary to navigate the complexities of my research. I am indebted to your belief in my potential and your investment in my growth.

To my friends P. Vergara, J. C. Lopez, N. Bañol, J. S. Giraldo, Silvia, Marcos, Jerson, J. D. Gómez, Leslie Herding and Roberto Barella-and to my colleagues at IIT-Comillas, especially those on the first floor of Santa Cruz de Marcenado, thank you for your friendship, thought-provoking conversations and unwavering support. Each of you has played an essential role in my journey, and I will carry your influence with me into the future.

Erik F. Alvarez – Madrid, Spain – November 2024

Funding

Abbreviations

AC/DC	Alternating/Direct Current
BESS	Battery Energy Etorage System
CCGT	Combined-Cycle Gas Turbine
DSM	Demand Side Management
DERs	Distributed Energy Resources
DSO	Distribution System Operator
ESS	Energy Storage System
GEP	Generation Expansion Planning
H2	Hydrogen
IEP	Integrated Expansion Planning
IRP	Integrated Resource Planning
KVL	Kirchhoff's Voltage Law
LP	Linear Programming
MG	Microgrid
MILP	Mixed-Integer Linear Programming
MINLP	Mixed-Integer Nonlinear Programming
MISOCP	Mixed-Integer Second-Order Conic Programming
NLP	Nonlinear Programming
OECD	Organization for Economic Co-operation and Development
OPF	Optimal Power Flow
PSH	Pumped-Storage Hydro
RES	Renewable Energy Sources
RPP	Reactive Power Planning
SEP	Storage Expansion Planning
SOCP	Second-Order Conic Programming
TEP	Transmission Expansion Planning
TSO	Transmission System Operator
UC	Unit Commitment
VRE	Variable Renewable Energy

Notation

Indexes:

i, j	Buses of the transmission network, $i, j \in \mathcal{B}^t$.
i', j'	Buses of the distribution network (within the same distribution grid).
m	Distribution network bus with a connected microgrid.
ij	Branch (edge or way) from node i to j.
c	Circuit, $c \in \mathcal{C}$ in branch ij.
ijc	Electricity line, $ijc \in \mathcal{L}$.
k	Cycle, $k \in \mathcal{K}$.
e	ESS unit (i.e., battery or PSH), $e \in \mathcal{E}_i$, and $\mathcal{E}_i \subseteq \mathcal{G}_i$.
g	Generation unit (i.e., thermal or RES), $g \in \mathcal{G}_i$.
r	Capacitor bank, $r \in \mathcal{R}_i$.
s	Synchronous compensator, $s \in \mathcal{S}_i$.
n	Time step, $n \in \mathcal{T}$.
o	Charging sample data, $o \in \mathcal{O}$.
p	Discharging sample data, $p \in \mathcal{P}$.

System Parameters:

S_B	Base power [MW].
D_n	Duration of the time step n.
C^{shed}	Cost of electricity not served [EUR/MWh].
P^{co2}	CO2 emission cost [EUR/tCO2].
P_{ni}^d, Q_{ni}^d	Active/reactive power demand [MW, Mvar].
Γ_n^u, Γ_n^d	Upward/downward operating reserve requirements [MW].

Generation and Storage Parameters:

C_g^{gen}	Annualized fixed investment cost of a candidate generation unit [MEUR].
C_e^{sto}	Annualized fixed investment cost of a candidate ESS unit [MEUR].
$\overline{P}_{ng}, \underline{P}_{ng}$	Maximum/minimum active power generation from thermal units [MW].
$\overline{P}_{ne}, \underline{P}_{ne}$	Maximum/minimum active power generation from storage units [MW].
$\overline{Q}_{ng}, \underline{Q}_{ng}$	Maximum/minimum reactive power generation [Mvar].
$\overline{P}_{ne}^c$	Maximum active power consumption of an ESS unit [MW].
CF_g	Intercept of the variable cost function of a generation unit [MEUR/h].
CV_g	Slope of the variable cost of a generation unit (It includes fuel, O&M, and emission costs) [MEUR/MWh].
CV_e	Slope of the variable cost of a storage unit [MEUR/MWh].
R_g^u, R_g^d	Ramp-up and ramp-down of a generation unit [MW/h].

T_g^u, T_g^d	Minimum up-time and down-time of a generation unit [h].
C_g^{su}	Startup cost of a generation unit [MEUR].
C_g^{sd}	Shutdown cost of a generation unit [MEUR].
η_e	Round-trip efficiency of the pump/turbine cycle of a hydropower. plant, or charge/discharge of an ESS unit [p.u.]
Ψ_e	Storage capacity of an ESS unit [MWh].
E_{ne}^i	Energy inflow (in hourly, daily, weekly, or monthly resolution) of an ESS unit [MWh].
E_g^{co2}	CO2 emission rate [t/MWh].

Transmission Parameters:

C_{ijc}^t	Annualized fixed cost of a candidate line [MEUR].
C_s^{sy}	Annualized fixed cost of a candidate synchronous compensator[MEUR].
C_r^{sh}	Annualized fixed cost of a candidate capacitor bank [MEUR].
R_{ijc}, X_{ijc}	Resistance and reactance of a line [p.u.].
Z_{ijc}^2, B_{ijc}^l	Squared series impedance and shunt susceptance of a line [p.u.].
B_r^{sh}	Shunt susceptance [p.u.].
$\overline{S}_{ijc}$	Maximum apparent power flow [MVA].
$\overline{\theta}_i, \underline{\theta}_i$	Maximum/minimum voltage angle at node i [rad].
$\overline{\theta}_{ijc}, \underline{\theta}_{ijc}$	Maximum/minimum voltage angle difference [rad].
$\overline{V}_{ni}, \underline{V}_{ni}$	Maximum/minimum voltage [p.u.].
V_{ni}^0	Initial value of the voltage magnitude [p.u.].

System Variables:

Continuous:

C^{ge}	Generation expansion cost [MEUR].
C^{te}	Transmission expansion cost [MEUR].
C^{se}	Storage expansion cost [MEUR].
C^{re}	Reactive power compensation expansion cost [MEUR].
C_n^{gen}	Electricity generation costs for each time step n [MEUR].
C_n^{con}	Electricity consumption costs for each time step n [MEUR].
C_n^{CO2}	CO2 emission costs for each time step n [MEUR].
C_n^{ens}	Electricity not served costs for each time step n [MEUR].

Generation and Storage Variables:

Continuous:

p_{ng}^{tg}, q_{ng}^{tg}	Active and reactive power generation [MW, Mvar].

p_{ne}^{tc}	Active power consumption from a ESS unit [MW].
p_{ng}^{sg}	Active power generation above the minimum output [MW].
p_{ne}^{sc}	Active power charged from a ESS unit [MW].
$r_{ng}^{p,u}, r_{ng}^{p,d}$	Upward/downward reserves from a power generation unit or ESS when it is discharging [MW].
$r_{ne}^{c,u}, r_{ne}^{c,d}$	Upward/downward reserves from an ESS when it is charging [MW].
y_{ne}	Stored energy from ESS unit [MWh].
s_{ne}	Spilled energy from ESS unit [MWh].
ei_{ne}	Energy inflows of a ESS unit [MWh].

Binary:

α_g^g	Candidate generation unit installed or not.
α_e^e	Candidate ESS unit installed or not.
uc_{ng}	Commitment of generation unit.
su_{ng}, sd_{ng}	Startup/shutdown of generation unit.

Transmission Variables:

Continuous:

l_{ni}^{ens}	Energy not served [p.u.].
v_{ni}^2	Square of voltage magnitude [p.u.^{2}].
i_{nijc}^2	Square of current magnitude [A^2].
θ_{ni}	Voltage angle [rad].
f_{nijc}^P	Active power flow [MW].
f_{nijc}^Q	Reactive power flow [Mvar].
q_{nijc}^{shl}	Reactive power nodal injection by an existing/candidate line [Mvar].
q_{nijc}^{shc}	Reactive power nodal injection by an existing/candidate capacitor bank [Mvar].
f_{nijc}^v	Auxiliary variable of voltage drop [p.u.].
f_{nijc}^θ	Auxiliary variable of voltage angle difference [rad].
θ_{nijc}^k	Auxiliary variable which represents the voltage angle difference for the branch between nodes i and j [rad].

Binary:

α_{ijc}^t	Candidate transmission line installed or not
α_s^q	Candidate synchronous compensator installed or not
α_r^s	Candidate capacitor bank installed or not

$\alpha_{ij}^{t,k}$ Auxiliary variable which specifies whether any of the candidate lines for the branch ij is built or not when stating the cycle constraints for cycle k

Contents

Introduction

> *You can't do better design with a computer, but you can speed up your work enormously.*
>
> — **Wim Crouwel**
> (Graphic designer and typographer)

The transition toward a zero-carbon economy is reshaping the power system landscape and introducing a new set of challenges that underscore the critical importance of transmission expansion planning (TEP). As we transition from the reliance on fossil fuels to a future dominated by renewable energy sources (RES), the need for a power system that is not only flexible, but also resilient, becomes only more and more evident. This transition requires a paradigm shift in how we approach optimisation models for power system operation and expansion. Traditional models must now evolve to incorporate the complexities introduced by intermittent renewable energy sources such as wind and solar, while navigating the nuances of electricity markets. This evolution is critical to ensuring the system's ability to efficiently and sustainably meet the demands of this new energy era.

The move towards integrated planning methodologies attempts to address multiple limitations by taking a more holistic approach to the expansion of generation, storage, and transmission infrastructure. These methods are laudable for their ability to potentially reduce reliance on thermal generation, minimise curtailment of renewable energy, and alleviate transmission congestion. However, the focus on integrated planning sometimes diverts attention from the unique and critical challenges specific to transmission expansion planning. Transmission systems play a critical role in ensuring the reliable and efficient delivery of electricity from diverse generation sources to load centers. The complexity of modern power systems, characterised by the increasing penetration of distributed energy resources (DERs) and the need for grid flexibility, exacerbates transmission planning challenges.

A particularly pressing issue in transmission expansion planning is the need for a comprehensive representation of the system operation. Traditional optimisation models to solve the TEP often overlook the dynamic interactions among various aspects of the functioning of modern power systems, including the operational

constraints of power plants, the variability of renewable energy sources, and the impact of demand-side management. This oversight can lead to an underestimation of the true value and capabilities of transmission infrastructure, potentially resulting in inefficient investment decisions and inadequate system performance.

In addition, as the energy sector evolves, integrating DERs, and the growing importance of local flexibility resources, require reevaluating how transmission systems are planned. The coordination between transmission and distribution systems, which is essential to harness local flexibility and ensure system adequacy, adds another layer of complexity to the TEP models.

1.1 Motivation

The motivation for this research stems from the urgent need to address the evolving needs of modelling the power system operation and expansion in the face of the transition to a zero-carbon economy. With the retirement of traditional fossil-fueled power plants and the increasing penetration of RES, power systems are undergoing a profound transformation. This transition poses new challenges related to ensuring grid adequacy and resilience while minimising environmental impacts and costs.

One of the key challenges in power system planning is transmission expansion optimisation, which involves finding the most cost-efficient and reliable ways to expand the transmission network to meet future demand and generation scenarios. Traditional approaches to transmission expansion planning, such as linear programming, mixed-integer programming and heuristic methods, often overlook the size and tightness of the resulting optimisation problem. Instead, they focus on decomposition techniques such as Benders decomposition or Lagrangian relaxation to deal with the complexity. However, these methods often fail to ensure that the optimisation formulation is sufficiently tight or efficient, leading to computational inefficiencies and excessive time and resources spent solving poorly developed formulations.

In addition, these approaches often fail to capture critical interdependencies among the functioning of generation, transmission and distribution infrastructure, such as the impact of transmission constraints on generation dispatch, or the impact of RES integration on grid stability. This can lead to sub-optimal solutions that do not fully take into account operational flexibility, resilience and cost efficiency. These issues are particularly challenging in large-scale networks with high uncertainty and variability, such as those with significant penetration of RES and evolving demand patterns.

Furthermore, providing flexibility within the grid, especially at the local level, is becoming increasingly important. The growth of DERs, such as rooftop solar, battery storage and electric vehicles, as well as increased level of coordination in their activities achieved by transmission and distribution system operators (TSOs and DSOs), requires considering the provision of the required (increased) levels of flexibility within the expansion planning process. Incorporating these factors is critical to maintaining grid adequacy while adapting to a rapidly changing energy landscape.

1.2 Research Questions

Based on the motivation and challenges outlined in section 1.1, within this thesis work, I have identified and addressed the following research questions (RQ):

- **RQ-1**: How can TEP models be improved in a computational manner while accurately accounting for the variability and dynamics introduced by RES?
- **RQ-2**: How does accounting for local flexibility, particularly from DERs, affect the TEP problem and its outcomes, and what value does it add in terms of increases in system efficiency and planning outcomes?
- **RQ-3**: What is the role of utility-scale storage in transmission expansion planning, and how does its integration affect the overall flexibility mix and system optimisation?

The RQs outlined here are designed to address key challenges in TEP amidst the increasing relevance of the integration of ever-larger amounts of RES generation and the evolving power system landscape. **RQ-1** seeks to explore how TEP models can be made more computationally efficient while still capturing the variability and dynamics introduced by RES. This question is critical because traditional TEP models often struggle with computational inefficiencies due to the complex, and non-linear, characteristics of the system, requiring the application of improved modelling techniques that balance accuracy and efficiency. **RQ-2** focuses on understanding the impact of incorporating local flexibility, particularly from DERs, into TEP. This question is important because the emergence of DERs, such as rooftop solar and battery storage, offers new opportunities for grid optimisation, potentially improving system efficiency. My aim here is to assess how DERs can add value to the TEP by reducing system costs or deferring large investments. Finally, in **RQ-3**, I examine the role of utility-scale storage in TEP and its impact on the flexibility mix to deploy and the overall system optimisation. As large-scale storage solutions such as batteries become more feasible, their integration into TEP could significantly change the way grid flexibility is managed, affecting both the short-term operation and the long-term investment strategies.

1.3 Aim and Scope of the Thesis

This thesis work aims to develop novel, advanced, TEP models, focusing on improving their computational efficiency and ensuring an accurate representation of the complex dynamics introduced by the integration of variable renewable energy sources. I address the optimisation of these models with the aim of allowing them to efficiently and accurately handle the variability of RES generation, thus examining the optimal balance between achieving a detailed representation of the system dynamics and computational manageability. In addition, this thesis work examines the impact of integrating local flexibility resources, particularly from DERs, on the performance of TEP, and evaluates the contribution of these resources to increasing the system efficiency and achieving planning effectiveness. The role of utility-scale storage is also examined, focusing on its potential to increase the overall system flexibility and increase the efficiency, flexibility, and resiliency of the energy mix, while minimising its negative environmental impact. Specifically, the key objectives of this research work are:

1. **To Optimise the Computational Efficiency of models:** Enhance the computational performance of TEP models to efficiently manage the increasing complexity introduced by the variability and dynamics of renewable energy source generation.

2. **To Evaluate the Local Flexibility Integration:** Investigate the impact of integrating local flexibility options, particularly from distributed energy resources (DERs), on the TEP process efficiency and ability to achieve its objectives. This includes assessing how local flexibility contributes to system efficiency, the expansion planning outcomes, and the overall grid resiliency.

3. **To Assess the Role of Utility-Scale Storage:** Investigate the integration of utility-scale storage into the TEP process and its impact on the flexibility mix and the efficiency, resiliency and environmental footprint of the system. In line with this objective, I seek to understand how storage solutions can support grid adequacy and efficiency.

This piece of research aims to contribute to the development of more efficient, resilient and sustainable electricity systems. Through comprehensive modelling and analysis, it provides insights and recommendations for optimising transmission system development during the transition to a low-carbon future. However, the study has certain limitations. The accuracy and availability of data, particularly for renewable energy generation, demand forecasts and technological advances, are critical factors that can affect the quality of the results. The assumptions made about the market conditions, the technology costs and the policy environment are

essential for modelling, but may limit the extrapolation of results to other contexts than that explored in the case studies. The computational constraints may limit the explored scenario complexity and the level of granularity considered by the model. In addition, the rapid evolution of energy technologies and market dynamics may affect the longevity and relevance of the results produced. Finally, while acknowledging the interconnectedness of transmission and distribution systems, this work focuses primarily on transmission planning, with limited emphasis on distribution-level challenges.

1.4 Main Contributions

In this thesis work, I make a number of significant advances in transmission expansion planning, divided into two distinct parts, each supporting the transition to a zero-carbon energy system, with a focus on improving model performance by ensuring the scalability of the problem formulation and resolution and integrating the modelling of the provision of flexibility at multiple scales.

Part 1 – Improvements in Modeling, here the emphasis is on improving the representation of system operations. By introducing advanced methods for accurate modelling of system behaviour, this research provides a refined framework that captures the complexities of modern power systems, in particular the variability of renewable generation. In addition, while the framework facilitates generation planning, the main contributions are in the area of network planning.

Part 2 – Assessing Flexibility and Storage Solutions, I also explore the value and impact of local flexibility and the strategic role of utility-scale storage in achieving an optimal mix of flexibility resources for power systems. In this work, I quantitatively assess how local flexibility, including DERs and demand side management, enhances the grid resilience and the system efficiency. I also explore the integration of utility-scale storage solutions. The results computed highlight the importance of this storage type in stabilising the grid, facilitating the integration of renewables, and reducing the overall system costs. The results of this part of the thesis work not only underscore the importance of both local and utility-scale flexibility in transmission expansion planning, but also provide insights into the strategic placement and sizing of storage assets, guiding stakeholders towards undertaking the most efficient investments in storage technologies.

Overall, through its focused and structured approach, this thesis work makes contributions to the field of transmission expansion planning by providing comprehensive methodologies and insights. These contributions are critical to supporting the energy

sector's transition to a sustainable and resilient future by helping address the evolving challenges of grid stability, RES-based generation integration, and environmental sustainability. The work described here lays a foundational path for future research and policy-making, guiding the energy sector towards the implementation of more efficient, scalable, and sustainable solutions.

1.5 Thesis Outline

This dissertation is organised in such a way that each chapter can be read independently, fully understanding its scientific content. The structure of the thesis:

Chapter 2 – Enhancing System Operation Representation

This chapter describes the development of advanced methods for accurately representing the system operation in transmission expansion planning models. It discusses the challenges of modeling the dynamic nature of power systems, particularly what concerns the integration of renewable energy source generation, and describes the proposed solutions to increase the accuracy and efficiency of these models.

Chapter 3 – Impact of the Flexibility Provided by Distributed Energy Resources

This chapter provides an assessment of the role and value of local flexibility in transmission expansion planning. In it, I quantitatively evaluate the system impact of integrating DERs and demand response mechanisms, highlighting how procuring local flexibility contributes to increasing the grid resilience and efficiency. In this chapter, I also explore the policy and regulatory implications of the aforementioned findings.

Chapter 4 – The Role of the Utility-Scale Storage in the Optimal Flexibility Mix

In this chapter, I explore the impact of the deployment of utility-scale storage solutions and analyse their strategic importance in achieving an optimal flexibility mix. I also examine the optimal placement and sizing of storage within the transmission system and assess its contribution to grid stability, RES-based generation integration, and cost reduction.

Chapter 5 – Conclusions

In this final chapter, I summarise the key findings of the thesis work, reflecting on this piece of research contributions and their implications for the field of transmission expansion planning. I also outline the limitations of my work and propose directions for future research, suggesting how this work can be extended and applied to other areas within energy system planning and policy-making.

1.6 List of Publications

The publications originated from this thesis are:

- **Erik F. Alvarez**. "The roles of the Utility-Scale Storage in the Optimal Flexibility Mix within the Transmission Expansion Planning". In: ArXiv (2024). **XXXXX**.
- **Erik F. Alvarez**, Juan Camilo López, Luis Olmos, Andres Ramos. "An Optimal Expansion Planning of Power Systems considering Cycle-Based AC Optimal Power Flow". In: Sustainable Energy, Grids and Networks. 2024 May 10:101413. DOI: https://doi.org/10.1016/j.segan.2024.101413. **Peer-reviewed**, JCR: 5,400 Q1 (2022) - SJR: 1,225 Q1 (2022), cite as [1].
- **Erik F. Alvarez**, Luis Olmos, Andres Ramos, Kyriaki Antoniadou-Plytaria, David Steen, and Le Anh Tuan. "Values and impacts of incorporating local flexibility services in transmission expansion planning." In: Electric Power Systems Research. 2022 Nov 1;212:108480. DOI: https://doi.org/10.1016/j.epsr.2022.108480. **Peer-reviewed**, JCR: 3,900 Q2 (2022); - SJR: 1,099 Q1 (2022), cite as [2].

Other publications by the author, not included in this thesis, are:

- Kristof Phillips, **Erik F. Alvarez**, Erik Delarue, Luis Olmos, and Andrés Ramos. "Assessment of System States Aggregation Methods for Transmission Expansion Planning with High Renewables Shares". In: ArXiv, (2024).
- **Erik F. Alvarez**, Pedro Sánchez Martín, and Andrés Ramos. "Self-Scheduling for a Hydrogen-Based Virtual Power Plant in Day-Ahead Energy and Reserve Electricity Markets". In: 20th International Conference on the European Energy Market, (2024). **Peer-reviewed**, cite as [3].
- Dilayne Santos, Sara Lumbreras, **Erik F. Alvarez**, Luis Olmos, Andrés Ramos. "Model-based energy planning: a methodology to choose and combine models to support policy decisions". In: International Journal of Electrical and Power Systems, 2024 Aug 1;159:110048. DOI: https://doi.org/10.1016/j.ijepes.2024.110048. **Peer-reviewed**, JCR: 5,200 Q1 (2022) - SJR: 1,533 Q1 (2022), cite as [4].
- Andrés Ramos, **Erik F. Alvarez**, and Sara Lumbreras. "openTEPES: open-source transmission and generation expansion planning". In: SoftwareX. (2022) Jun 1;18:101070. DOI: https://doi.org/10.1016/j.softx.2022.101070. **Peer-reviewed**, JCR: 3,400 Q2 (2022); - SJR: 0,574 Q2 (2022), cite as [5].
- Sara Lumbreras, Jesús David Gómez, **Erik F. Alvarez**, and Sebastien Huclin. "The Human Factor in Transmission Network Expansion Planning: The Grid That a Sustainable Energy System Needs". In: Sustainability. (2022)

May 31;14(11):6746. DOI: https://doi.org/10.3390/su14116746. **Peer-reviewed**, JCR: 3,900 Q2 (2022); - SJR: 0,664 Q1 (2022), cite as [6].

- Daniel Huppmann, Matthew J. Gidden, Zebedee Nicholls, Jonas Hörsch, Robin Lamboll, Paul N. Kishimoto, Thorsten Burandt, Oliver Fricko, Edward Byers, Jarmo Kikstra, Maarten Brinkerink, Maik Budzinski, Florian Maczek, Sebastian Zwickl-Bernhard, Lara Welder, **Erik F. Alvarez** and Christopher J. Smith. "pyam: Analysis and visualisation of integrated assessment and macro-energy scenarios". In: Open Research Europe. 2021;1. DOI: https://doi.org/10.12688/openreseurope.13633.2. **Peer-reviewed**, cite as [7].

1.7 Contributions to the Scientific Open-Source Community Work

Contributing to the activities carried out by the open source community is critical to advancing research in TEP and the broader field of energy systems. Open source initiatives promote transparency, reproducibility and collaboration between researchers, which is essential for validating results and building on existing work. In this thesis, several open source tools written in Python and Julia have been used and extended.

Tools directly used in this thesis are

- **ITEPO**, https://github.com/IIT-EnergySystemModels/ITEPO, is a specialised tool for transmission expansion planning and can also be used for generation expansion planning, storage expansion planning, topology optimisation and reactive power planning. Its comprehensive mathematical framework integrates AC-OPF, unit commitment and operating reserves. The tool offers various network modelling options, including DC-OPF, linear and second-order conic bus injection-based AC-OPF, and linear branch flow-based AC-OPF with and without cycle constraints. Developed entirely by the author of this thesis in Julia using JuMP, ITEPO is noted for its flexibility and detailed capabilities.

- **openTEPES**, https://github.com/IIT-EnergySystemModels/openTEPES. This tool will be rigorously updated to improve its efficiency and scalability, which are crucial for the design of electrical systems that integrate RES and storage. The importance of the project is underlined by its role in strategic initiatives such as Spain's National Energy and Climate Plan. With a focus on long-term operational and expansion planning, openTEPES serves as a critical tool for researchers and policy makers seeking to navigate the complexities of the transition to sustainable energy systems. In addition to my efforts, Andrés

Ramos Galán, the architect of openTEPES, has played a key role in improving this important energy system model. Developed in Python using Pyomo, openTEPES has benefited from our joint contributions, which have significantly advanced it and influenced numerous research projects since 2019.

Other tools contributed by the author and not used in this thesis are:

- **StarNet**, https://github.com/IIT-EnergySystemModels/StarNet. This tool supports generation and transmission expansion planning, either together or separately. It employs a robust formulation for single-node approaches or transmission expansion with DC-OPF. It integrates renewables, storage, and transmission network reinforcement. With a single script and minimal constraints, it optimises CPU time and serves as a basic tool for targeted analysis. Initially created by Andrés Ramos Galán in GAMS, it was later rewritten in Python using Pyomo through our joint efforts.

- **openENTRANCE**, https://github.com/openENTRANCE/openentrance. This tool standardises definitions and terms for linking energy system models in the Horizon 2020 project, focusing on Europe's energy transition. It provides a Python library with YAML files for common definitions, units and regional specifications, and a Python package for scenario analysis. This promotes interoperability between models that study energy systems and climate policy, and supports collaborative research for sustainable European energy strategies.

- **openSDUC**, https://github.com/IIT-EnergySystemModels/openSDUC. This tool features an Open Stochastic Daily Unit Commitment model for thermal and energy storage systems. It optimises the scheduling of large power systems, balancing cost-effective generation with uncertainties from RES and demand. The model supports detailed time partitioning and various storage options, yielding insights into operational efficiency, emissions reduction, and marginal costs. The project emphasises ease of implementation, with guidance on solver selection and installation. Developed collaboratively with Andrés Ramos Galán in Python, this tool is based on the SDUC model written in GAMS.

- **oHySEM**, https://github.com/IIT-EnergySystemModels/oHySEM, optimises the self-scheduling of a hydrogen-based virtual power plant within electricity and hydrogen networks. Developed by Andrés Ramos Galán, Pedro Sánchez Martín and myself, the model integrates RES, battery, electrolysers and hydrogen storage to maximise profits. It effectively manages the complexities and optimising resources for energy and reserve markets while accounting for interactions between electricity and hydrogen systems. Built using Python and Pyomo, the model is typically solved in about 15 seconds, enabling efficient bid generation for 15-minute interval electricity markets.

2 Enhancing System Operation Representation

> *The most dangerous phrase in the language is,*
> *"We've always done it this way."*

— **Grace Hooper**
Pionner in computer science

Contents of this chapter are based on

Alvarez, Erik F., et al. "An Optimal Expansion Planning of Power Systems considering Cycle-Based AC Optimal Power Flow." Sustainable Energy, Grids and Networks (2024): 108480. DOI: `https://doi.org/10.1016/j.segan.2024.101413`

Declaration

I carried out all study elements and authored the initial draft. Co-authors edited and reviewed paragraphs and validated some results.

2.1 Introduction

The energy sector is undergoing significant changes to achieve sustainability. The shift from fossil fuels to renewable energy sources introduces complexities in the operation and expansion of power systems. This transition requires an innovative approach to transmission expansion planning (TEP), which is essential to adapt our energy infrastructure to the variability of wind and solar generation. As fossil fuel plants retire and renewable resources fluctuate, the power system must find new ways to increase flexibility and resiliency [8]. Traditional power system optimisation models are being reexamined and improved to incorporate low-carbon technologies and take advantage of emerging electricity markets that support renewable energy. These advances are critical for TEP models, which are key to ensuring technical and environmental sustainability at minimal cost.

Current enhancements to TEP models focus on the integration of flexibility devices and a more accurate representation of system operations within the TEP framework. This chapter examines potential enhancements aimed at achieving a more accurate representation of operational realities. Identified enhancements include:

1. More accurate representation of power flows: Prioritizing accurate simulation of power flows within the grid is critical. This improvement ensures that the model more accurately reflects how electricity is transmitted across the grid, taking into account both physical and regulatory constraints.

2. Modelling Unit Commitment for Thermal Plants: It's important to address the rigidity of the power generation system by accurately modelling the unit commitment of thermal plants. Since the operation of these plants is heavily influenced by the variability of renewable energy sources, this representation is key to realistic TEP modelling.

3. Continuous Storage Management Modelling: Incorporating a continuous storage management model into TEP allows for a dynamic and realistic representation of how energy storage systems can be deployed and optimized over time. This includes understanding how storage can mitigate issues such as renewable intermittency and peak demand challenges to provide a more robust and flexible grid.

By focusing on these critical areas of improvement, this chapter aims to provide an in-depth examination of the TEP in the context of the transition to zero-carbon energy systems. It explores the incorporation of linearized alternating-current optimal power flow (AC-OPF), customized unit commitment, and continuous storage management. This exploration sheds light on how these components collectively capture the operational dynamics of today's power systems, highlighting the ability of advanced TEP models to adapt and thrive skillfully in the changing energy landscape.

Specifically, this chapter presents an extension and linearization of the cycle-based formulation for the Second Order Cone Programming (SOCP)-based OPF as described in [9]. The adaptation allows this formulation to be used in the context of transmission expansion planning for medium to large electrical systems involving the deployment of new resources, including reactive power compensation devices. The formulation of cycle constraints for the expansion planning problem builds on the concepts introduced by [10]. In contrast to the direct current (DC) OPF used by the authors in [10], this work uses an AC branch flow model. The AC OPF-based formulation is comprehensive, covering a variety of generation and storage resources, as well as reactive power compensation devices. It provides a detailed representation of system operations, considering all relevant operational constraints with sufficient

temporal granularity to effectively manage the economic operation of key energy resources, including short-, medium-, and long-term storage.

To ensure the tractability of this complex problem, efficient size reduction techniques are applied. These include the use of a cycle-based AC-OPF model and a procedure for deriving tight bounds on voltage magnitude and angle variables. Given the hourly resolution considered, a static scheduling approach is used to keep the problem size within manageable limits for medium to large power systems.

The specific contributions of this work are outlined below:

- Introduction of a novel linear, branch-flow-based, AC-OPF model using cycle constraints adapted to the transmission expansion planning problem.
- Modification of typically used boundary conditions on voltage magnitude and angle variables, incorporating them into a linearized AC-OPF within the framework of expansion planning. These constraints have not previously been incorporated into this type of problem formulation in the existing literature.
- A representative case study is used to demonstrate the benefits of incorporating bound-tightening and cycle constraints into the AC-OPF formulation. These adjustments significantly reduce both the size and computational complexity of the problem, thereby increasing the efficiency of the expansion planning process.
- The applicability and effectiveness of the proposed formulation are further validated by applying it to compute the optimal integrated expansion plan for a realistically scaled medium-scale power system based on the deployment of renewable energy sources (RES)-based generation. Comparative analyses show that this approach outperforms other relevant formulations also suitable for such problems.

This chapter begins by describing the current challenges and advances in TEP. It continues with a critical review of both traditional and contemporary methodologies, emphasising the predominant mathematical formulations used in the field. Special attention is given to the importance of advanced modelling techniques, such as linearised AC-OPF, unit commitment and continuous storage management, and their integration into TEP. Subsequent sections explore the improvements introduced by recent research, with a particular focus on how these advanced modelling techniques and strategies contribute to solving the complexity of TEP problems while maintaining their tractability. The chapter concludes by discussing the broader implications of these advances for the future development and sustainability of power systems, and how they can support the evolving needs of modern power grids.

2.2 A Brief Review of TEP Formulations

This section presents the mathematical formulations often cited in the literature to address the challenge of transmission expansion planning. Following this review, a basic formulation is introduced to serve as a reference for further discussion. This initial formulation plays a critical role in the subsequent extensions and developments explored in later sections and chapters.

2.2.1 Mathematical Formulations

Since 1980, various regions of the world have undergone a significant transition from regulated to deregulated power systems, dramatically affecting transmission expansion planning strategies and objectives. Initially, efforts focused on providing cost-effective and reliable services within a unified planning framework. Additionally, the move toward deregulation ushered in a new era that emphasized economic efficiency, market dynamics, and adaptability in the face of uncertainty. This pivotal shift has spurred the innovation of sophisticated planning algorithms and tools, marking a profound change in the way transmission expansion projects are designed and implemented [11]. In this context, optimisation models representing the TEP as a complex problem requiring strategic solutions have gained prominence. These models, characterized by their mathematical formulations, aim to define investment plans and include an objective with constraints, thereby guiding the future operation of the power system and evaluating different investment options for expansion.

One of the leading methods for solving TEP problem is the mixed integer linear programming (MILP) model, which incorporates the DC network model. This model assumes a consistent voltage magnitude of 1 per unit (p.u.), a concept introduced by Villasana et al. in [12]. Their work refined the seminal efforts of Garver et al. in [13], which were among the first-if not the first-to apply linear programming to solve the TEP. The contribution of Villasana et al. was crucial in embedding the DC model in the TEP. However, their framework did not allow for binary variables indicating investment decisions, a limitation that was later addressed.

The introduction of binary variables and disjunctive constraints into TEP by Bahiense et al, as detailed in [14], was a major advance in the field. Their pioneering mathematical model led to the now-prevalent mixed-integer linear formulation that incorporates the DC network model for TEP. This formulation has become the leading approach for solving TEP problems, and its practical application is presented in several papers such as [15].

In contrast, a more flexible version of the previous model introduces an interesting approach known as the transportation network model. This adaptation, which avoids the constraints imposed by Kirchhoff's second law, represents a major shift in analytical techniques. Inspired by the foundational work of Garver et al. and operationalized in [16], it offers a new perspective on solving complex problems.

Subsequently, the research presented in [17] extends the work of Bahiense and colleagues by integrating energy loss considerations to improve the relaxation of the DC network model, thereby addressing the nonlinear and nonconvex nature of the AC model. This pivotal development has led scholars to further expand the range of methodologies designed to address the complex challenges of network modelling. They have identified clear research directions, including 1) convexification of the AC network model, 2) integration of market dynamics, 3) improvement of system adequacy, 4) development of reduction methods, 5) exploration of multiple power transmission technologies, and 6) incorporation of uncertainties, as thoroughly reviewed in [18]. This chapter focuses on the convexification of the AC network model within the context of the TEP problem and on enhancing system adequacy through improved representation of power system operations.

2.2.2 A Basic Formulation

As previously outlined in Section 2.2.1, the proposed formulation introduced by Villasana et al. remains a cornerstone in the field due to its simplicity and versatility in accommodating various features for studying the expansion of current power systems. The essence of its enduring relevance lies in the simplicity of the formulation and its well-documented scalability, making it exceptionally suitable for application in large-scale case studies. Following this exposition, the mixed-integer linear programming (MILP) formulation is presented as follows:

$$\min C = C^{te} + \sum_{n \in \mathcal{T}} C_n^{gen} + C_n^{ens} \tag{2.1a}$$

$$C^{te} = \sum_{ijc \in \mathcal{L}^c} C_{ijc}^t \alpha_{ijc}^t \tag{2.1b}$$

$$C_n^{gen} = \sum_{g \in \mathcal{G}_i} D_n CV_g p_{ng}^{tg} \qquad : \forall n, \tag{2.1c}$$

$$C_n^{ens} = \sum_{i \in \mathcal{B}^t} D_n C^{shed} l_{ni}^{ens} P_{ni}^d \qquad : \forall n, \tag{2.1d}$$

$$\sum_{g \in \mathcal{G}_i} p_{ng}^{tg} = P_{ni}^d \left(1 - l_{ni}^{ens}\right) + \sum_{ijc \in \mathcal{L}} f_{nijc}^P - \sum_{jic \in \mathcal{L}} f_{njic}^P \qquad \forall ni \tag{2.1e}$$

$$\frac{f_{nijc}^P}{\overline{S}_{ijc}'} - \left(\theta_i - \theta_j\right)\frac{S_B}{X_{ijc}\overline{S}_{ijc}'} = 0 \qquad : \forall nijc | ijc \in \mathcal{L}^e, \tag{2.1f}$$

$$\left| \frac{f_{nijc}^P}{\overline{S}'_{ijc}} - (\theta_i - \theta_j)\frac{S_B}{X_{ijc}\overline{S}'_{ijc}} \right| \leq 1 - \alpha_{ijc}^t \qquad\qquad : \forall nijc | ijc \in \mathcal{L}^c, \text{ (2.1g)}$$

$$\left| f_{nijc}^P \right| \leq \overline{S}'_{ijc} \qquad\qquad : \forall nijc | ijc \in \mathcal{L}^e, \text{ (2.1h)}$$

$$0 \leq l_{ni}^{ens} \leq 1 \qquad\qquad : \forall ni, \text{ (2.1i)}$$

$$\underline{P}_g \leq p_{ng}^{tg} \leq \overline{P}_g \qquad\qquad : \forall ng, \text{ (2.1j)}$$

$$\theta_{ni} = 0 \qquad\qquad : \forall ni | i = \text{reference node, (2.1k)}$$

The MILP formulation for the TEP problem is formulated as a series of equations, described in (2.1). Within this formulation, parameters are written in upper case, while variables are written in lower case. This formulation encapsulates objectives aimed at minimizing the total cost, which includes both investment and system operating costs, outlined from (2.1a) to (2.1d). The equation (2.1e) ensures active power balance, while the application of Kirchhoff's second law to both existing and candidate lines is articulated in (2.1f) and (2.1g), respectively. The limits on active power flow over existing lines are given in (2.1h). The limit on unserved electricity is defined in (2.1i). The limits on the electricity production per unit per time step are specified in (2.1j), and the voltage angle reference is set to zero as per (2.1k).

Understanding both the size of the problem and the architecture of the matrix is key to comparing different formulations. However, the CPU time required to solve a formulation depends not only on the problem size but also on the architecture of the matrix, including whether it is dense or sparse. This means that a smaller problem can sometimes take longer to solve than a larger one, depending on the complexity of the constraints and the structure of the matrix.

2.3 Extension of TEP through Comprehensive System Operation Modelling

In section 2.2.2, a basic formulation for TEP is introduced. This formulation is capable of incorporating renewable energy sources, candidate lines, and all time steps of one year (8760 hours) within a static planning framework. Planning approaches are identified as either static, targeting a specific year, or dynamic, projecting multiple years into the future with detailed operational simulations for each time step considered within each year. These methods were sufficient for transmission planning until recent developments required a greater focus on system flexibility. Such flexibility can be achieved by reinforcing existing branches (adding new corridors to existing paths) or by expanding the network.

In addition, the flexibility of the system is significantly influenced by the unit commitment of thermal units, the management of storage technologies (such as batteries or hydro reservoirs) that involve inter-temporal constraints, and the modelling of power flows. These

factors, which are critical for modifying the investment plan to meet evolving needs, are not addressed in the basic formulation. Integrating these elements is critical to update the TEP problem. It will ensure that the expansion planning remains robust, adaptable, and capable of supporting a resilient and efficient electric grid amidst the growing integration of variable energy sources and increasing demand for electricity.

The transition to comprehensive system operation within the TEP can be achieved by incorporating specific features that reveal potential problems related to the flexibility capacity of the system. These features include:

1. **Unit commitment of thermal units:** This includes operating reserves and divides the unit's production into fixed and variable blocks. It also includes logical constraints related to startup and shutdown procedures, as well as symmetry-breaking constraints to speed decision-making between two similar units.

2. **Storage management:** This includes the use of storage systems to contribute to operating reserves during both the charge and discharge phases. The modelling of the energy storage system strategically considers the division of the capacity to charge and discharge energy in each time step, optimizing the compactness of the formulation and making it possible to avoid binary variables whose purpose is to limit simultaneous charging and discharging.

3. **Power flow modelling:** This process uses an AC-OPF based branch flow model instead of the classical bus injection model. The branch flow model is chosen to avoid the more complex nonlinearities of the bus injection model. In addition, cycle constraints are applied within this model to provide a more accurate relaxation, which improves the handling of non-linearities compared to previous approaches.

These enhancements are essential to accurately capture the complexities of future power system operations. They play a critical role in evaluating the integration of renewable energy sources, assessing the need for energy storage over a range of capacities - from short to long storage cycles - and identifying the need for flexibility and reactive power compensation. This comprehensive approach ensures more effective management of energy resources and facilitates the transition to sustainable power systems. The mathematical formulation of TEP that incorporates these features is presented in the following subsections, and the resulting model will also enable generation and storage expansion planning:

2.3.1 Objective Function

$$\min C = C^{te} + C^{re} + \sum_{n \in \mathcal{T}} C_n^{gen} + C_n^{con} + C_n^{CO2} + C_n^{ens} \tag{2.2}$$

$$C^{te} = \sum_{ijc \in \mathcal{L}^c} C_{ijc}^t \alpha_{ijc}^t \tag{2.3a}$$

$$C^{re} = \sum_{s \in \mathcal{S}_i^c} C_s^{sy} \alpha_s^q + \sum_{r \in \mathcal{R}_i^c} C_r^{sh} \alpha_r^q \tag{2.3b}$$

$$C_n^{gen} = \sum_{g \in \mathcal{G}_i} D_n (CV_g p_{ng}^{tg} + CF_g uc_{ng}) + C_g^{su} su_{ng} + C_g^{sd} sd_{ng} \qquad : \forall n, \tag{2.4a}$$

$$C_n^{con} = \sum_{e \in \mathcal{G}_i} D_n CV_e p_{ne}^{tc} \qquad : \forall n, \tag{2.4b}$$

$$C_n^{CO2} = \sum_{g \in \mathcal{G}_i} D_n P^{co2} E_g^{co2} p_{ng}^{tg} \qquad : \forall n, \tag{2.4c}$$

$$C_n^{ens} = \sum_{i \in \mathcal{B}^t} D_n C^{shed} l_{ni}^{ens} \left(P_{ni}^d + Q_{ni}^d \right) \qquad : \forall n, \tag{2.4d}$$

In the equations (2.2)–(2.4d), the sets $\mathcal{L}^c$, $\mathcal{S}_i^c$, $\mathcal{R}_i^c$, $\mathcal{G}_i$, and $\mathcal{B}^t$ represent candidate lines, synchronous compensators, capacitor banks, generating units, and nodes, respectively. In addition, the binary variables α_{ijc}^t, α_s^q, and α_r^q indicate the decisions to install a candidate line (i.e., a circuit c between nodes i and j), a synchronous compensator s, and a capacitor bank r. These variables are used in conjunction with the fixed annualized installation costs of each asset, denoted by C_{ijc}^t, C_s^{sy}, and C_r^{sh}, respectively.

Incorporating AC-OPF into the TEP allows the simultaneous installation of lines, synchronous compensators and capacitor banks, which is equivalent to solving the TEP and reactive power planning. This comprehensive approach, only possible with AC-OPF, enables coordinated investment decisions and operational strategies. In contrast, the use of DC-OPF in the TEP does not allow for such simultaneous considerations. With DC-OPF, reactive power planning must be done separately, either before or after transmission expansion planning, due to its inability to handle reactive power flows.

The binary variables uc_{ng}, su_{ng} and sd_{ng} reflect the decisions for commitment, startup and shutdown of a generation unit. The variable p_{ng}^{tg} represents the active power output of a generation unit, while p_{ne}^{tc} represents the active power consumption of an ESS unit. The variable l_{ni}^{ens} quantifies the percentage of load shedding at the node i.

The operating costs are specified by CV_g and CF_g for the variable and fixed costs of a generation unit, respectively. The parameters C_g^{su} and C_g^{sd} denote the startup and shutdown costs of a generation unit. For an ESS unit, CV_e represents the variable cost during storage. The cost of unserved energy is represented by C^{shed}.

In addition, the parameters D_n, P^{co2}, E_g^{co2}, P_{ni}^d, and Q_{ni}^d specify the duration of a time step, the cost of CO2 emissions, the CO2 emission rate, and the active and reactive power demand, respectively.

2.3.2 Investment Decisions Bounds for Operational Variables

Transmission lines

Investments related to transmission lines include constraints that limit current flow and thus implicitly limit power flows in candidate lines, as shown in (2.5), where $\mathcal{L}^c$ denotes the subset of candidate lines. In AC-OPF, the relationship between power flows and current flows is described by (2.10). For DC-OPF, limiting the active power flow alone is sufficient, as illustrated in [5].

$$\frac{i^2_{nijc}}{\overline{S}^2_{ijc}/\overline{V}^2_{ni}} \leq \alpha^t_{ijc} \qquad\qquad\qquad : \forall nijc | ijc \in \mathcal{L}^c, \ (2.5)$$

Synchronous compensators

The output (injection or absorption) of candidate synchronous compensators is constrained by the investment decision associated with each compensator, as shown in (2.6a) and (2.6b), where $\mathcal{S}^c_i$ represents the subset of candidate synchronous compensators. It's important to note that synchronous compensators are modelled as power generation units that can only provide reactive power. Investment decisions regarding capacitor banks set limits on the reactive power compensation of these assets, as illustrated in (2.14b) and (2.14c).

$$\frac{q^{tg}_{ns}}{\overline{Q}_s} \leq \alpha^q_s \qquad\qquad\qquad : \forall ns | s \in \mathcal{S}^c_i, \ (2.6a)$$

$$\frac{q^{tg}_{ns}}{-\underline{Q}_s} \geq -\alpha^q_s \qquad\qquad\qquad : \forall ns | s \in \mathcal{S}^c_i, \ (2.6b)$$

2.3.3 AC Optimal Power Flow: Branch Flow Model

In the field of power flow analysis, optimisation and its applications, the modelling of transmission lines plays a central role, with the PI model often being the standard assumption. Currently, two basic methodologies for defining the variables of the PI model have emerged, leading to the development of the Bus Injection Model (BIM) and the Branch Flow Model (BFM). The BIM, which uses a polar coordinate formulation, is favoured primarily for its intuitive approach to modelling based on the voltage magnitude and angle of the PI model, although it does not explicitly represent power flows. Conversely, the BFM, a more recent innovation in the field, has been shown to be equivalent to the BIM, a validation described in [19]. This advancement diversifies the suite of modelling tools at our disposal and significantly expands our capabilities by offering different approaches to tackle the OPF problem. The BFM addresses similar challenges to traditional power flow analysis by explicitly illustrating power flows, as shown in the PI model diagram of a transmission line (see Figure 2.1). This figure also highlights the variables associated with the BFM. The BFM integrates quadratic variables, second-order equality constraints, and variable multiplications by streamlining the nonlinear complexities inherent in power system modelling. This approach introduces a unique set of challenges that are, in some respects, less complex than those posed by alternative models. In addition, the pioneering work of Farivar et al. documented in [20] introduces a more intuitive and simplified approach to
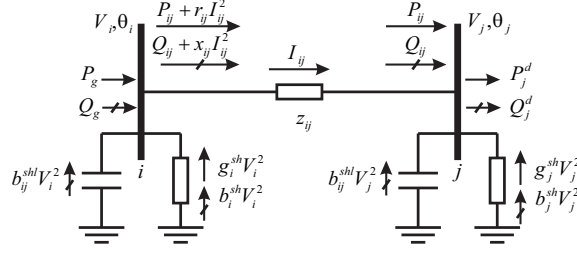
Fig. 2.1.: Diagram considered for the BFM. [Source: Author's own illustration]

the relaxation of the BFM. This methodology converts second-order equality constraints into rotated second-order conic constraints and implements transformations for quadratic variables. This innovation significantly streamlines the BFM relaxation process, providing a simpler and more effective solution compared to previous efforts.

This section focuses on the BFM and its significant advantages in facilitating a linear OPF formulation. The framework of the BFM provides an advanced approach to the complex challenges of TEP. Unlike conventional formulations that either struggle with the nonlinear and non-convex dilemmas of the power flow equations or default to the DC power flow model for simplicity, the BFM skillfully reduces these complexities. This reduction makes the BFM particularly suitable for the TEP. The linearization process significantly improves computational efficiency, thereby increasing the practicality and scalability of expansion planning efforts. Leveraging the BFM's ability to transform complex power flow equations into manageable linear forms, this research seeks to make a significant contribution to the TEP field by providing insightful findings and groundbreaking methodologies.

After the introductory discussion, the basic formulation for TEP, as presented in (2.1) and initially incorporating DC-OPF, is modified to include a BFM-based AC-OPF. This modification aligns with the formulation proposed in [21] and the respective mathematical formulation is as follows:

Active and reactive power balance

This formulation includes specific constraints to ensure active and reactive power balance, as described in (2.7). The active power balance, defined in (2.7a), is similar to that described in (2.1e), but refers specifically to active power flows within the BFM. The reactive power balance, described in (2.7b), includes the production and consumption of generation units, synchronous compensators, capacitor banks (only injects to the grid) and transmission lines.

$$\sum_{g \in \mathcal{G}_i} p_{ng}^{tg} = \sum_{e \in \mathcal{G}_i} p_{ne}^{tc} + P_{ni}^d (1 - l_{ni}^{ens}) + \sum_{ijc \in \mathcal{L}} f_{nijc}^P - \sum_{jic \in \mathcal{L}} f_{njic}^P - R_{jic} i_{njic}^2 \qquad : \forall ni, \quad (2.7a)$$

$$\sum_{g \in \{\mathcal{G}_i \cup \mathcal{S}_i\}} q_{ng}^{tg} + \sum_{r \in \mathcal{R}_i} q_{nr}^{shc} = Q_{ni}^d (1 - l_{ni}^{ens})$$
$$+ \sum_{ijc \in \mathcal{L}} f_{nijc}^Q - q_{nijc}^{shl} - \sum_{jic \in \mathcal{L}} f_{njic}^Q + q_{njic}^{shl} - X_{jic} i_{njic}^2 \qquad : \forall ni, \qquad (2.7b)$$

Note that it is the squared current flow (i^2_{nijc}) that is considered a variable in our formulation instead of the current flow. This is also the case for the square of the voltage magnitude (v^2_{nijc}), which is considered in the following constraints.

Voltage magnitude drop

The equations (2.8) quantify the voltage magnitude drop between nodes for each branch. Specifically, (2.8a) calculates this drop for existing lines, while (2.8b) and (2.8c) are formulated for the candidate lines. Importantly, these latter equations are disjunctive inequalities designed to handle the interaction between a line's "current flow" and "power flow" variables and its associated investment (binary) variable, as defined in the original formulation.

$$v^2_{ni} - v^2_{nj} = Z^2_{ijc} i^2_{nijc} + 2 \left(R_{ijc} f^P_{nijc} + X_{ijc} f^Q_{nijc} \right) \qquad : \forall nijc | ijc \in \mathcal{L}^e, \text{ (2.8a)}$$

$$v^2_{ni} - v^2_{nj} - f^v_{nijc} = Z^2_{ijc} i^2_{nijc} + 2 \left(R_{ijc} f^P_{nijc} + X_{ijc} f^Q_{nijc} \right) \qquad : \forall nijc | ijc \in \mathcal{L}^c, \text{ (2.8b)}$$

$$\left| f^v_{nijc} \right| \leq \left(\overline{V}^2_{ni} - \underline{V}^2_{ni} \right) (1 - \alpha^t_{ijc}) \qquad : \forall nijc | ijc \in \mathcal{L}^c, \text{ (2.8c)}$$

Voltage angle difference

The equations (2.9) quantify the voltage angle differences along branches ij. Equation (2.9a) addresses these differences for existing lines, while (2.9b) and (2.9c) address them for candidate lines. Similar to the approach applied for the voltage magnitude drop, disjunctive inequalities are also defined here. The nonlinear equations (2.9a) and (2.9b) can be linearized by assuming that $v^2_{ni} = V^0_{ni}$ and $\sin(\theta_{ni} - \theta_{nj}) = (\theta_{ni} - \theta_{nj})$, as done in the initial step in [21].

$$\sqrt{v^2_{ni}} \sqrt{v^2_{nj}} \sin(\theta_{ni} - \theta_{nj}) = X_{ijc} f^P_{nijc} - R_{ijc} f^Q_{nijc} \qquad : \forall nijc | ijc \in \mathcal{L}^e, \text{ (2.9a)}$$

$$\sqrt{v^2_{ni}} \sqrt{v^2_{nj}} \sin(\theta_{ni} - \theta_{nj}) = f^\theta_{nijc} + X_{ijc} f^P_{nijc} - R_{ijc} f^Q_{nijc} \qquad : \forall nijc | ijc \in \mathcal{L}^c, \text{ (2.9b)}$$

$$\left| f^\theta_{nijc} \right| \leq 2 \overline{V}_{ni} \overline{V}_{nj} \overline{\theta}_{nijc} (1 - \alpha^t_{ijc}) \qquad : \forall nijc | ijc \in \mathcal{L}^c, \text{ (2.9c)}$$

Current flow

The nonlinear and non-convex constraint (2.10) calculates current flow based on concurrent power flows and voltage magnitudes. Several methods are available to address the challenges posed by a nonlinear constraint. The primary approaches include: a) using relaxation techniques to convert it into a rotated second-order conic constraint that bounds the squares of the power flows; and b) applying a piecewise linearization process to the square terms. In this model, the latter approach, as detailed in [21], is applied to (2.10).

$$(f^P_{nijc})^2 + (f^Q_{nijc})^2 = v^2_{ni} i^2_{nijc} \qquad : \forall nijc, \text{ (2.10)}$$

And, the constraint (2.10) is replaced by (2.11) that is defined as follows:

$$\left(V^0_{ni} \right)^2 i^2_{nijc} = \sum_{k=1}^{K} \left[m^s_{nijc,k} \Delta f^P_{nijc,k} \right] + \sum_{k=1}^{K} \left[m^s_{nijc,k} \Delta f^Q_{nijc,k} \right] \qquad : \forall nijc, \text{ (2.11a)}$$

$$f^{P+}_{nijc} + f^{P-}_{nijc} = f^P_{ijc} \qquad : \forall nijc, \text{ (2.11b)}$$

$$f_{nijc}^{P+} - f_{nijc}^{P-} = \sum_{k=1}^{K} \left[\Delta f_{nijc,k}^{P} \right] \qquad\qquad : \forall nijc, \text{ (2.11c)}$$

$$f_{nijc}^{Q+} + f_{nijc}^{Q-} = f_{nijc}^{Q} \qquad\qquad : \forall nijc, \text{ (2.11d)}$$

$$f_{nijc}^{Q+} - f_{nijc}^{Q-} = \sum_{k=1}^{K} \left[\Delta f_{nijc,k}^{Q} \right] \qquad\qquad : \forall nijc, \text{ (2.11e)}$$

$$0 \leq \Delta f_{nijc,k}^{P} \leq \overline{\Delta S}_{nijc,k} \qquad\qquad : \forall nijc, \forall k \in K \text{ (2.11f)}$$

$$0 \leq \Delta f_{nijc,k}^{Q} \leq \overline{\Delta S}_{nijc,k} \qquad\qquad : \forall nijc, \forall k \in K \text{ (2.11g)}$$

$$0 \leq f_{nijc}^{P+}, f_{nijc}^{P-}, f_{nijc}^{Q+}, f_{nijc}^{Q-} \qquad\qquad : \forall nijc, \text{ (2.11h)}$$

Within the piecewise linearization of $(f_{nijc}^{P})^2$ and $(f_{nijc}^{Q})^2$, the set K represents the piecewise partitions considered, $\Delta S_{nijc} = \overline{V}_{nj} i_{nijc}^2 / \text{card}(K)$ and $m_{nijc,k}^{S} = (2k-1)\Delta S_{nijc}$. Δf_{nijc}^{P}, Δf_{nijc}^{Q}, f_{nijc}^{P+}, f_{nijc}^{P-}, f_{nijc}^{Q+}, and f_{nijc}^{Q-} are auxiliary variables.

Bound of the current flow

Limits on current flow magnitudes for existing transmission lines are set by (2.12a). Similarly, the current flow magnitude of a candidate line is limited by (2.12b), with these limits depending on the investment decision for each candidate line.

$$0 \leq \frac{i_{nijc}^2}{\left(\overline{S}_{ijc}/\overline{V}_{ni}\right)^2} \leq 1 \qquad\qquad : \forall nijc | ijc \in \mathcal{L}^e, \text{ (2.12a)}$$

$$0 \leq \frac{i_{nijc}^2}{\overline{S}_{ijc}^2/\overline{V}_{i}^2} \leq \alpha_{ijc}^{t} \qquad\qquad : \forall nijc | ijc \in \mathcal{L}^c, \text{ (2.12b)}$$

Reactive power injection or consumption to the grid from a transmission line

The injection or consumption by existing lines is determined according to (2.13a), and that by candidate lines according to the disjunctive inequalities in (2.13b)-(2.13c).

$$q_{nijc}^{shl} = v_{ni}^2 B_{ijc}^{l} \qquad\qquad : \forall nijc | ijc \in \mathcal{L}^e, \text{ (2.13a)}$$

$$-\overline{V}_{ni}^2 \left(1-\alpha_{ijc}^{t}\right) \leq q_{nijc}^{shl} - v_{ni}^2 B_{ijc}^{l} \leq \underline{V}_{ni}^2 \left(1-\alpha_{ijc}^{t}\right) \qquad\qquad : \forall nijc | ijc \in \mathcal{L}^c, \text{ (2.13b)}$$

$$\underline{V}_{ni}^2 B_{ijc}^{l} \alpha_{ijc}^{t} \leq q_{nijc}^{shl} \leq \overline{V}_{ni}^2 B_{ijc}^{l} \alpha_{ijc}^{t} \qquad\qquad : \forall nijc | ijc \in \mathcal{L}^c, \text{ (2.13c)}$$

Reactive power compensation to the grid from a capacitor bank

The injection or consumption by existing lines is determined according to (2.14a), and that by candidate lines according to the disjunctive inequalities in (2.14b)-(2.14c).

$$q_{nr}^{shc} = v_{ni}^2 B_{r}^{sh} \qquad\qquad : \forall nr | r \in \mathcal{R}_i^e, \text{ (2.14a)}$$

$$-\overline{V}_{ni}^2 (1-\alpha_{r}^{s}) \leq q_{nr}^{shc} - v_{ni}^2 B_{r}^{sh} \leq \underline{V}_{ni}^2 (1-\alpha_{r}^{s}) \qquad\qquad : \forall nr | r \in \mathcal{R}_i^c, \text{ (2.14b)}$$

$$\underline{V}_{ni}^2 B_{r}^{sh} \alpha_{r}^{s} \leq q_{nr}^{shc} \leq \overline{V}_{ni}^2 B_{r}^{sh} \alpha_{r}^{s} \qquad\qquad : \forall nr | r \in \mathcal{R}_i^c, \text{ (2.14c)}$$

2.3.4 Cycle Constraints

In the branch-flow-based AC-OPF model, Kirchhoff's voltage law is represented by equations for voltage magnitude drop (2.8), voltage angle difference (2.9), and current flow (2.10). Based on the cycle constraints outlined in [9], it is proposed to replace the voltage angle difference constraints (2.9) with cycle constraints to improve the efficiency and robustness of the AC-OPF formulation within the expansion planning problem. Consequently, the formulation of the linear branch flow-based AC-OPF model differs from previous works as it incorporates cycle flow constraints and reformulates equation (2.9) using equation (2.15) along with a new set of linear and efficiently defined equations (2.16) as discussed in [9]. Note that in this model, cycles are defined as closed loops formed by branches (e.g., transmission lines) and nodes (e.g., buses) within the network topology. These loops exclude any active or reactive power compensation devices connected in series with the transmission lines. This concept aligns with graph theory, where a cycle is a closed path in a graph: a sequence of edges connecting vertices that starts and ends at the same vertex, without revisiting any other vertex along the path as shown in Figure 2.2.
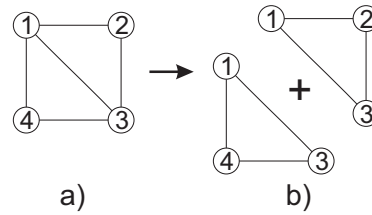
Fig. 2.2.: (a) Representation of the electricity network as a graph, and (b) decomposition of the graph into two distinct cycles. [Source: Author's own illustration]

The cycles are defined and classified based on the approach proposed in [10]. Accordingly, two sets of cycles are distinguished: the existing cycles, which are computed based on the existing transmission network, and the candidate cycles, which include at least one branch where only candidate lines are considered. The sets $\mathcal{K}^e$ and $\mathcal{K}^c$ correspond to the existing and candidate cycles, respectively. The set $\mathcal{K}^e$ is derived from the cycle basis calculated for the existing network only. In contrast, the set $\mathcal{K}^c$ is obtained by removing all cycles within $\mathcal{K}^e$ from the cycle basis computed for the entire network (including both existing and candidate lines). Consequently, $\mathcal{K}^c$ represents the difference between the cycle basis for the entire network and the set $\mathcal{K}^e$.

All cycles containing only existing lines are included in $\mathcal{K}^e$, while those containing at least one candidate line are included in $\mathcal{K}^c$. Finally, the voltage angle differences along the cycles $k \in \mathcal{K}$, where $\mathcal{K} = \mathcal{K}^e \cup \mathcal{K}^c$, are expressed as a directed linear combination of those for branches $'ij'$, using the incidence matrix $H_{ijc,k}$ in (2.15a).

Note that, according to the proposed formulation, the KVL is not enforced for those initially defined cycles that include at least one branch for which only candidate lines are considered if none of these lines is eventually built.

$$
H_{ijc,k} = \begin{cases} 1 & \text{if} \quad \text{line } ijc \in k \\ -1 & \text{if} \quad \text{line } jic \in k \\ 0 & \text{if} \quad \text{otherwise} \end{cases} \tag{2.15a}
$$

For those cycles in $\mathcal{K}^e$, the voltage angle differences along them can be represented by the corresponding sum of voltage angle differences along the lines in (2.15b).

$$
\sum_{ijc \in k | k \in \mathcal{K}^e} H_{ijc,k} \theta_{nijc}^k = 0 \qquad \forall n \tag{2.15b}
$$

For every cycle $k \in \mathcal{K}^e$, the equations (2.15b)-(2.15e) are defined as proposed in [9]. Where it is considered that the sum of voltage angle differences across all the lines in every cycle k must add up to zero, as imposed by (2.15b), and (2.15c) links the auxiliary variable $\theta_{nijc}^k, \forall nijc | ijc \in \mathcal{L}^e$ to its respective voltage angle difference.

$$
\theta_{nijc}^k = \theta_{ni} - \theta_{nj} \qquad \forall nijc | ijc \in \mathcal{L}^e, \tag{2.15c}
$$

Finally, (2.9a) is relaxed into (2.15d) and (2.15e).

$$
\theta_{nijc}^k \geq \frac{X_{ijc} f_{nijc}^P - R_{ijc} f_{nijc}^Q}{\overline{V}_{ni} \overline{V}_{nj} \cos \frac{\Theta_{nijc}^m}{2}} - \tan \frac{\Theta_{nijc}^m}{2} + \frac{\Theta_{nijc}^m}{2} \qquad \forall nijc | ijc \in \mathcal{L}^e, \tag{2.15d}
$$

$$
\theta_{nijc}^k \leq \frac{X_{ijc} f_{nijc}^P - R_{ijc} f_{nijc}^Q}{\underline{V}_{ni} \underline{V}_{nj} \cos \frac{\Theta_{nijc}^m}{2}} + \tan \frac{\Theta_{nijc}^m}{2} - \frac{\Theta_{nijc}^m}{2} \qquad \forall nijc | ijc \in \mathcal{L}^e, \tag{2.15e}
$$

Equations (2.15c)-(2.15e), as defined in [9], do not include cycles with candidate lines. Note that Θ_{nijc}^m is a parameter and is calculated as $\Theta_{nijc}^m = \max[|\underline{\theta}|, |\overline{\theta}|]$, which makes the equations (2.15d)-(2.15e) linear. And, the term $-\tan \frac{\Theta_{nijc}^m}{2} + \frac{\Theta_{nijc}^m}{2}$ in the previous equations is derived from the envelopes of the sine function, assuming that the voltage magnitudes and angles are relatively small, as discussed in [9].

In this study, a new set of equations, (2.16), is proposed for cycles consisting exclusively of branches containing only candidate lines, called candidate cycles. These equations are applied to a given candidate cycle if, and only if; there is at least one line per branch ij within the cycle that is either under construction or already exists. In practice, a candidate cycle is considered closed, and the cycle constraints are enforced, only if each branch within the cycle that contains only candidate lines has its investment variable set to 1. This requirement is detailed in equations (2.16a) through (2.16c).

For this purpose, auxiliary variables are utilized, specifically ($\theta_{nijc}^k, \forall nijc | ijc \in \mathcal{L}^c$ and $\alpha_{ij}^{t,k}, \forall ij | ij \in \mathcal{L}^c$) and the set $\mathcal{L}^p$ comprising those candidates lines that belong to the same branch and are in parallel. Note that constraint (2.15b), which is defined for existing cycles ($k \in \mathcal{K}^e$), is extended to candidate cycles through the constraint (2.16a) considering the

previously defined auxiliary variables θ_{nijc}^k. Within the latter constraint, the sum of the voltage angle differences along the branches is set to zero when the cycle (k in $\mathcal{K}^c$) is closed, i.e., when at least one line is built for each branch without an existing line within the cycle. This sum is zero if all complementary auxiliary investment variables $\alpha_{ij}^{t,k}$ defined for the branches within the cycle are zero. Otherwise, the sum of the voltage angle differences along the branches in the cycle is set to free.

$$| \sum_{ijc\in k|k\in\mathcal{K}^c} H_{ijc,k}\theta_{nijc}^k | \leq \sum_{ijc\in k,ijc\in\mathcal{L}^c|k\in\mathcal{K}^c} \alpha_{ij}^{t,k}\overline{\theta}_{nijc} \qquad \forall n, \text{ (2.16a)}$$

In the same way, (2.15c) is extended to (2.16b) and (2.16c) by considering the auxiliary variable θ_{nijc}^k equal to its respective voltage angle difference when a candidate line is built; otherwise, that auxiliary variable is equal to zero in order not to be considered in the sum of the left side in (2.16a).

$$-(1-\alpha_{ijc}^t)\overline{\theta}_{nijc} \leq \theta_{nijc}^k-(\theta_{ni}-\theta_{nj}) \leq (1-\alpha_{ijc}^t)\overline{\theta}_{nijc} \qquad \forall nijc, \text{ (2.16b)}$$

$$-\alpha_{ijc}^t\underline{\theta}_{nijc} \leq \theta_{nijc}^k \leq \alpha_{ijc}^t\overline{\theta}_{nijc} \qquad \forall nijc, \text{ (2.16c)}$$

Note that the value of the auxiliary variable $\alpha_{ij}^{t,k}$, related to the investment for branch $'ij'$, is determined by constraint (2.16d) for those branches $'ij'$ for which there is only one candidate line, while this is determined by constraints (2.16e)-(2.16f) for those branches $'ij'$ for which there are multiple candidate lines in parallel. This auxiliary variable for branch $'ij'$ takes a value of 0 if at least one candidate line is built for branch $'ij'$. Otherwise, it takes a value of 1

$$\alpha_{ij}^{t,k} = 1 - \alpha_{ijc}^t \qquad \forall nijc|ijc \in \mathcal{L}^c, ijc \notin \mathcal{L}^p, \text{ (2.16d)}$$

$$0 \leq \alpha_{ij}^{t,k} \leq 1 - \alpha_{ijc}^t \qquad \forall nijc|ijc \in \mathcal{L}^p, \text{ (2.16e)}$$

$$1 - \sum_{c\in\mathcal{C}} \alpha_{ijc}^t \leq \alpha_{ij}^{t,k} \qquad \forall ij|ij \in \mathcal{L}^p, \text{ (2.16f)}$$

Finally, as it was defined for cycles comprised of only existing lines, the envelopes in (2.16g)-(2.16h) are used to define the bounds for the auxiliary variable θ_{nijc}^k for candidate lines. Note that Θ_{nijc}^m is a parameter that makes the equations linear. And, it is computed as follows $\Theta_{nijc}^m = \max[|\underline{\theta}|, |\overline{\theta}|]$.

$$\theta_{nijc}^k \geq \frac{X_{ijc}f_{nijc}^P-R_{ijc}f_{nijc}^Q}{\overline{V}_{ni}\overline{V}_{nj}\cos\frac{\Theta_{nijc}^m}{2}} - \tan\frac{\Theta_{nijc}^m}{2} + \frac{\Theta_{nijc}^m}{2} \qquad \forall nijc|ijc \in \mathcal{L}^c, \text{ (2.16g)}$$

$$\theta_{nijc}^k \leq \frac{X_{ijc}f_{nijc}^P-R_{ijc}f_{nijc}^Q}{\underline{V}_{ni}\underline{V}_{nj}\cos\frac{\Theta_{nijc}^m}{2}} + \tan\frac{\Theta_{nijc}^m}{2} - \frac{\Theta_{nijc}^m}{2} \qquad \forall nijc|ijc \in \mathcal{L}^c, \text{ (2.16h)}$$

An illustrative 3-bus case example where either one single existing or one single candidate cycle is defined is shown in Figure 2.3. There, v^2 represents the squared voltage magnitude, θ represents the voltage angle, k_1 corresponds to the cycle defined, and c represents a specific line. This figure shows the 3-bus system in three different cases: a) when there are only existing lines within the system and there is just one existing cycle: 1-2-3-1; b) when there is only one candidate line connecting nodes 1 and 3, and the only cycle defined is candidate cycle is 1-2-3-1; and c) when there are just two candidate lines in parallel connecting nodes 1 and 3, and the only cycle defined is candidate cycle 1-2-3-1.
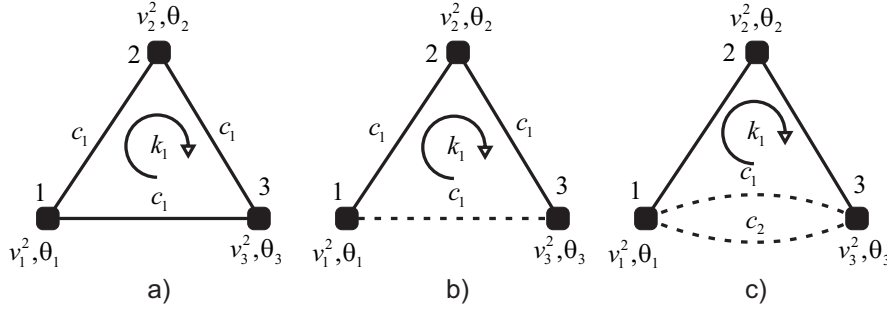
Fig. 2.3.: a) 3-bus system where there are only existing lines; b) 3-bus system where one branch within the cycle defined comprises one candidate line; and c) 3-bus system where one branch within the single cycle defined comprises two candidate lines in parallel. [Source: Author's own illustration]

For case a), as shown in Figure 1a, the equation (2.15b) simplifies to $\theta_{12a}^k + \theta_{23a}^k - \theta_{13a}^k = 0$ when considering a single time step (one hour). In addition, the set of equations (2.15c) contains three equations, namely: $\theta_{12a}^k = \theta_1 - \theta_2$, $\theta_{23a}^k = \theta_2 - \theta_3$, and $\theta_{13a}^k = \theta_1 - \theta_3$.

For case b), as shown in Figure 1b, given that there is a branch comprising just one candidate line, equation (2.16a) applies, and it reads $-\alpha_{13}^{t,k}\overline{\theta}_{13a} \leq \theta_{12a}^k + \theta_{23a}^k - \theta_{13a}^k \leq \alpha_{13}^{t,k}\overline{\theta}_{13a}$. Equation set (2.15c) is a two-equation set reading: $\theta_{12a}^k = \theta_1 - \theta_2$, and $\theta_{23a}^k = \theta_2 - \theta_3$. For the candidate line for branch $1-3$, equation (2.16b) applies, and it reads $-(1-\alpha_{13a}^t)\overline{\theta}_{13a} \leq \theta_{13a}^k - (\theta_1 - \theta_3) \leq (1-\alpha_{13a}^t)\overline{\theta}_{13a}$. Together with the former, equation (2.16c) also applies, reading $-\alpha_{13a}^t\underline{\theta}_{13a} \leq \theta_{13a}^k \leq \alpha_{13a}^t\overline{\theta}_{13a}$. Besides, equation (2.16d) applies, reading $\alpha_{13}^{t,k} = 1 - \alpha_{13a}^t$.

Finally, for case c), as shown in Figure 1c, given that there is a branch comprising two candidate lines in parallel, equation (2.16a) applies, reading $-\alpha_{13}^{t,k}(\overline{\theta}_{13a} + \overline{\theta}_{13b}) \leq \theta_{12a}^k + \theta_{23a}^k - \theta_{13a}^k - \theta_{13b}^k \leq \alpha_{13}^{t,k}(\overline{\theta}_{13a} + \overline{\theta}_{13b})$. Equation set (2.15c) also applies, and it is a two-equation set reading the same as that in case b). Besides, for candidate lines $'a'$ and $'b'$ in branch $1-3$, equation set (2.16b) applies, reading $-(1-\alpha_{13a}^t)\overline{\theta}_{13a} \leq \theta_{13a}^k - (\theta_1 - \theta_3) \leq (1-\alpha_{13a}^t)\overline{\theta}_{13a}$, and $-(1-\alpha_{13b}^t)\overline{\theta}_{13b} \leq \theta_{13b}^k - (\theta_1 - \theta_3) \leq (1-\alpha_{13b}^t)\overline{\theta}_{13b}$. Also, equation set (2.16c) applies, reading $-\alpha_{13a}^t\underline{\theta}_{13a} \leq \theta_{13a}^k \leq \alpha_{13a}^t\overline{\theta}_{13a}$ and $-\alpha_{13b}^t\underline{\theta}_{13b} \leq \theta_{13b}^k \leq \alpha_{13b}^t\overline{\theta}_{13b}$. Since there are two parallel lines defined for branch $1-3$, equation set (2.16e) reads to $0 \leq \alpha_{13}^{t,k} \leq 1 - \alpha_{13a}^t$ and $0 \leq \alpha_{13}^{t,k} \leq 1 - \alpha_{13b}^t$, while equation (2.16f) reads $1 - \alpha_{13a}^t - \alpha_{13b}^t \leq \alpha_{13}^{t,k}$.

2.3.5 Operation of Power Generation and Energy Storage Systems

Reserves supplied by power generation units, and energy storage systems in GW

It is assumed that variable renewable energy (VRE) units, such as solar photovoltaic (PV) and wind, cannot contribute to operating reserves. Consequently, only generation units (such as hydro-reservoirs and combined cycle gas turbines (CCGTs)) and energy storage systems (ESS) (such as battery energy storage systems (BESS)) can contribute to reserves. Note that $r^{p,u}$ and $r^{p,d}$ refer to the upward and downward reserve contributions of hydro or thermal units, as well as the contributions of storage units when they are discharging or injecting electricity into the grid. Meanwhile, $r^{c,u}$ and $r^{c,d}$ represent the contributions to upward and downward reserves specifically when storage units are charging or discharging electricity from the grid for storage purposes.

$$\sum_{g \in \mathcal{G}_i} r^{p,u}_{ng} + \sum_{e \in \mathcal{E}_i} r^{c,u}_{ne} = \Gamma^u_n \qquad\qquad : \forall n, \ (2.17\text{a})$$

$$\sum_{g \in \mathcal{G}_i} r^{p,d}_{ng} + \sum_{e \in \mathcal{E}_i} r^{c,d}_{ne} = \Gamma^d_n \qquad\qquad : \forall n, \ (2.17\text{b})$$

Logic rules for ESS that contribute reserves in GW

An important aspect to consider is that Energy Storage Systems (ESS) can support operating reserves through their charge and discharge capabilities. However, to do so, an ESS must either have the capacity to store energy or already have stored energy when the operating reserves are needed. During their discharging phase, ESSs can only contribute to upward reserves if they have stored energy at that time, as indicated in the equation (2.18a). Similarly, they can support downward reserves if there is available storage capacity, as described in the equation (2.18b). Conversely, in charge mode, ESS can support upward reserves by reducing the amount of charge if there is already stored energy, as described in equation (2.18c). Contributions to downward reserves can be achieved by increasing the charge rate or consumption, but sufficient storage capacity is required, as specified in equation (2.18d).

$$r^{p,u}_{ne} \leq \frac{y_{ne}}{D_n} \qquad\qquad : \forall ne, \ (2.18\text{a})$$

$$r^{p,d}_{ne} \leq \frac{\Psi_e - y_{ne}}{D_n} \qquad\qquad : \forall ne, \ (2.18\text{b})$$

$$r^{c,u}_{ne} \leq \frac{\Psi_e - y_{ne}}{D_n} \qquad\qquad : \forall ne, \ (2.18\text{c})$$

$$r^{c,d}_{ne} \leq \frac{y_{ne}}{D_n} \qquad\qquad : \forall ne, \ (2.18\text{d})$$

The following operational constraints relate to storage management and apply to various technologies, including hydro reservoirs, pumped-storage hydro (PSH), battery energy storage systems (BESS), and other types of energy storage technologies.

Energy inventory of an ESS in GWh

The constraint (2.19a) establishes a relationship between the current state of charge (SoC) of an ESS, its SoC in previous periods and the decisions made for charging and discharging. This constraint is formulated based on the proposal presented by Wang et al. in [22]. It is designed to model the different management strategies and charge/discharge cycles specific to different types of ESSs, which can range from hourly to daily or even weekly cycles. And the parameter τ represents the seasonality/storage cycle of the ESS unit. The constraint reflects the characteristic behaviour of each type of ESS. For example, battery systems typically operate on an hourly cycle due to their rapid charge and discharge capabilities. This means that the current SoC and the recent history of charge/discharge actions within the past hour influence decisions to charge or discharge. In contrast, pumped hydro systems have slower response times and larger storage capacities, and often operate on longer cycles such as daily or weekly. The constraints for such systems take into account the SoC evolution over these longer periods and the corresponding charge/discharge decisions made to optimize their operation within these extended time frames.

$$y_{n-\tau_e,e} - y_{ne} + s_{ne} + \sum_{n'=n+1-\tau_e}^{n} D_{n'} \left(ei_{n'e} - p_{n'e}^{tg} + \eta_e p_{n'e}^{tc} \right) = 0 \qquad : \forall ne, \ (2.19a)$$

Maximum and minimum charge of an ESS in p.u.

The maximum and minimum electricity consumption capacity required to charge the ESS storage is determined by (2.19b).

$$\frac{p_{ne}^{sc} - r_{ne}^{c,u}}{\overline{P}_e^c - \underline{P}_e^c} \geq 0; \quad \frac{p_{ne}^{sc} + r_{ne}^{c,d}}{\overline{P}_e^c - \underline{P}_e^c} \leq 1 \qquad : \forall ne, \ (2.19b)$$

Avoid simultaneous charge and discharge of an ESS in p.u

The equation (2.19c), developed based on [22], represents a continuous storage model that divides the storage capacity into charge and discharge portions. The sum of these portions is constrained to be within the range defined by the minimum power required for discharge and the maximum charge capacity. In addition, the variables controlling charging and discharging are influenced by their contribution to the operating reserves.

$$\frac{p_{ne}^{sg} + r_{ne}^{c,u}}{\overline{P}_e - \underline{P}_e} + \frac{p_{ne}^{sc} + r_{ne}^{c,d}}{\overline{P}_e^c} \leq 1 \qquad : \forall ne, \ (2.19c)$$

Total charge of an ESS in p.u.

The total charge or power consumption of an ESS unit is defined by the equation (2.19d). The power consumption is divided into fixed and variable components: 1) a fixed part that ensures the minimum consumption, denoted by $\underline{P}_e^c$, and 2) a variable part that adjusts the consumption within the range $[\underline{P}_e^c, \overline{P}_e^c]$. This approach is inspired by the formulation

presented in [23], which is part of a comprehensive formulation of the Unit Commitment (UC) problem.

$$\frac{p_{ne}^{tc}}{\underline{P}_e^c} = \frac{p_{ne}^{sc} + r_{ne}^{c,d} - r_{ne}^{c,u}}{\underline{P}_e^c} \qquad\qquad : \forall ne, \quad (2.19\text{d})$$

The production block approach is used in the UC formulation. Under this approach, a unit's production is divided into fixed and variable blocks: the fixed block covers the unit's minimum output level and includes the startup/shutdown processes, while the variable block represents the remaining output capacity, whether dispatched to the system or not, and its interaction with various output products such as reserves and ramps. These constraints are derived from [24], which presents a comprehensive UC problem formulation that incorporates considerations of reserves, ramps, startup and shutdown constraints.

Variable block of electricity production from generation units in p.u.

The maximum and minimum electricity production associated with a unit's variable block (excluding VRE units) are defined by the equations (2.20a) and (2.20b).

$$\frac{p_{ng}^{sg} - r_{ng}^{p,d}}{\overline{P}_g - \underline{P}_g} \geq 0 \qquad\qquad : \forall ng, \quad (2.20\text{a})$$

$$\frac{p_{ng}^{sg} + r_{ng}^{p,u}}{\overline{P}_g - \underline{P}_g} \leq uc_{ng} \qquad\qquad : \forall ng, \quad (2.20\text{b})$$

Total production of a committed unit

This constraint applies to all generating units except VRE units.

$$\frac{p_{ng}^{tg}}{\underline{P}_g} = uc_{ng} + \frac{p_{ng}^{sg} + \Gamma^{ua} r_{ng}^{p,u} - \Gamma^{da} r_{ng}^{p,d}}{\underline{P}_g} \qquad\qquad : \forall ng, \quad (2.20\text{c})$$

Logic rules for commitment of a generation unit in p.u.

The initial commitment and unit output are determined based on the merit order given by the fixed and variable costs of each unit, including the RES and ESS units.

$$uc_{ng} - uc_{n-1,g} = su_{ng} - sd_{ng} \qquad\qquad : \forall ng, \quad (2.20\text{d})$$

Ramps affecting the variable block of production in p.u.

The maximum ramp-up and ramp-down constraints that affect the variable block of electricity produced by generation units-excluding variable renewable energy (VRE) units-are detailed in equations (2.20e) and (2.20f). [25].

$$\frac{-p_{n-1,g}^{sg} - r_{n-1,g}^{p,d} + p_{ng}^{sg} + r_{ng}^{p,u}}{D_n R_{ng}^u} \leq uc_{ng} - su_{ng} \qquad\qquad : \forall ng, \quad (2.20\text{e})$$

$$\frac{-p_{n-1,g}^{sg} + r_{n-1,g}^{p,u} + p_{ng}^{sg} - r_{ng}^{p,d}}{D_n R_{ng}^d} \geq -uc_{n-1,g} + sd_{ng} \qquad\qquad : \forall ng, \quad (2.20\text{f})$$

Time coupling of the unit commitment in hours

The minimum up and down time of a committed unit, as stated in [26].

$$\sum_{n'=n+1-T_g^u}^{n} su_{n'g} \le uc_{ng} \qquad\qquad : \forall ng, \ (2.20\text{g})$$

$$\sum_{n'=n+1-T_g^d}^{n} sd_{n'g} \le 1-uc_{ng} \qquad\qquad : \forall ng, \ (2.20\text{h})$$

Bounds for variables related to generation units

The limits related to the operating reserve variables are defined by equations (2.21), which include the variables representing the contribution of a unit to the operating reserves when it is producing or injecting electricity into the network, and the variables representing the contribution to the operating reserves when it is consuming electricity from the network. The limits of the variables related to storage management are defined in (2.22). The limits for active power production are defined in (2.23), and those for reactive power compensation (production or consumption) are detailed in (2.24). Note that reactive power compensation limits of a synchronous compensator are defined in (2.24d).

$$0 \le r_{ng}^{p,u} \le \overline{P}_g - \underline{P}_g \qquad\qquad : \forall ng, \ (2.21\text{a})$$

$$0 \le r_{ng}^{p,d} \le \overline{P}_g - \underline{P}_g \qquad\qquad : \forall ng, \ (2.21\text{b})$$

$$0 \le r_{ne}^{c,u} \le \overline{P}_e^c - \underline{P}_e^c \qquad\qquad : \forall ne, \ (2.21\text{c})$$

$$0 \le r_{ne}^{c,d} \le \overline{P}_e^c - \underline{P}_e^c \qquad\qquad : \forall ne, \ (2.21\text{d})$$

$$0 \le p_{ne}^{tc} \le \overline{P}_e^c \qquad\qquad : \forall ne, \ (2.22\text{a})$$

$$0 \le p_{ne}^{sc} \le \overline{P}_e^c \qquad\qquad : \forall ne, \ (2.22\text{b})$$

$$0 \le y_{ne} \le \Psi_e \qquad\qquad : \forall ne, \ (2.22\text{c})$$

$$0 \le s_{ne} \qquad\qquad : \forall ne, \ (2.22\text{d})$$

$$0 \le p_{ng}^{tg} \le \overline{P}_g \qquad\qquad : \forall ng, \ (2.23\text{a})$$

$$0 \le p_{ng}^{sg} \le \overline{P}_g - \underline{P}_g \qquad\qquad : \forall ng, \ (2.23\text{b})$$

$$\underline{Q}_g \le q_{ng}^{tg} \le \overline{Q}_g \qquad\qquad : \forall ng, \ (2.24\text{a})$$

$$\left| q_{ng}^{tg} \right| \le p_{ng}^{tg} \tan(\cos^{-1}(pf)) \qquad\qquad : \forall ng, \ (2.24\text{b})$$

$$\left| q_{ng}^{tg} \right| = \begin{cases} q_{ng}^{tg} & \text{if} \quad pf = pf^{\text{cap}} \\ -q_{ng}^{tg} & \text{if} \quad pf = pf^{\text{ind}} \end{cases} \qquad\qquad : \forall ng, \ (2.24\text{c})$$

$$\underline{Q}_s \le q_{ns}^{tg} \le \overline{Q}_s \qquad\qquad : \forall ns, \ (2.24\text{d})$$

Bounds for network variables

The limits of the variable associated with unserved energy are defined in (2.25). Similarly, the limits of the voltage magnitude variable are specified in (2.26), and those for the reference node voltage angle are outlined in (2.27).

$$0 \le l_{ni}^{ens} \le 1 \qquad\qquad\qquad\qquad : \forall ni, \quad (2.25)$$

$$\underline{V}_i^2 \le v_{ni}^2 \le \overline{V}_i^2 \qquad\qquad\qquad\qquad : \forall ni, \quad (2.26)$$

$$\theta_{ni} = 0 \qquad\qquad\qquad : \forall ni | i = \text{reference node}, \quad (2.27)$$

2.3.6 Bound-Tightening Procedure

Based on the results of relevant case studies, it is concluded that implementing the proposed convex relaxations of the AC-OPF formulation, along with tightened bounds for the variables v_{ni}^2 and θ_{nijc}^k, leads to a significant reduction in problem-solving time without compromising the quality of expansion planning solutions. As outlined in [27], a minimal network and bound-consistency algorithm is proposed to determine tight bounds for these variables, thus accelerating the problem-solving process.

This tightening process employs propagation techniques that systematically exploit the structure of the problem constraints to update variable bounds based on the information provided by each constraint. Similar to the approach in [27], the algorithm is used in a preliminary procedure before solving the proposed expansion planning problem as follows:

1. The binary variables defined in the expansion planning problem are relaxed so that they can take any value in [0,1], and the minimal network and bound-consistency algorithm [27] per hour (i.e., time step, here made to coincide with each operation hour) $'n'$ is run.

2. The voltage magnitude bounds $(\overline{V}_{ni}, \underline{V}_{ni})$ and voltage angle bounds $(\overline{\theta}_{ni}, \underline{\theta}_{ni})$ are updated. Additionally, constraint (2.28) is tightened by defining the convex envelopes of the square voltages as in [28].

$$v_{ni}^2 \in \langle x \rangle \begin{cases} x \ge V_{ni}^{sqr} \\ x \le (\overline{V}_{ni} + \underline{V}_{ni})\sqrt{V_{ni}^{sqr}} - \overline{V}_{ni}\underline{V}_{ni} \end{cases} \qquad : \forall ni, \quad (2.28)$$

where V_{ni}^{sqr} is a parameter who takes the value of v_{ni}^2 previously computed in Step 1. Moreover, the feasible region for the voltage angle can be tightened according to (2.29), where Θ^Δ is the voltage angle difference, defined as a parameter whose value is made to coincide with the difference of the variables θ_{ni} and θ_{nj} previously computed in Step 1.

$$-\pi/3 \le -\Theta_{nijc}^\Delta \le \theta_i - \theta_j \le \Theta_{nijc}^\Delta \le \pi/3 \qquad : \forall nijc, \quad (2.29)$$

3. Solving the proposed expansion planning problem, including the updated bounds for the voltage angles and magnitudes as well as (2.28) and (2.29).

2.4 Overview of Formulation and Case Study Setup

This section provides an overview of the proposed mathematical formulation and describes the case studies, scenarios, test system, and assumptions used in the simulations that validated the performance of the proposed model. All formulated optimisation problems were solved using Gurobi 10.0.1, a commercial mixed integer programming (MIP) solver, on a computer equipped with a 3.40 GHz Intel Core i7-10875H processor and 32 GB of RAM. Simulations were performed in Julia 1.8.5 using JuMP 1.7.0 for optimisation model development.

2.4.1 Overview of the Proposed Mathematical Formulation

This section illustrates the potential of the mathematical formulation introduced in section 2.3 by providing an overview of the equations. Table 2.1 summarizes these equations, links each to its subsection, and describes its content.

Tab. 2.1.: Overview of the formulation.

Subsection	Content	Number	Equations
Objective function	Main function	2.3.1	(2.2)
	Investment cost related to transmission lines		(2.3a)
	Investment cost related to reactive power compensation		(2.3b)
	Operating cost related to power generation		(2.4a)
	Operating cost related to power consumption		(2.4b)
	Operating cost related to CO2 emission		(2.4c)
	Operating cost related to energy not served		(2.4d)
Expansion planning	Bound set by investment decisions in lines	2.3.2	(2.5)
	Bound set by investment decisions in reactive power compensation		(2.6)
AC OPF: Branch flow model	Active and reactive power flow balance	2.3.3	(2.7)
	Voltage magnitude drop		(2.8)
	Voltage angle difference		(2.9)
	Current flow		(2.11)
	Bounds for the current flow on existing branches		(2.12)
	Reactive power injection by branch devices (transmission lines)		(2.13)
	Reactive power injection by bus devices (capacitor banks)		(2.14)
Cycle Constraints	Cycle constraints within the Branch flow-based model	2.3.4	(2.15)-(2.16)
Operating Reserves	Reserves supplying by power generation and ESS units	2.3.5	(2.17)
	Logical rules for ESSs' contributions		(2.18)
Energy Storage Management	Energy inventory	2.3.5	(2.19a)
	Maximum and minimum charge		(2.19b)
	Avoid simultaneous charge and discharge		(2.19c)
	Total charge		(2.19d)
Unit Commitment	Bounds of the variable block of electricity production	2.3.5	(2.20a)-(2.20b)
	Total production of a committed unit		(2.20c)
	Logic rules for commitment of a generation unit		(2.20d)
	Ramps that affects the variable block		(2.20e)-(2.20f)
	Time coupling of the unit commitment		(2.20g)-(2.20h)
Bounds	Variables related to generation units	2.3.5	(2.21a)-(2.24d)
	Bounds for network variables		(2.25)-(2.27)
Bound-tightening	Bounds for the voltage magnitude	2.3.6	(2.28)-(2.29)
	Bounds for the voltage angle difference		(2.29)

Note that the comprehensive MILP TEP formulation that considers cycle-based AC-OPF, operating reserves, unit commitment, energy storage management, and tight bounds presented is highly flexible, allowing for the inclusion or exclusion of specific constraints and features based on requirements. For example, unit commitment and operating reserves can be included as needed. Similarly, if the test system does not include ESS, the corresponding management equations for ESS are omitted. This flexible approach extends to the type of OPF considered, whether AC-OPF or DC-OPF.

Tab. 2.2.: Features of the proposed model (M-A) and alternatives.

Model	Description	Equations
M-A	GEP+TEP+SEP+RPP+Cycle-based AC-OPF+UC	(2.34), (2.3a)–(2.4d), (2.30), (2.31), (2.32), (2.33), (2.5), (2.6) (2.17), (2.19), (2.20), (2.21), (2.22), (2.23), (2.24), (2.25), (2.26), (2.27) (2.7), (2.8), (2.11), (2.15), (2.16)
M-B	GEP+TEP+SEP+RPP+AC-OPF+UC	(2.34), (2.3a)–(2.4d), (2.30), (2.31), (2.32), (2.33), (2.5), (2.6) (2.17), (2.19), (2.20), (2.21), (2.22), (2.23), (2.24), (2.25), (2.26), (2.27) (2.7), (2.8), (2.9), (2.11)
M-C	GEP+TEP+SEP+RPP+AC-OPF	(2.34), (2.3a)–(2.4d), (2.30), (2.31), (2.32), (2.33), (2.5), (2.6) (2.17), (2.19), (2.22), (2.23a), (2.24), (2.25), (2.26), (2.27) (2.7), (2.8), (2.9), (2.11)
M-D	GEP+TEP+SEP+DC-OPF+UC	(2.35), (2.3a), (2.4a)–(2.4c), (2.36), (2.30), (2.31), (2.32), (2.33), (2.5) (2.17), (2.19), (2.20), (2.21), (2.22), (2.23), (2.25), (2.27) (2.1e)–(2.1h)

2.4.2 Case Studies

To validate the formulation presented, four different cases were defined, each representing a distinct configuration of the comprehensive expansion and operation problem, resulting in four unique formulations. These cases are illustrated in Table 2.2 and encompass a variety of scenarios, each characterized by specific fuel and carbon prices. The expansion includes investments in transmission infrastructure—such as lines, synchronous compensators, and capacitor banks—as well as in power generation and energy storage systems, incorporating multiple technologies within each category.

In addition, all cases use a static planning and deterministic approach, with the full year 2030 as the time horizon. This methodology was chosen to assess the impact of incorporating cycle-based AC-OPF and investments in reactive power compensation on investment decisions, system operation, and CPU time. System operation was analyzed over 8,736 hours of the target year, a number strategically chosen to be a multiple of the number of weekly hours significant to the storage capacities of the pumped storage units. Initial voltage magnitude limits were set at $\underline{V} = 0.95$ p.u. and $\overline{V} = 1.05$ p.u..

To ensure that the different configurations based on the formulation presented can accommodate investments in power generation and energy storage systems, the following constraints must be added to them:

$$C^{ge} = \sum_{g \in \mathcal{G}_i^c} C_g^{gen} \alpha_g^g \tag{2.30}$$

$$C^{se} = \sum_{e \in \mathcal{E}_i^c} C_e^{sto} \alpha_e^e \tag{2.31}$$

$$uc_{ng} \leq \alpha_g^g \qquad\qquad : \forall ng | g \in \mathcal{G}_i^c, \tag{2.32a}$$

$$\frac{p_{ng}^{tg}}{\overline{P}_g} \leq \alpha_g^g \qquad\qquad : \forall ng | g \in \mathcal{G}_i^c, \tag{2.32b}$$

$$\frac{p_{ne}^{tg}}{\overline{P}_e} \leq \alpha_e^e \qquad\qquad : \forall ne | e \in \mathcal{E}_i^c, \tag{2.33a}$$

$$\frac{p_{ne}^{tc}}{\overline{P}_e^c} \leq \alpha_e^e \qquad\qquad : \forall ne | e \in \mathcal{E}_i^c, \tag{2.33b}$$

Furthermore, the original objective function as described in the equation (2.2) is replaced by the equation (2.34). This new objective function includes additional terms, C^{ge} and C^{se}, to capture the costs of generation expansion and storage expansion, respectively.

$$\min C = C^{ge} + C^{te} + C^{se} + C^{re} + \sum_{n \in \mathcal{T}} C_n^{gen} + C_n^{con} + C_n^{CO2} + C_n^{ens} \qquad (2.34)$$

The four expansion planning formulations presented are M-A, M-B, M-C, and M-D. M-A represents the most comprehensive formulation, while the others serve as alternatives. These alternative models are extensively implemented and widely used in addressing the expansion planning problem for medium and large systems, and provide a detailed representation of system operations. The main features of these models are summarized in Table 2.2, which also includes the associated equations. The M-C and M-D formulations are inspired by classical approaches often referenced in the literature and are widely used to address challenges in power system expansion planning. Depending on the specific requirements, these formulations (M-*) can use either a DC or AC Optimal Power Flow (OPF) model, incorporate UC constraints, and consider cycle constraints.

In M-D, the DC-OPF, UC and operating reserve constraints are considered, which modifies the objective function and replaces it by (2.35). The equation (2.4d) is also modified and replaced by (2.36). Then, the resultant formulation is set up with the following equations: (2.35) s.t. (2.30), (2.3a), (2.31), (2.4a), (2.4b), (2.4c), (2.36), (2.32), (2.5), (2.33), (2.17), (2.19), (2.20), (2.21a)–(2.23), (2.25), (2.27), and the DC-OPF's equations (2.1e)–(2.1h) are taken from the basic TEP formulation presented in section 2.2.2.

$$\min C^{ge} + C^{se} + \sum_{n \in \mathcal{T}} C_n^{gen} + C_n^{con} + C_n^{CO2} + C_n^{ens} \qquad (2.35)$$

$$C_n^{ens} = \sum_{i \in \mathcal{B}^t} D_n C^{ens,P} l_{ni}^{ens} P_{ni}^d \qquad : \forall n, \quad (2.36)$$

Definition of the performance metrics

The proposed model formulation (M-A) is compared to others previously discussed in the literature (M-B, M-C, and M-D) using two main performance metrics: i) the efficiency or quality of the planning solutions generated by each formulation, and ii) the computational resources, specifically CPU time, required to solve the expansion planning problem. For a given test system, the efficiency of an expansion plan is primarily evaluated based on the total expansion and operating costs. However, given the limited resources available for system expansion, the efficiency of a plan can also be evaluated on a per-unit basis. This involves calculating the reduction in total system cost per unit of investment cost achieved by implementing this plan compared to a plan derived from the reference formulation (M-A). Additionally, in regions or systems where minimizing RES energy spillage is a goal of expansion planning or system operation, the efficiency of a plan can also be measured in terms of the RES energy spillage it causes. If implemented, this would serve as a complementary measure of plan efficiency, in addition to the primary measures related to the system costs incurred under the plan.
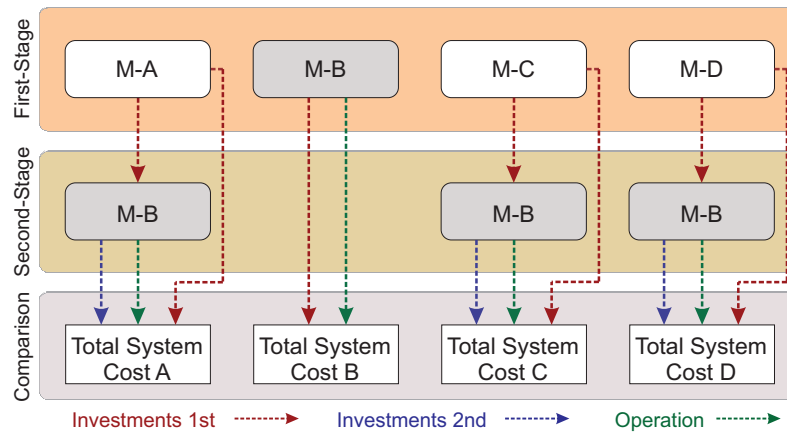
Fig. 2.4.: The proposed 2-stage comparative analysis approach. [Source: Author's own illustration]

Planning methodology adopted: a 2-stage approach for the computation of the system costs resulting from an expansion solution

This section outlines the methodology used to calculate the total system cost resulting from the implementation of each expansion planning solution calculated using the M-X formulation. Because the system representation varies among the formulations, this method ensures a fair comparison of their system operating costs by providing a standardized basis for cost calculation. Different expansion planning formulations use different approaches to calculating operating costs, which can lead to significantly different estimates of the costs associated with a given system expansion solution. To facilitate a fair comparison, a two-step approach to calculating the total cost of implementing an expansion planning solution has been developed. This approach is illustrated in Figure 2.4. In the first phase, the system expansion solution is calculated for each formulation, called M-X, across different scenarios. Then, in the second phase, the total system cost is determined using the comprehensive reference formulation, M-B, which accurately represents system operation. These costs include both the investment and operational costs of implementing the improvement solutions derived in the first phase for each scenario.

In addition, the second phase considers the implementation of additional investments over a 2-3 year period beyond those identified in the first phase. These additional investments are strategically planned to mitigate any operational infeasibilities that may result from the implementation of the expansion plans developed in the first phase with some of the compared formulations. Such infeasibilities could manifest themselves as significant instances of non-served energy during certain operating hours. In addition, these investments are aimed at improving the economic efficiency of the development of the system.

In the expansion planning process, the types of investments considered in Stage 2 are strategically limited to specific technologies to ensure realistic planning. The initial planning in Stage 1 accounts for each formulation over the long term, providing ample opportunity to deploy investments in any technology well before the target year designated for evaluating the impact of these investments on system operation.

Tab. 2.3.: Fuel and carbon price levels considered in each of the scenarios considered

		Carbon		
	Times	**0.5x**	**1x**	**2x**
Fuel	**0.5x**	A1B1	A0B1	X
	1x	A1B0	A0B0	A2B0
	2x	X	A0B2	A2B2

However, adhering to standard practices in expansion planning analyses, the detailed assessment of the expansion plans' effects on system operation, designated as Stage 2, is scheduled to occur only 3-4 years prior to when the planned investments are expected to become operational. This timing aligns with 3-4 years before the year in which the impact of these investments on system operation is analyzed. By the commencement of Stage 2 analyses, only certain technologies are feasible for identification and deployment within the limited timeframe before the start of the period used to assess each plan's impact on system operation.

The generation investment options considered in Stage 2, referenced in Figure 2.4, include technologies such as gas, BESS, wind, and solar PV. Additionally, grid investments like transmission lines, capacitor banks, and synchronous compensators are also feasible for inclusion in this stage. These technologies typically require an average construction or installation period of approximately 3-4 years, as indicated in [29], with an allowance of about 1-2 years for potential delays, making them suitable choices for medium-term reinforcements.

The expansion planning problem is addressed in two distinct stages, with the types of investments in the second stage being considerably restricted. This approach is applied to all formulations except for formulation M-B. For M-B, the expansion plan, operating costs, and total system costs computed in the first stage are considered definitive and are directly compared with the outcomes computed in the second stage for the other formulations. This exception allows for a direct evaluation of M-B's initial results against the more refined analyses conducted for the remaining formulations in the subsequent stage.

2.4.3 Scenario Characterization

Within the case studies, several scenarios were created to represent different potential future trajectories for fuel (especially gas) and carbon prices, as these parameters have a significant impact on achieving a low-carbon future. The level of both gas and carbon prices has a direct impact on the deployment of RES and storage technologies, making them more or less attractive depending on the scenario. This variation in attractiveness is critical for strategic planning as it informs the viability and selection of technologies in different economic environments. The level of fuel and carbon prices in the scenarios has been determined by applying scaling factors to the base values of these parameters. Specifically, the prices are adjusted by factors of 2x, 1x, and 0.5x, as detailed in Table 2.3. This approach allows for the analysis of how variations in fuel and carbon prices influence strategic decisions under different economic conditions.

The base values for the 2030 prices of coal, natural gas, and oil have been sourced from the *European Resources Adequacy Assessment* [30], listed as 6.62, 9.32, and 12.30 USD/MMBtu, respectively. Similarly, the base value for the carbon price, also derived from [30], is 110 USD/tCO2. Despite the high uncertainty surrounding future fuel prices, energy policies are expected to continue promoting Low Carbon Emission (LCE) technologies, influencing future price levels as indicated in the latest projections [31].

The scaling factors applied to these base values to determine the prices in each scenario are documented in Table 2.3. These factors account for two key considerations: 1) the historical propensity for crude oil and natural gas prices to experience sudden deviations within a generally rising trend, and 2) the expectation that future incremental increases in the carbon price will be less volatile compared to recent history.

2.4.4 Test System

The RTS-GMLC test system, referenced in [32], is employed in the case studies to assess the proposed formulation's performance. This system is an updated version of the traditional IEEE Reliability Test System (RTS) and is designed to simulate modern power systems that incorporate significant amounts of RES-based generation while still maintaining the substantial capacities of fossil fuel power plants.

The primary variable input parameters—namely, the output from RES generation and the demand—are sourced from [32]. Geographically, the system represents a region in the southwestern United States. The network model for this area includes 73 nodes, representing substations distributed across three main areas, each divided into two sub-areas. The system operates at voltage levels of 230 kV and 138 kV and features an existing network infrastructure of 104 transmission lines (36 at 138 kV and 68 at 230 kV) and 16 power transformers.

The case studies focus on the RTS-GMLC system, which models system operations at an hourly resolution across 73 nodes. The proposed formulation showcases significant versatility by incorporating representative periods that may span hours, days, or weeks, also at hourly resolution. This adaptability allows the modelling approach to be applied to much larger test systems, enhancing its practical utility and relevance for comprehensive system analyses and planning.

Candidate network investments include duplicating all existing lines. The transmission lines retain the admittance, impedance, and apparent power limits from the original RTS test case. Despite considering a set of candidate lines, the number of cycles in the power grid remains unchanged. Additional parameters in the case studies include the susceptance of the capacitor banks, set at 0.2 p.u., with each unit costing MUSD 0.05 ($(C_r^{sh}, \forall r \in \mathcal{R}_i^c)$). The costs of the transmission lines vary based on their characteristics. Six synchronous compensators, each offering 200/-150 Mvar and costing 0.25 MUSD/Mvar, are proposed at specific nodes (107, 122, 207, 222, 307, and 322) identified as needing voltage regulation

Tab. 2.4.: Installed capacities of generation, storage, and reactive power compensation technologies within the test system.

	Technology	Existing				Candidate			
		$\overline{P}$	$\underline{P}$	$\overline{Q}$	$\underline{Q}$	$\overline{P}$	$\underline{P}$	$\overline{Q}$	$\underline{Q}$
Thermal	Coal	2317	924	1070	-575	-	-	-	-
	Gas-CC	3550	1700	1500	-250	8400	3780	3600	-1800
	Gas-CC-90CCS	-	-	-	-	12000	5400	4800	-2400
	Gas-CT	1485	594	554	-390	6000	2700	2400	-1200
	Nuclear	400	396	200	-50	-	-	-	-
	Oil	324	131	162	-	-	-	-	-
RES	Solar-PV	2716	-	-	-	4050	-	-	-
	Onshore-Wind	2508	-	-	-	3800	-	-	-
	Hydro	1000	-	320	-200	-	-	-	-
	PSH	-	-	-	-	5900	-	1888	-1180
	Solar-CSP	200	30	-	-	4600	450	-	-
	BESS	50	-	-	-	4380	-	-	-
Reactive Power	Synch. condenser	-	-	600	-150	-	-	1200	-300
	Capacitor bank	-	-	-	-	-	-	3650	-
	Filter	-	-	-	-300	-	-	-	-

via load flow analysis. Additionally, each node is considered for a candidate capacitor bank of 50 Mvar. The system's total projected peak active and reactive loads are 12,287.8 MW and 9,377.5 Mvar, respectively, with an annual electricity demand of 56.2 TWh, which is 1.5 times the original demand. Approximately 46% of this demand is located at nodes operating at 138 kV. The cost of non-served energy is set at $10,000 USD/MWh.

The power generation mix includes 372 units, 158 of which are pre-installed, and the remainder are candidates. The installed generation capacities are detailed in Table 2.4 and span six thermal technologies and two RES-based ones (Solar-PV and Onshore-Wind). Storage plays a significant role in the system, with candidate investments considered only for technologies like Gas-CC, Gas-CC-90CCS (90% CCS), Gas-CT, Solar-CSP with Thermal Energy Storage, Solar-PV, Onshore-Wind, PSH, and BESS. The term *Hydro* refers to conventional hydro-power with reservoirs.

Within thermal generation, gas exhibits the most flexibility in terms of its minimum up-time and down-time, while nuclear operations are comparatively less flexible. Nuclear energy is primarily utilized to meet the base demand. Coal and oil offer additional flexibility to adjust the overall power production in response to changes in the net demand.

All parameters representing the characteristics of the existing generation, storage and reactive power units have been obtained from the RTS-GMLC system. The characteristics of the candidate units reflect those of the existing units. The technical characteristics of all technologies except Gas-CC-90CCS and PSH have been taken from the technical guide in [29]. Their investment costs are also taken from [29], while the fuel costs are taken from [30]. All costs are expressed in 2020 USD using the U.S. Bureau of Labor Statistics Consumer Price Index for 2021 [29]. The inflows of the hydro units are taken from [32], and those of the PSH are equal to those of the hydro units. The candidate PSH units mirror the existing hydro units in number, parameters, and location, except that PSH units can pump water. The output profiles of solar and wind generation, which vary with geographic location, were generated using the System Advisor model provided by the National Renewable Energy Laboratory (NREL) [33]. The storage capacity and round-trip efficiency of all BESS are
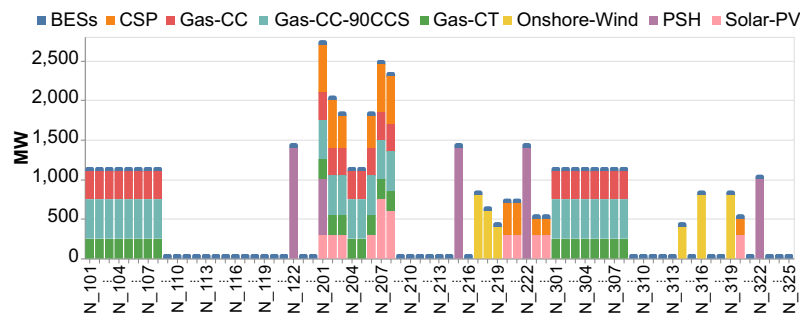
Fig. 2.5.: Installed capacity of candidate generation & storage per technology and node. [Source: Author's own illustration]

assumed to be 4 hours and 0.85, respectively. For solar CSP and PSH and general storage hydro, the storage capacity is 24 hours with a round-trip efficiency of 0.8. PSH units have a storage capacity of 1 week and a round-trip efficiency of 0.75.

The deployment of candidate generation and storage units is calculated separately for each node, as shown in Figure 2.5. Many candidate solar PV units are located in Area 2, while fewer units are located in Area 1, where natural gas-based technologies predominate due to limited primary renewable resources. Most of these candidate units are in the same locations as existing units. The complete data set for this system is available in the repository[1] of the openTEPES model [5].

2.5 Simulation Results

As mentioned above, this section presents the performance of the proposed formulation. Table 2.5 shows the total system cost (including expansion and operating costs) in millions of US dollars (MUSD) for each formulation and scenario discussed in section 2.4.2. It's important to note that there is no unserved energy in any scenario for any formulation. Furthermore, the cost difference between formulations M-A and M-B is negligible, with a maximum variance of only 0.0017% observed in one scenario. In contrast, the percentage difference between formulations M-C and M-D compared to M-B is in the range of [7.10%, 9.57%] and [6.29%, 8.39%], respectively. This highlights that ignoring the constraints of the UC or AC-OPF models in an expansion planning problem can result in significant cost increases.

Both carbon and fuel prices influence the selection and deployment of technologies. The impact of each factor on the total cost depends on several key considerations: the range of analyzed price fluctuations analyzed, the emission intensity of the power output of the studied technologies, and the eventual selection of technologies for deployment, as shown in Figure 2.6. This figure shows the capacity of installed generation and storage in gigawatts (GW), the extent of transmission lines in 1000 MW-km, which quantifies construction per unit length and power capacity, and reactive power compensation in gigavolt-amperes reactive

---

[1] openTEPES' GitHub repository

Tab. 2.5.: Total system costs (MUSD) per formulation M-X and scenario. Yearly amortized cost is given in parenthesis next to each total system cost.

	Cycle-based AC+UC	AC+UC	AC	DC+UC
	M-A	M-B	M-C	M-D
A0B0	2119.4 (1081.2)	2119.4 (1081.2)	2315.5 (1277.4)	2291.4 (1253.7)
A0B1	1800.2 (937.0)	1800.2 (936.6)	1972.1 (1124.5)	1951.2 (1090.5)
A0B2	2705.5 (1126.2)	2705.5 (1126.2)	2910.6 (1333.2)	2887.1 (1302.3)
A1B0	1908.6 (998.7)	1908.5 (998.6)	2091.1 (1179.5)	2068.1 (1155.7)
A1B1	1535.7 (682.6)	1535.7 (681.7)	1663.4 (835.2)	1648.2 (826.7)
A2B0	2455.5 (1262.3)	2455.4 (1262.2)	2686.4 (1500.7)	2655.2 (1456.9)
A2B2	3063.8 (1193.4)	3063.8 (1193.2)	3281.5 (1412.4)	3256.5 (1377.9)
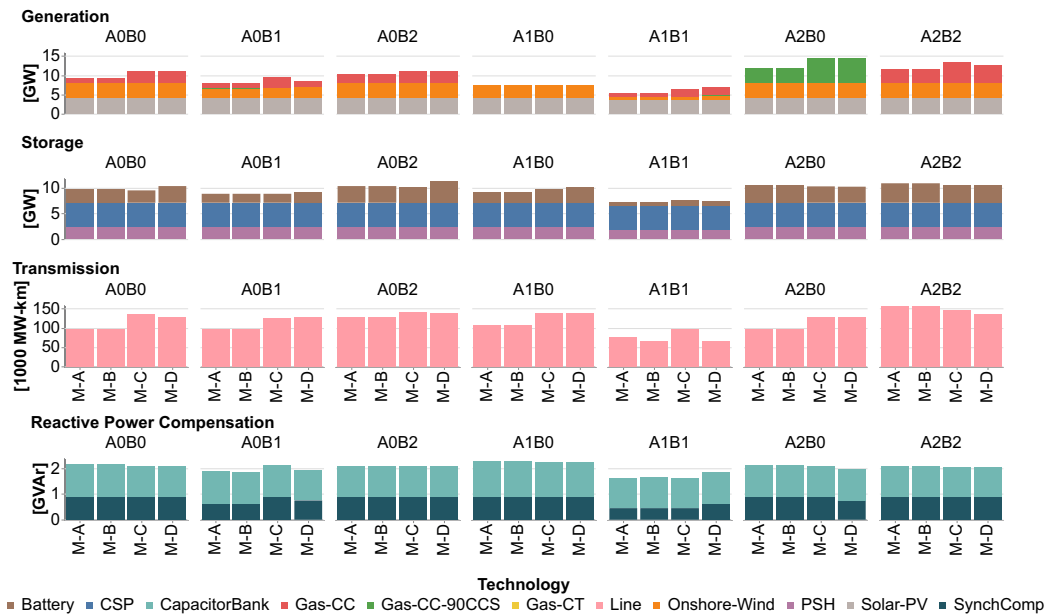
Fig. 2.6.: Installed capacity in power generation, energy storage, transmission network and reactive power compensation assets per scenario and formulation. [Source: Author's own illustration]
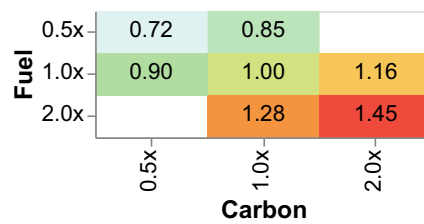
Fig. 2.7.: Ratio of total system costs in each scenario to those in the base scenario A0B0 for formulation M-A. [Source: Author's own illustration]

(GVAr). Both carbon pricing and fuel costs have a significant impact on the decision process regarding technology deployment and utilization. In particular, new thermal units show significant variability across scenarios, as do the quantity of storage (batteries) installed. Figure 2.7 illustrates that, for the proposed M-A formulation, reasonable variations in fuel prices can lead to changes in total system cost in the range of [15%, 29%].

Tab. 2.6.: Annual curtailment of the Solar-PV and Onshore-Wind output in TWh. Relative curtailment is given in parenthesis next to each annual curtailment.

	Solar-PV			Onshore-Wind		
	Cycle-based AC+UC	AC	DC+UC	Cycle-based AC+UC	AC	DC+UC
	M-A	M-C	M-D	M-A	M-C	M-D
A0B0	0.57 (4.11%)	3.48 (18.08%)	2.24 (13.00%)	0.66 (5.00%)	4.39 (23.21%)	2.31 (16.15%)
A0B1	0.83 (8.20%)	3.91 (27.90%)	2.46 (17.32%)	1.18 (9.82%)	5.22 (28.60%)	3.26 (20.78%)
A0B2	0.41 (2.91%)	2.18 (9.94%)	1.96 (8.96%)	0.47 (3.57%)	1.54 (8.47%)	1.07 (8.47%)
A1B0	0.69 (5.40%)	3.82 (22.88%)	2.34 (16.10%)	0.85 (6.69%)	4.94 (26.44%)	2.67 (17.26%)
A1B1	1.19 (10.27%)	4.17 (30.30%)	2.85 (20.57%)	1.75 (11.30%)	5.38 (29.50%)	4.72 (27.54%)
A2B0	0.46 (3.30%)	2.79 (12.47%)	1.72 (9.19%)	0.42 (3.13%)	2.82 (15.54%)	1.60 (11.00%)
A2B2	0.28 (1.73%)	1.68 (6.57%)	1.35 (5.30%)	0.30 (2.27%)	1.04 (5.23%)	0.84 (4.64%)

In addition, Table 2.6 shows the curtailment for solar PV and onshore wind output in absolute terms and as a percentage of gross output for each formulation and scenario. The curtailment ratio for the M-A formulation shows a lower percentage of gross output compared to M-C and M-D across all scenarios. Therefore, M-A tends to achieve higher levels of utilization of gross output from RES-based generation compared to M-C or M-D.

The formulations at hand can also be compared in terms of the computational time required to solve them. Table 2.7 shows, for each formulation and scenario, the CPU time required to compute an expansion planning solution for the first stage problem of the 2-stage process followed.

Tab. 2.7.: CPU time (h) required to solve the first stage problem using each formulation.

	Cycle-based AC+UC	AC+UC	AC	DC+UC
	M-A	M-B	M-C	M-D
A0B0	7.41	10.18	6.45	5.71
A0B1	7.27	8.83	6.65	5.70
A0B2	7.44	9.43	6.63	5.65
A1B0	7.40	9.71	6.67	5.63
A1B1	7.27	9.49	7.11	5.67
A2B0	7.73	9.66	7.62	5.82
A2B2	7.25	9.61	6.83	5.61

And, the total CPU time required to solve both stage 1 and stage 2 problems is provided in Table 2.8. The two-stage approach aims to compute an initial long-term expansion planning solution and refine it in the medium term (second stage) for the M-C and M-D formulations to ensure feasibility. The time savings achieved by M-A compared to M-B range from 17.67% to 27.21%, considering their times in the first stage.

Tab. 2.8.: Total CPU time (h) required to solve the problems in both stage 1 and stage 2.

	Cycle-based AC+UC	AC+UC	AC	DC+UC
	M-A	M-B	M-C	M-D
A0B0	14.53	10.18	17.19	15.49
A0B1	15.74	8.83	18.35	16.34
A0B2	14.88	9.43	17.04	15.74
A1B0	14.12	9.71	17.15	15.98
A1B1	13.24	9.49	16.36	14.53
A2B0	13.57	9.66	16.38	14.38
A2B2	13.29	9.61	16.36	14.93

However, the total CPU time required to solve both stages is longer than that required for the stage 1 problem alone, as shown for M-A, M-C, and M-D formulations that produce expansion plans that may require refinement in stage 2. Formulations with less detailed representations of system operation have lower computational burdens in the first stage. However, when considering the total CPU time for both planning stages, the merits of each formulation differ. The total time to compute the final expansion plan is the longest for the M-C and M-D formulations, with M-C being more computationally expensive. For example, when comparing the total CPU time for expansion plans based on M-C and M-A formulations, M-C's time is 3.9% to 23.6% longer, depending on the case study, due to the omission of UC constraints in stage 1, which significantly affects the hourly representation of system operation. Switching from a DC to an AC OPF model (comparing M-A and M-D) increases the CPU time for the first stage problem by 27.54% to 34.68%, which remains within reasonable limits.

The impact of considering UC constraints is minimal (comparison between M-A and M-C), because few generators are subject to UC constraints within the considered time horizon, resulting in a similar computational burden for M-A and M-C due to the small number and impact of these constraints and associated binary variables on the problem solution time. The increase in computation time due to these constraints is greater when cycle constraints are not considered. As expected, formulation M-D has the lowest computational cost. Comparing formulations M-A and M-B in terms of the CPU time required to solve the expansion planning problem in the first stage and the size of this problem (see Table 2.7-2.8 and Table 2.9), it is evident that both time and problem size are essentially proportional.

Tab. 2.9.: Sizes of the stage 1 problem after the presolve[2], when considering scenario A0B0. The size of the stage 2 problem is given within parenthesis next to the stage 1 value.

		Cycle-based AC+UC	AC+UC	AC	DC+UC
		M-A	M-B	M-C	M-D
Variables	Continuous	13010112 (9497382)	15336949	10735864 (13803254)	7668475 (13419830)
	Binary	155889 (69215)	155889	539 (140300)	85739 (116917)
Constraints	-	10534324 (7268684)	13875521	9019089 (12141081)	6937761 (12141081)

Considering the cycle constraints, the problem size in the first stage for the M-A formulation is reduced compared to M-B as follows: a) the number of continuous variables by 15.17%; b) the number of binary variables by 26.00%; and c) the number of constraints by 24.08%. Although the problem size is smaller for M-A than for M-B, the quality of the solution computed for the former is not inferior to that of the latter. The representation of the system operation using the M-A formulation is more accurate compared to the M-C and M-D formulations. This results in a smaller stage 1 problem size for M-C and M-D, but a smaller stage 2 problem size for M-A. Formulations M-C and M-D neglectUC constraints and use DC-OPF instead of AC-OPF. For example, M-C includes only a small number of binary variables in Stage 1 related to investment decisions, while M-D uses DC-OPF and does not consider investments in reactive power compensation devices. As a result, the number of

---

[2]The presolve includes techniques and procedures used by optimisation solvers to simplify the problem before attempting to solve it with more complex algorithms.

binary variables in the Stage 1 problem is higher for the M-A and M-B formulations than for the M-C and M-D formulations. However, the system operation computed in Step 1 for formulation M-A is very similar to that of the reference formulation M-B compared to formulations M-C and M-D. This means that a significantly larger amount of investment must be calculated in Step 2 to make the resulting operation feasible and improve the system expansion efficiency when starting from the expansion plans calculated using formulations M-C and M-D.

Tab. 2.10.: Electricity production per technology for the proposed formulation (M-A) in the base scenario (A0B0).

	Technology	[TWh]	[%]
	Coal	0.0000	0.0
	Gas-CC	12.2322	20.9
Thermal	Gas-CC-90CCS	0.0000	0.0
	Gas-CT	0.0000	0.0
	Nuclear	3.0707	5.2
	Oil	0.0000	0.0
RES	Solar-PV	13.2367	22.6
	Onshore-Wind	12.5079	21.3
	Hydro	3.9706	6.8
	PSH	3.8688	6.6
	Solar-CSP	8.5931	14.7
	BESS	1.1525	2.0

The proposed formulation (M-A) supports the design of an electricity system in a low-carbon future context, with nearly 80% of electricity generation coming from RES, as shown in Table 2.10. This contrasts with the initial electricity generation profile of the RTS-GMLC system, shown in Table 8 of [32], where there remains a significant amount of electricity generation from coal and a notable use of gas CC units. Table 2.10 highlights Gas-CC as the only operational fossil fuel-based thermal technology that plays a significant role in the energy mix. Nuclear power also makes a significant contribution. Solar PV, onshore wind, solar-CSP, and hydro dominate electricity generation, with various forms of storage playing a significant role. The emissions of CO_2 are all attributed to gas-fired power plants. Solar-CSP production is notable for its hybridization with thermal storage, which provides benefits to the system.

In the base scenario (A0B) for the M-A formulation, the average utilization of interconnections between areas is 54.31%. In addition, there are 179 hours when the interconnections experience congestion. Within areas, the average network utilization is significantly lower at 20.05%, with 48 hours of internal congestion. During these instances, the flexibility available within each area (primarily provided by storage) is insufficient to prevent congestion. Since demand response is not considered, flexibility requirements are measured based on changes in net demand (electricity demand minus solar and wind generation). The largest upward and downward ramps are 8953.57 MW and -1111.55 MW, respectively, requiring system flexibility to accommodate these ramps. Ramp margins assess the system's ability to handle these ramps, represented as the ratio of the maximum ramp the system can handle to the largest ramp it faces during calculated system operation. In the base scenario A0B0 with formulation M-A, the ramp-up and ramp-down margins are 1.10% and 1.81%, respectively.

Tab. 2.11.: Average and maximum computation error per scenario after the first stage of the computation process for the power flows, the voltage magnitudes and the angles, making use of the M-A formulation. The errors made are determined by comparing the values computed for these variables with those resulting from considering the fundamental power flow equations.

Scenario	Feature	V_{ni}, [%]	θ_{ni}, [%]	P_{nijc}, [%]	Q_{nijc}, [%]
A0B0	Max. error	0.925	0.865	0.489	0.557
	Avg. error	0.028	0.032	0.068	0.072
A0B1	Max. error	0.910	0.981	0.572	0.563
	Avg. error	0.043	0.039	0.060	0.084
A0B2	Max. error	0.087	0.072	0.068	0.041
	Avg. error	0.032	0.059	0.070	0.057
A1B0	Max. error	0.916	0.821	0.516	0.683
	Avg. error	0.025	0.049	0.074	0.067
A1B1	Max. error	0.096	0.928	0.341	0.793
	Avg. error	0.041	0.039	0.077	0.076
A2B0	Max. error	0.048	0.062	0.005	0.006
	Avg. error	0.013	0.025	0.032	0.037
A2B2	Max. error	0.032	0.051	0.004	0.008
	Avg. error	0.019	0.026	0.013	0.028

The accuracy of operations computed using the M-A formulation, as opposed to the full original AC power flow equations, is evaluated. A model that incorporates the nonconvex and nonlinear fundamental AC power flow equations has been employed. This model calculates system operations independently for each hour (time step) in the base scenario, A0B0. The power flow solutions computed in this manner are compared with those obtained using the M-A formulation in Step 1. In the AC power flow calculation, the investment plan (represented by binary variables) and the active and reactive power generated by the units as determined by the M-A formulation are fixed. These fixed values are used to calculate the power flows, voltage magnitudes and angles. In particular, the reference node is treated as the slack bus with both voltage magnitude and angle fixed. For each storage unit, such as PSH or BESS, the net generation is considered individually for each hour. The net generation level of a storage unit is calculated as the difference between its generation and consumption levels in the respective hour. The energy inventory for storage units is managed separately for each unit. Furthermore, the procedure used for this comparison follows the approach described by the authors in [21].

Table 2.11 shows both the average and the maximum errors that occur in the calculation of power flows, as well as voltage magnitudes and angles. These calculations used the proposed formulation, M-A, across all scenarios and serve as a basis for comparison with the solutions derived from the nonlinear model executed per time step considering the solution provided by M-A. It is important to note that these errors, both average and maximum, are within acceptable limits. The maximum error made over all the considered system states (8736 hours in total per scenario) is less than 1%.

In addition, the produced output data reveals the existence of complex relationships among the several variables considered across the different scenarios. In particular, there is a moderate positive correlation between the errors made when computing the active power flows (P_{nijc}) and the reactive power flows (Q_{nijc}). This can be observed across all the scenarios, highlighting the interconnectedness of these critical system variables.

The analysis conducted has also allowed us to identify significant correlations existing among the errors made when computing key variables, such as the active and reactive power flows and voltage angles (θ_{ni}), for specific scenarios, such as A0B0, A1B1 and A2B2, highlighting the complex interplay among these variables. Despite the differences between these scenarios, the calculated results show a consistent upward trend in the errors correlated to the increase in the ratio of fuel and carbon price levels between the scenarios. In terms of the voltage magnitude (V_{ni}), the maximum and average errors show opposite trends when comparing scenarios A0B1, or A0B2, to scenarios A0B0 or A1B0, i.e. in the latter the maximum error is larger while the average error is lower than in the former.

This suggests that the error distribution in the former scenarios is significantly different from that in the later scenarios. The largest deviations from the accurate values of the system operation variables are observed for the voltage magnitudes and angles. However, in average terms, the accuracy of these voltage-related variables exceeds the errors of the active and reactive power flows. This trend can be attributed to the assumptions made when deriving the M-A equations for current flows. The fact that significant maximum errors are made for the voltage variables, particularly those associated with insufficient reactive power generation - a key challenge in power systems with high shares of RES. In this regard, it is noteworthy the fact that the voltage at the nodes is largely affected by the production and consumption of reactive power within each system area.

2.6 Conclusions

This chapter outlines a novel approach to TEP that provides significant detail on system operations. The methodology integrates a comprehensive set of operational constraints with a high degree of temporal granularity. By improving computational efficiency through the inclusion of cycle constraints and refined bounds, this formulation directly addresses Research Question 1 (RSQ-1) presented in Section 1.2 by improving both temporal resolution and representation of system operations.

A one-hour time step is considered for system operations, with computations spanning 8,736 time steps. Although the current model, the RTS-GLMC, includes 73 nodes, the approach is designed to be flexible. It can be adapted to consider different representative periods - from hours to weeks - at an hourly resolution. This adaptability makes it suitable for application to medium- to large-scale systems.

To keep the problem manageable, a compact representation of the AC-OPF model is employed using cycle constraints. In addition, the bounds on the voltage magnitude and angle variables are optimized to ensure that they are tightly controlled. This strategy allows for efficient computation of expansion planning solutions within acceptable time limits. The solutions are capable of accommodating all types of energy resources and technologies while maintaining accurate management of short-, medium-, and long-term storage technologies.

Another key aspect of the formulation is the relaxation of the charge and discharge state variables. This technique relaxes the binary nature of the charge/discharge operation decisions, further reducing the complexity of the problem. By allowing a more efficient solution process, this approach contributes to the scalability and applicability of the model to large systems.

The proposed formulation has been used to compute the optimal expansion plan for a medium-sized system, specifically the RTS-GMLC test system. This was done under different scenarios, and the results were compared to those obtained from alternative formulations that deviate in specific ways from the original proposal. These variations include Formulation M-B, which omits cycle constraints; Formulation M-C, which omits UC constraints; and formulation M-D, which uses a DC-OPF model instead of a linear AC model.

Literature reviews indicate that more complex formulations are generally not appropriate for this type of system. The integrated expansion plan derived from the proposed formulation does not focus solely on transmission lines and reactive power compensation devices (such as synchronous compensators and capacitor banks). It also considers multiple power generation and storage technologies as viable candidates within the case studies.

First, the proposed formulation has demonstrated its applicability to the system in question by successfully solving the corresponding expansion planning problem within a reasonable time frame. This achievement is notable given the substantial size of the problem, which includes approximately 13 million continuous variables, about 100000 binary variables, and nearly 10 million constraints. The application of bound tightening and cycle constraints facilitated the successful solution of this complex problem. In particular, the implementation of cycle constraints had a negligible impact on the quality of the planning solution, with a maximum cost difference of only 0.00017% compared to the costs incurred under Formulation M-B. More importantly, these constraints significantly reduced the CPU time across the scenarios considered, with an average reduction of 22.53%.

Second, the results obtained using the proposed formulation and those from simplified alternative formulations underscore the superior efficiency of the proposed expansion plan. Significant reductions in total system costs were observed when implementing plans computed with the proposed formulation (M-A) compared to those that either neglected UC constraints (M-C) or replaced the AC optimal power flow with a DC model (M-D). Specifically, the cost savings achieved with the proposed formulation compared to using a DC-OPF model ranged from 5.92% to 7.74%, and the savings compared to plans that neglected UC constraints ranged from 6.63% to 8.73%.

The significant cost savings achieved by the proposed formulation are primarily due to reduced capital expenditures. Specifically, investment costs for the proposed formulation are 15.33% to 18.27% lower than those calculated using a DC-OPF model, and 13.36% to 17.43% lower than scenarios that neglect UC constraints.

In addition, the expansion schedules generated by the proposed formulation effectively limit renewable curtailment. For example, the maximum curtailment for solar-PV output across different scenarios is 10.27% and for onshore wind it is 11.30%.

The operational solutions provided by the proposed formulation, referred to as M-A, ensure a feasible system operation over the 8736 hours of the target year by enforcing basic AC power flow constraints and successfully avoiding any load shedding. The deviations in system operation due to the enforcement of these constraints are less than 1%.

Another key advantage of the proposed formulation is its flexibility, which allows different elements to be considered separately within the TEP framework. This includes the choice between DC- or AC-OPF models, UC constraints, operating reserves, and energy storage management. It also facilitates the seamless integration of generation and storage investments, effectively transforming TEP into an integrated expansion planning problem.

Future research will focus on developing weather scenarios based on historical data for use in expansion planning analyses. In addition, the incorporation of stochastic elements and contingencies into the current formulation will be explored to assess their impact on investment decisions and the feasibility of achieving climate goals under extreme weather.

Impact of the Flexibility Provided by Distributed Energy Resources

3

> *Coming together is a beginning; keeping together is progress; working together is success.*
>
> — **Henry Ford**
> Founder of Ford Motor Company

Contents of this chapter are based on

Alvarez, Erik F., et al. "Values and impacts of incorporating local flexibility services in transmission expansion planning." Electric Power Systems Research 212 (2022): 108480. DOI: `10.1016/j.epsr.2022.108480`

Declaration

I was responsible for executing the implementation of the mathematical formulation and played a pivotal role in co-authoring every component of the study, including both the initial draft and the final publication. The contributions of other authors primarily encompassed reviewing and co-editing the manuscript.

3.1 Introduction

This chapter looks at the significant transitions and challenges in achieving a zero-carbon economy, with a particular focus on the increased need for flexibility in power systems. Traditionally, transmission expansion planning has played a critical role in improving system flexibility. However, to better meet today's challenges, there is an urgent need for novel tools to develop technically and economically efficient plans. In addition, the increasing use of distributed generation and storage suggests that distributed energy resources (DERs) should also contribute to this flexibility. This requires transmission and distribution system operators (TSOs & DSOs) to coordinate the operation of their networks more closely. The provision of massive flexibility services (FSs) at the local level within the distribution network could have a significant impact not only on the operation but also on the expansion of the transmission network.

The literature defines and evaluates several TSO-DSO operational coordination models, such as the work presented in [34, 35, 36]. Some studies consider the provision of local flexibility in the context of operational coordination between TSOs and DSOs, but they often overlook system expansion. A notable exception is the work in [37], which models the joint planning of transmission and distribution expansion as a three-level problem aimed at minimising investment costs while optimising system operation through economic dispatch. However, this study does not consider the potential of DERs to provide flexibility at both the operational and expansion planning levels under different operational strategies. To date, the impact of providing local flexibility on the operation and expansion of the transmission system and the associated costs under centralised and decentralised operation schemes remains under-explored.

This work defines optimisation models at different levels of network operation to formulate and solve problems related to the study cases outlined in section 3.3. The objective is to coordinate the planning of transmission network expansion, its operation, and the operation of downstream distribution networks connected to microgrids (MGs) with flexible DERs. By comparing the results of grid expansion and operation with the associated costs derived from these problem solutions, it determines the impact of local DERs on transmission expansion planning (TEP) and system operation, as well as the economic value provided by DERs. The models include detailed representations of the transmission and distribution networks, including the MGs where the DERs are located.

Transmission expansion and system operation are modelled as a mixed-integer programming (MIP) problem using the DC power flow model at the transmission level and the AC branch flow model at the distribution level. This merging creates a multi-level optimisation problem that is computationally demanding and typically only amenable to small test systems. Following an approach similar to that of the authors in [37], this multilevel problem is transformed into an equivalent single-level problem. Furthermore, the complex operation of the MGs is represented by a multi-follower approach, where the power exchanges between the transmission grid, the distribution grid, and the MGs are considered variables in the coordination of the addressed problems.

The main research questions addressed in our work are as follows:

1. How does the choice of the model considered for the TSO-DSO coordination affect the operation of the system and, specifically, the dispatch of local flexibility resources (DERs providing flexibility)?

2. How does this choice of coordination model affect the amount, allocation, and value of the local FSs?

3. How does the provision of local FSs affect the expansion of the transmission grid?

The main contributions of this work are described next:

- An optimisation model to solve the TEP, taking into account the TSO-DSO coordination and the use of locally provided FSs. The local flexibility can be procured centrally by the TSO or in a decentralised manner, i.e. by each DSO. The model is

used to evaluate the flexibility value of the system and to determine its impact on transmission expansion and system operation.

- A detailed representation of the provision of local flexibility considering two FSs: 1) a baseline product, which quantifies flexibility as the deviation from a power profile and is typically used in recent studies, and 2) a capacity constraint product, which quantifies flexibility as the peak power reduction from an upper capacity limit and was introduced in [38] to avoid possible market manipulation. Comparing the results of transmission system expansion and operation considering these FSs offered at different system levels allows us to determine which approach provides higher benefits to the TSO.

- A bilevel optimisation problem formulated using: 1) a multi-follower approach for the MGs connected at the distribution level, and 2) the variables of the optimisation model representing the power exchanges between networks as a means to coordinate optimisation problems at different network levels. This bilevel problem is then transformed into an equivalent single-level problem, allowing scalable solutions for any system. This is in contrast to previous efforts, which have often struggled with scalability when addressing similar types of problems.

3.2 Mathematical Formulation

The TSO-DSO model consists of three primary components: a) the TEP and operational problem addressed by the TSO; b) the operational problem addressed by the DSO; and c) the energy and flexibility dispatch problem overseen by each MG providing energy services to its customers and FSs to the upstream connected grids. Each problem can be solved independently by calculating the energy exchanges with the neighbouring upstream grid, using the exchanges with downstream grids as input parameters. To represent the coordinated operation between the DSO grid and the MGs, a bilevel optimisation problem is delineated, following the emerging research trend of using bilevel programming to represent interactions between resource aggregators (or MGs) and prosumers [39, 40], as well as interactions between grid or market operators and aggregators, MGs, or prosumers [41, 42]. The bilevel problem is transformed into an equivalent single-level MIP problem by substituting the lower-level problem with its Karush-Kuhn-Tucker (KKT) conditions and applying the strong duality theorem [43]. The coordination of TSO and DSO network operations is modelled by integrating this single-level optimisation problem into the TEP problem, merging the objective functions of both problems into one, and treating power flows through transformers at boundary buses between transmission and distribution networks as common variables. This section provides a detailed formulation of each aspect of the overall model. The problem formulations for each test case, representing specific coordination paradigms, are elaborated in section 3.3.

3.2.1 TEP Problem: Constraints

The proposed formulation for the transmission planning problem is the same as presented as the basic TEP formulation in section 2.2.2, where network investment decisions are calculated for future years with hourly resolution in the expected system operation. User-defined candidate lines are specified in advance, allowing the model to determine the optimal investment decisions from the specified options using a DC-OPF linearised approximation. The formulation of the TEP problem faced by the TSO is described by (3.1) s.t. (3.2)–(3.10).

Objective Function
The objective of the TSO is to minimise, as expressed in (3.1), both the total investment cost (first term) and the total operating cost associated with generation dispatch and load shedding (last two terms):

$$\min \sum_{ijc \in \mathcal{L}^c} C_{ijc}^t \alpha_{ijc}^t + \sum_{ng} \Delta t CV_g p_{ng}^{tg} + \sum_{ni} \Delta t C^{shed} l_{ni}^{ens}. \tag{3.1}$$

The parameters $C_{ijc}^t, CV_g, C^{shed}$ represent the annualised fixed cost of a candidate line, the variable cost of generation, and the cost of unserved energy, respectively. The variable costs include fuel, operation and maintenance (O&M), and emissions costs. Additionally, Δt denotes the duration of the time discretisation step. The variables $l_{ni}^{ens}, p_{ng}^{tg}$, and the (relaxed) binary variable α_{ijc}^t denote load shedding, active power generation, and the decision to install candidate lines, respectively.

Power Balance
The balance of generation and demand at each node, neglecting ohmic losses, is given by

$$\sum_{g \in \mathcal{G}_i} p_{ng}^{tg} - P_{ni}^d - \sum_{i' \in \mathcal{B}_i^d} p_{ni'}^{SS} - l_{ni}^{ens} - \sum_{ijc \in \mathcal{L}} f_{nijc}^P + \sum_{jic \in \mathcal{L}} f_{njic}^P = 0 \qquad \forall n \in \mathcal{T}, \ \forall i \in \mathcal{B}^t, \tag{3.2}$$

where the parameter P_{ni}^d represents the active power demand, and the variables f_{nijc}^P and $p_{n,i'}^{SS}$ represent the active power flow on the lines and the active power transferred to the connected distribution networks via the border substations, respectively.

Logical Investment Bounds
The transfer capacity conditioned by the investment decision in candidate transmission lines is expressed as

$$-\alpha_{ijc}^t \leq \frac{f_{nijc}^P}{\overline{S}_{ijc}} \leq \alpha_{ijc}^t \qquad \forall nijc, ijc \in \mathcal{L}^c \tag{3.3}$$

where $\overline{S}_{ijc}$ is the total transfer capacity of the line multiplied by a security factor (e.g. 0.67 in our approach).

Power Flow Bounds
The DC power flow equations for existing and candidate lines (following Kirchhoff's second law) are expressed as

$$\frac{f_{nijc}^P}{\overline{S}_{ijc}'} = (\theta_{ni} - \theta_{nj}) B_{ijc} \frac{S_B}{\overline{S}_{ijc}'} \qquad \forall nijc, ijc \in \mathcal{L}^e \tag{3.4}$$
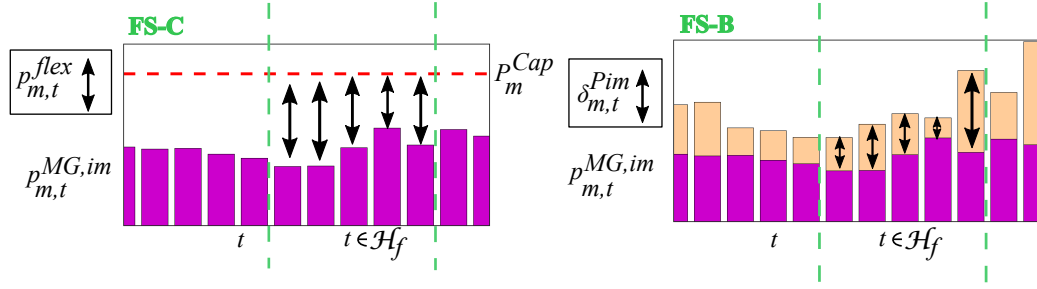
Fig. 3.1.: The capacity limitation (left) and baseline flexibility services (right).

$$\left|\frac{f^P_{nijc}}{\overline{S}'_{ijc}} - (\theta_{ni} - \theta_{nj})B_{ijc}\frac{S_B}{\overline{S}'_{ijc}}\right| \leq 1 - \alpha^t_{ijc} \qquad \forall nijc, ijc \in \mathcal{L}^c \quad (3.5)$$

Where θ_{ni} and B_{ijc} represent the bus voltage angle and the susceptance of each line in per unit (p.u.), respectively. $\overline{S}'_{ijc}$ serves as the big M value for the disjunctive constraint.

Transmission System Bounds

The bounds on generation, load shedding, and transmission network transfer capacity are defined by Eqs. (3.6)-(3.8), while the decision variables for line installation are constrained by (3.9).

$$\underline{P}_g \leq p^{tg}_{ng} \leq \overline{P}_g \qquad \forall n \in \mathcal{T}, \forall g \in \mathcal{G}_i, \quad (3.6)$$

$$0 \leq l^{ens}_{ni} \leq P^d_{ni} \qquad \forall n \in \mathcal{T}, \ \forall i \in \mathcal{B}^t, \quad (3.7)$$

$$-\overline{S}_{ijc} \leq f^P_{nijc} \leq \overline{S}_{ijc} \qquad \forall nijc, ijc \in \mathcal{L}^e, \quad (3.8)$$

$$\alpha^t_{ijc} \in \{0, 1\} \qquad \forall ijc, ijc \in \mathcal{L}^c. \quad (3.9)$$

$\underline{P}_g$ and $\overline{P}_g$ represent the minimum load and maximum power of each generator, respectively, while $\overline{S}_{ijc}$ is the maximum transfer capacity of a line. Additionally, the voltage angle of the reference node is set to 0 for each time step according to the constraint (3.10).

$$\theta_{n,node_{ref}} = 0 \qquad \forall n \in \mathcal{T}. \quad (3.10)$$

3.2.2 DSO: Optimal Network Operation Problem (Upper Level)

The distribution system operator (DSO) optimises its operations by utilising flexible services (FS) provided by grid-connected microgrids (MGs) acting as flexible service providers (FSPs). The two types of FSs considered are illustrated in Figure 3.1 and described in detail in this section: FS-C, representing flexibility offered as a capacity limitation product; and FS-B, representing flexibility offered as a basic product.

Objective Function

The DSO's objective is to minimise both its peak power costs and the costs associated with provisioning local flexibility, which minimises the subscription fee paid to the TSO. The objective function is formulated as follows:

$$\min f^{UL,peak} = c^{peak} + c^{flex}, \tag{3.11}$$

where c^{peak} is the peak power cost and c^{flex} is the cost associated with purchasing local flexibility from the MGs.

Power Flow Equations

The LinDistFlow equations (3.13)–(3.21) $\forall n \in \mathcal{T}$ model the linearised lossless AC power flow according to the convex branch flow model [20].

This model is derived by applying voltage angle relaxation and neglecting the capacitance and the line losses. The equation (3.12) $\forall n \in \mathcal{T}$ is included to calculate c^{peak}.

$$c^{peak} \geq \Lambda^{peak} p_{ni'}^{SS}, \qquad\qquad \forall n \in \mathcal{T}, \forall i' \in \mathcal{B}^d \cup \mathcal{B}_i^d, \tag{3.12}$$

$$\sum_{i' \in \mathcal{B}_i^d} p_{ni'}^{SS} + \sum_{j' \in \mathcal{B}_{i'}^t} (p_{nj'i'} - p_{ni'j'}) = \sum_{m \in \mathcal{B}_{i'}^m} (p_{nm}^{MG,im} - p_{nm}^{MG,ex}) + P_{ni'}^L, \qquad \forall n \in \mathcal{T}, \forall i', j' \in \mathcal{B}^d, \tag{3.13}$$

$$\sum_{j' \in \mathcal{B}_{i'}^t} (q_{nj'i'} - q_{ni'j'}) = q_{ni'}^{SS} + Q_{ni'}^L + \sum_{m \in \mathcal{B}_{i'}^m} Q_{nm}^{MG}, \qquad \forall n \in \mathcal{T}, \forall i', j' \in \mathcal{B}^d, \tag{3.14}$$

$$v_{nj'} - v_{ni'} + 2(p_{ni'j'} R_{i'j'} + q_{ni'j'} X_{i'j'}) = 0, \qquad \forall n \in \mathcal{T}, \forall i' \in \mathcal{B}^d, \forall j' \in \mathcal{B}_{i'}^t, \tag{3.15}$$

$$v_{ni'} \leq \overline{V} \quad \text{and} \quad v_{ni'} \geq \underline{V}, \qquad \forall n \in \mathcal{T}, \forall i' \in \mathcal{B}^d, \tag{3.16}$$

$$v_{ni'} = V^{SB}, \qquad \forall n \in \mathcal{T}, \forall i' \in \mathcal{B}_i^d, \tag{3.17}$$

$$p_{ni'j'} = 0, \qquad \forall n \in \mathcal{T}, \forall i' \in \mathcal{B}^d, \forall j' \notin \mathcal{B}_{i'}^t, \tag{3.18}$$

$$q_{ni'j'} = 0, \qquad \forall n \in \mathcal{T}, \forall i' \in \mathcal{B}^d, \forall j' \notin \mathcal{B}_{i'}^t, \tag{3.19}$$

$$p_{ni'j'} + p_{nj'i'} = 0, \qquad \forall n \in \mathcal{T}, \forall i' \in \mathcal{B}^d, \forall j' \in \mathcal{B}_{i'}^t, \tag{3.20}$$

$$q_{ni'j'} + q_{nj'i'} = 0, \qquad \forall n \in \mathcal{T}, \forall i' \in \mathcal{B}^d, \forall j' \in \mathcal{B}_{i'}^t, \tag{3.21}$$

The variables $p_{nm}^{MG,ex}/p_{nm}^{MG,im}$ denote the power exported from or imported into an MG. The variables $v_{ni'}$ and $p_{ni'j'}/q_{ni'j'}$ refer to the square of the voltage magnitude and the active/reactive power flows. The parameters Λ^{peak}, $R_{i'j'}/X_{i'j'}$ and V^{SB} refer to the peak imported power tariff paid by the DSO to the TSO, the line resistance/reactance and the square of the voltage at the substation of the distribution system (boundary bus). And the parameters $P_{ni'}^L$, $Q_{ni'}^L$ refer to the active and reactive power demand at the distribution nodes, respectively.

FSs

This section refers to the next FSs: FS-C and FS-B.

FS-C: Regarding the flexibility product FS-C, the term c^{flex} of (3.11) becomes

$$c^{flex} = \sum_{n \in \mathcal{T}_f} \sum_{n \in \mathcal{B}_{i'}^m} \pi_{flex}^{Cap} p_{nm}^{flex} = \pi_{flex}^{Cap}(P_m^{Cap} - p_{nm}^{fl,im}) \qquad (3.22)$$

and the MG imported/exported power are given by

$$p_{nm}^{MG,im} = p_{nm}^{im}, \qquad\qquad\qquad \forall n \in \mathcal{T}, \ \forall m \in \mathcal{B}_{i'}^m, \ (3.23)$$

$$p_{nm}^{MG,ex} = p_{nm}^{ex}, \qquad\qquad\qquad : \ \forall n \in \mathcal{T}, \ \forall m \in \mathcal{B}_{i'}^m, \ (3.24)$$

The positive variables π_{flex}^{Cap} and p_{nm}^{flex} represent the flexibility price and the offered amount of flexibility (averaged over δt) during the flexibility activation period $\mathcal{T}_f! \subseteq !\mathcal{T}$, respectively. Additionally, $p_{nm}^{fl,im}$ denotes the imported power of the MG at each time step within the flexibility activation period. It's important to note that the amount of flexibility is determined in terms of power capacity reduction. For example, the activation of the FS-C flexibility product results in an "updated" capacity represented by $P_m^{Cap} - p_{nm}^{flex}$ to the DSO. The parameter P_m^{Cap} is the upper capacity limit, typically agreed between the DSO and the MG operator, often based on values such as the capacity at the connection point.

FS-B: Regarding the flexibility product FS-B, the term c^{flex} of (3.11) becomes

$$c^{flex} = \sum_{n \in \mathcal{T}_f} \sum_{m \in \mathcal{B}_{i'}^m} -\pi_{flex}^{im} \delta^{Pim} + \pi_{flex}^{ex} \delta^{Pex}, \qquad (3.25)$$

and the MG imported/exported power are given by

$$p_{nm}^{MG,im} = p_{nm}^{im} + \delta^{Pim}, \qquad\qquad : \ \forall n \in \mathcal{T}, \ \forall m \in \mathcal{B}_{i'}^m, \ (3.26)$$

$$p_{nm}^{MG,ex} = p_{nm}^{ex} + \delta^{Pex}, \qquad\qquad : \ \forall n \in \mathcal{T}, \ \forall m \in \mathcal{B}_{i'}^m, \ (3.27)$$

where the positive variables π_{flex}^{im} and π_{flex}^{ex} represent the prices associated with flexibility, while δ^{Pim} and δ^{Pex} denote the amounts of flexibility procured. Specifically, in this FS, the amount of flexibility provided, denoted by δ^{Pim} or δ^{Pex}, represents the deviation from the baseline power exchange profile. It is assumed here that the baseline profile corresponds to the optimal energy dispatch of the MG ($p_{nm}^{ex} - p_{nm}^{im}$), determined as the solution to the optimal MG energy management problem in the absence of any flexibility services.

3.2.3 Energy and Flexibility Dispatch of the MGs (Lower Level)

The formulation of the original LL problem differs depending on whether FS-C is considered, as given by (3.28) subject to (3.29)–(3.52) for all $m \in \mathcal{B}_{i'}^m$, or FS-B is considered as given by (3.28), subject to (3.29)–(3.49) and (3.53)–(3.59), $\forall m \in \mathcal{B}_{i'}^m$. It's worth noting that the dual variables, denoted by λ or μ, are defined for each constraint. Due to space limitations, inequality constraints are presented together with their complementarity slackness (CS) conditions. Although the CS conditions are not explicitly part of the primal problem, they are used later to derive the Karush-Kuhn-Tucker (KKT) conditions (see Section 3.2.4).

Objective Function

The microgrid (MG) operator aims to minimise the energy cost of the MG, represented by $c_m^{im} - r_m^{ex}$ in (3.28), where c_m^{im} and r_m^{ex} are the energy cost and revenue of the MG, respectively. At the same time, the operator tries to maximise the revenue from the flexibility services (FSs) provided, denoted by r^{flex}.

$$\min f_m^{LL} = c_m^{im} - r_m^{ex} - r^{flex}, \qquad\qquad (3.28)$$

$$c_m^{im} = \sum_{n \in \mathcal{T}} (\Lambda_n + C^{im}) p_{nm}^{MG,im} \Delta t, \qquad\qquad : \forall m \in \mathcal{B}_{i'}^m, \;\; (3.29)$$

$$r_m^{ex} = \sum_{n \in \mathcal{T}} (\Lambda_n + C^{ex}) p_{nm}^{MG,ex} \Delta t, \qquad\qquad : \forall m \in \mathcal{B}_{i'}^m, \;\; (3.30)$$

where the parameter Λ_t represents the energy price [USD/MWh], while C^{im} and C^{ex} refer to the distribution grid tariff and the compensation fee associated with the imported and exported energy of the microgrid, respectively.

Power Balance

For a MG connected at bus m with Photovoltaic (PV) and Battery Energy Storage systems (BESS), it is essential to comply with (3.31) $\forall n \in \mathcal{T}$. This requirement is due to the fact that the electricity consumption of the MG customers is met by the resources of the MG and/or the connection to the upstream distribution grid at each time step.

$$P_{nm}^{PV} + p_{nm}^{dis} - p_{nm}^{ch} = p_{nm}^{MG,ex} - p_{nm}^{MG,im} + P_{nm}^{MG,L}, \qquad : \lambda_{nm}^{PB}, \quad \forall n \in \mathcal{T}, \; \forall m \in \mathcal{B}_{i'}^m, \;\; (3.31)$$

In (3.31), P_{nm}^{PV}, P_{nm}^{MGL}, and the positive variables p_{nm}^{ch}/p_{nm}^{dis} respectively refer to the PV generation of the MG's PV systems, the electric power consumption of the MG customers, and the charging/discharging power of the MG's BES. It is assumed that the BES draws power from both the main distribution grid and the PVs and injects power into both the main grid and the MG's consumption points.

BESS model

The BESS model, described by the equations (3.32)–(3.49) $\forall n \in \mathcal{T}, \; \forall m \in \mathcal{B}_{i'}^m$. This model, originally introduced in [44], uses a measurement-based approach using data extracted from charge/discharge curves. The parameters SoE_{mk}^{ch}, P_{mk}^+, P_{mk}^{ch}, SoE_{mp}^{dis}, P_{mp}^-, and P_{mp}^{dis} take values from the sample data.

The positive variables p_n^- and p_n^+ denote the power output/input of the BESS cells before/after accounting for BESS losses. E^{max} denotes the installed BESS capacity, while soe_{nm} denotes the state-of-energy (SoE) or state of charge, constrained between lower and upper limits (SoE^{min} and SoE^{max}, respectively). The equation (3.36) ensures that the soe_{nm} of the BES at the end of the dispatch period (soe_m^{end}) is equal to its initial value (SoE_m^{init}). This assumption is often used in the literature as a means of regulating the state of energy (SoE) within the time boundaries of the study.

The continuous variables x_{nmp} and y_{nmk}, associated with the selection of discharging or charging sample data, allow the creation of convex combinations involving soe_{nm}, p_{nm}^+, and p_{nm}^{ch}. In addition, this model accounts for the variable charging/discharging efficiencies of the BESS system, which are influenced by internal BESS losses and DC/DC converter losses, affecting p_{nm}^{ch}/p_{nm}^{dis} and soe_{nm}. The charge/discharge efficiencies are defined as $\eta_{nm}^{ch} = p_{nm}^+/p_{nm}^{ch}$ and $\eta_{nm}^{dis} = p_{nm}^{dis}/p_{nm}^-$, $\forall n \in \mathcal{T}, \forall m \in \mathcal{B}_{i'}^m$, respectively, [44].

$$soe_{nm} = \begin{cases} soe_{nm} = SoE_m^{init}, & : \lambda_{nm}^{start}, t = 1 \\ soe_{n-1,m} + \frac{p_{n-1,m}^+ \Delta t}{E_m^{max}} - \frac{p_{n-1,m}^- \Delta t}{E_m^{max}}, & : \lambda_{nm}^{BES}, t > 1 \end{cases}, \tag{3.32}$$

$$soe_m^{end} = soe_{nm} + \frac{p_{nm}^+ \Delta t}{E_m^{max}} - \frac{p_{nm}^- \Delta t}{E_m^{max}}, \qquad \qquad : \lambda_{nm}^{BES,end}, \tag{3.33}$$

$$0 \geq SoE_m^{min} - soe_{nm} \quad \text{to be consistent} \quad \underline{\mu}_{nm}^{SoE} \geq 0, \tag{3.34}$$

$$0 \geq soe_{nm} - SoE_m^{max} \quad \text{to be consistent} \quad \overline{\mu}_{nm}^{SoE} \geq 0, \tag{3.35}$$

$$soe_m^{end} = SoE_m^{init}, \qquad \qquad : \lambda_{nm}^{end}, \tag{3.36}$$

$$p_{nm}^- = \sum_{p \in \mathcal{P}} P_{mp}^- x_{nmp}, \qquad \qquad : \lambda_{nm}^-, \tag{3.37}$$

$$p_{nm}^{dis} = \sum_{p \in \mathcal{P}} P_{mp}^{dis} x_{nmp}, \qquad \qquad : \lambda_{nm}^{dis}, \tag{3.38}$$

$$p_{nm}^+ = \sum_{k \in \mathcal{K}} P_{mk}^+ y_{nmk}, \qquad \qquad : \lambda_{nm}^+, \tag{3.39}$$

$$p_{nm}^{ch} = \sum_{k \in \mathcal{K}} P_{mk}^{ch} y_{nmk}, \qquad \qquad : \lambda_{nm}^{ch}, \tag{3.40}$$

$$0 \geq -p_{nm}^{ch} \quad \text{to be consistent} \quad \mu_{nm}^{ch} \geq 0, \tag{3.41}$$

$$0 \geq -p_{nm}^{dis} \quad \text{to be consistent} \quad \mu_{nm}^{dis} \geq 0, \tag{3.42}$$

$$0 \geq -p_{nm}^+ \quad \text{to be consistent} \quad \mu_{nm}^+ \geq 0, \tag{3.43}$$

$$0 \geq -p_{nm}^- \quad \text{to be consistent} \quad \mu_{nm}^- \geq 0, \tag{3.44}$$

$$soe_{nm} = \sum_{p \in \mathcal{P}} SoE_{mp}^{dis} x_{nmp} + \sum_{k \in \mathcal{K}} SoE_{mk}^{ch} y_{nmk} \qquad \qquad : \lambda_{nm}^{SoE}, \tag{3.45}$$

$$\sum_{p \in P} x_{nmp} = 1, \qquad \qquad : \lambda_{nm}^x, \tag{3.46}$$

$$0 \geq -x_{nmp} \quad \text{to be consistent} \quad \mu_{nmp}^x \geq 0, \qquad \qquad \forall p \in \mathcal{P}, \tag{3.47}$$

$$\sum_{k \in K} y_{nmk} = 1, \qquad \qquad : \lambda_{nm}^y, \tag{3.48}$$

$$0 \geq -y_{nmk} \quad \text{to be consistent} \quad \mu_{nmk}^y \geq 0, \qquad \qquad \forall k \in \mathcal{K}, \tag{3.49}$$

A three-dimensional feasibility region is defined by the equations (3.37)–(3.38), (3.42), (3.44), and (3.45)–(3.47), using discharge sample data $(SoE_{mp}^{dis}, P_{mp}^{-}, P_{mp}^{dis})$ to constrain the variables $(soe_{nm}, p_{nm}^{-}, p_{nm}^{dis})$ that are interdependent during discharge. Similarly, the equations (3.39)–(3.40), (3.41), (3.43), (3.45), and (3.48)–(3.49) describe the feasibility range of the variables $(soe_{nm}, p_{nm}^{+}, p_{nm}^{ch})$ during charging, using charging sample data $(SoE_{mk}^{ch}, P_{mk}^{+}, P_{mk}^{ch})$. Any convex combination of the BESS operation variables $(soe_{nm}, p_{nm}^{+}, p_{nm}^{ch}, p_{nm}^{-}, p_{nm}^{dis})$ depends on the variables x_{nmp} and y_{nmk} which correspond to the selection of the discharging and charging sample data, respectively.

Flexibility as a Capacity Limitation Product

The term r^{flex} in (3.28) becomes

$$r_m^{flex} = \sum_{n \in \mathcal{T}_f} \pi_{flex}^{Cap}(P_m^{Cap} - p_{nm}^{fl,im}) \tag{3.50}$$

and the following constraints are added, $\forall n \in \mathcal{T}, \forall m \in \mathcal{B}_{i'}^m$:

$$0 \geq p_{nm}^{im} - p_{nm}^{fl,im} \quad \text{to be consistent} \quad \mu_{nm}^{fl,Cap} \geq 0, \tag{3.51}$$

$$0 \geq -p_{nm}^{fl,im} \quad \text{to be consistent} \quad \mu_{nm}^{fl,+} \geq 0, \tag{3.52}$$

Flexibility as a Baseline Product

The imported/exported power of the MG are defined by the equations (3.26)–(3.27), and the following constraints are also included $\forall n \in \mathcal{T}, \forall m \in \mathcal{B}_{i'}^m$:

$$0 \geq -p_{nm}^{im} \quad \text{to be consistent} \quad \mu_{nm}^{im,+} \geq 0, \tag{3.53}$$

$$0 \geq -p_{nm}^{ex} \quad \text{to be consistent} \quad \mu_{nm}^{ex,+} \geq 0, \tag{3.54}$$

$$0 \geq \delta_{nm}^{Pim} \quad \text{to be consistent} \quad \mu_{nm}^{fl,im+} \geq 0, \tag{3.55}$$

$$0 \geq -\delta_{nm}^{Pex} \quad \text{to be consistent} \quad \mu_{nm}^{fl,ex+} \geq 0, \tag{3.56}$$

$$0 \geq -p_{nm}^{im} - \delta_{nm}^{Pim} \quad \text{to be consistent} \quad \mu_{nm}^{fl,im} \geq 0, \tag{3.57}$$

$$0 \geq -p_{nm}^{ex} - \delta_{nm}^{Pex} \quad \text{to be consistent} \quad \mu_{nm}^{fl,ex} \geq 0, \tag{3.58}$$

The term r_m^{flex} in (3.28) becomes

$$r_m^{flex} = \sum_{n \in \mathcal{T}_f} \pi_{flex}^{ex}\delta_{nm}^{Pex} + \pi_{flex}^{im}\delta_{nm}^{Pim}. \qquad \forall m \in \mathcal{B}_{i'}^m \tag{3.59}$$

3.2.4 Bilevel Optimization: DSO and MGs

The conversion of the bilevel problem into a single-level equivalent problem is accomplished by integrating the KKT conditions from the LL problem into the DSO's upper-level (UL) problem. The KKT conditions include all equality and inequality constraints of the LL problem, including the CS conditions associated with LL inequalities, as described in Sections 3.2.3. In addition, the KKT conditions include equality constraints derived from the partial derivatives of the LL Lagrangian function with respect to the LL primal variables, where these derivatives must equal zero. These conditions are represented by the equations (3.60)–(3.78), $\forall m \in \mathcal{B}_{i'}^m$, where T denotes the last time step of the dispatch period. It's noteworthy that all primal and dual variables of the LL problem become primal variables in the context of the single-level equivalent problem.

$$\frac{\partial \mathcal{L}}{\partial p_{nm}^{ch}} = 0 = -\lambda_{nm}^{PB} + \lambda_{nm}^{ch} - \mu_{nm}^{ch}, \qquad\qquad : \forall n \in \mathcal{T}, \quad (3.60)$$

$$\frac{\partial \mathcal{L}}{\partial p_{nm}^{dis}} = 0 = \lambda_{nm}^{PB} + \lambda_{nm}^{dis} - \mu_{nm}^{dis}, \qquad\qquad : \forall n \in \mathcal{T}, \quad (3.61)$$

$$\frac{\partial \mathcal{L}}{\partial x_{nmp}} = 0 = -P_{mp}^- \lambda_{mt}^- - P_{mp}^{dis} \lambda_{nm}^{dis} - SoE_{mp}^{dis} \lambda_{nm}^{SoE} - \lambda_{nm}^x - \mu_{nmp}^x, \quad : \forall n \in \mathcal{T}, \; \forall p \in \mathcal{P}, \quad (3.62)$$

$$\frac{\partial \mathcal{L}}{\partial y_{nmk}} = 0 = -P_m^+ \lambda_{nm}^+ - P_{mp}^{ch} \lambda_{nm}^{ch} - SoE_{mk}^{ch} \lambda_{nm}^{SoE} - \lambda_{nm}^y - \mu_{nmk}^y, \quad : \forall n \in \mathcal{T}, \; \forall k \in \mathcal{K}, \quad (3.63)$$

$$\frac{\partial \mathcal{L}}{\partial soe_{nm}} = 0 = -\lambda_{nm}^{BES} + \lambda_m^{start} + \lambda_{nm}^{SoE} + \overline{\mu}_{nm}^{SoE} - \underline{\mu}_{nm}^{SoE}, \qquad : n = 1, \quad (3.64)$$

$$\frac{\partial \mathcal{L}}{\partial soe_{nm}} = 0 = \lambda_{n,m}^{BES} - \lambda_{n+1,m}^{BES} + \lambda_{nm}^{SoE} + \overline{\mu}_{nm}^{SoE} - \underline{\mu}_{nm}^{SoE}, \qquad : \forall n \in \mathcal{T} \setminus \{1, T\}, \quad (3.65)$$

$$\frac{\partial \mathcal{L}}{\partial soe_{nm}} = 0 = \lambda_{nm}^{BES} - \lambda_m^{BES,end} + \lambda_{nm}^{SoE} + \overline{\mu}_{nm}^{SoE} - \underline{\mu}_{nm}^{SoE}, \qquad : n = T, \quad (3.66)$$

$$\frac{\partial \mathcal{L}}{\partial p_{nm}^{im}} = 0 = (\Lambda_n + C^{im}) \Delta t + \lambda_{nm}^{PB} + \mu_{nm}^{im,+} - \mu_{nm}^{fl,im}, \qquad : \forall n \in \mathcal{T}_f, \quad (3.67)$$

$$\frac{\partial \mathcal{L}}{\partial p_{nm}^{ex}} = 0 = -(\Lambda_n + C^{ex}) \Delta t - \lambda_{nm}^{PB} + \mu_{nm}^{ex,+} - \mu_{nm}^{fl,ex}, \qquad : \forall n \in \mathcal{T}_f, \quad (3.68)$$

$$\frac{\partial \mathcal{L}}{\partial p_{nm}^+} = 0 = -\frac{\Delta t}{E_m^{max}} \lambda_{n+1,m}^{BES} + \lambda_{nm}^+ - \mu_{nm}^+, \qquad : \forall n \in \mathcal{T} \setminus \{T\}, \quad (3.69)$$

$$\frac{\partial \mathcal{L}}{\partial p_{nm}^+} = 0 = -\frac{\Delta t}{E_m^{max}} \lambda_{n,m}^{BES,end} + \lambda_{nm}^+ - \mu_{nm}^+, \qquad : t = T, \quad (3.70)$$

$$\frac{\partial \mathcal{L}}{\partial p_{nm}^-} = 0 = -\frac{\Delta t}{E_m^{max}} \lambda_{n+1,m}^{BES} + \lambda_{nm}^- - \mu_{nm}^-, \qquad : \forall n \in \mathcal{T} \setminus \{T\}, \quad (3.71)$$

$$\frac{\partial \mathcal{L}}{\partial p_{nm}^-} = 0 = -\frac{\Delta t}{E_m^{max}} \lambda_{n,m}^{BES,end} + \lambda_{nm}^- - \mu_{nm}^-, \qquad : t = T, \quad (3.72)$$

$$\frac{\partial \mathcal{L}}{\partial \delta_{nm}^{Pim}} = 0 = (\Lambda_n + C^{im}) \Delta t + \pi_{flex}^{im} + \lambda_{nm}^{PB} + \mu_{nm}^{fl,im+} - \mu_{nm}^{fl,im}, \qquad : \forall n \in \mathcal{T}_f, \quad (3.73)$$

$$\frac{\partial \mathcal{L}}{\partial \delta_{nm}^{Pim}} = 0 = (\Lambda_n + C^{im}) \Delta t + \lambda_{nm}^{PB} + \mu_{nm}^{fl,im+} - \mu_{nm}^{fl,im}, \qquad : \forall n \in \mathcal{T} \cap \mathcal{T}_f', \quad (3.74)$$

$$\frac{\partial \mathcal{L}}{\partial \delta_{nm}^{Pex}} = 0 = -(\Lambda_n + C^{ex})\Delta t - \pi_{flex}^{ex} - \lambda_{nm}^{PB} - \mu_{nm}^{fl,ex+} - \mu_{nm}^{fl,ex}, \qquad\qquad : \forall n \in \mathcal{T}_f, \quad (3.75)$$

$$\frac{\partial \mathcal{L}}{\partial \delta_{nm}^{Pex}} = 0 = -(\Lambda_n + C^{ex})\Delta t - \lambda_{nm}^{PB} - \mu_{nm}^{fl,ex+} - \mu_{nm}^{fl,ex}, \qquad\qquad : \forall n \in \mathcal{T} \cap \mathcal{T}_f', \quad (3.76)$$

$$\frac{\partial \mathcal{L}}{\partial p_{nm}^{fl,im}} = 0 = \pi_{flex}^{Cap} - \mu_{nm}^{fl,+} - \mu_{nm}^{fl,Cap}, \qquad\qquad : \forall n \in \mathcal{T}_f, \quad (3.77)$$

$$\frac{\partial \mathcal{L}}{\partial p_{nm}^{fl,im}} = 0 = -\mu_{nm}^{fl,+} - \mu_{nm}^{fl,Cap}, \qquad\qquad : \forall n \in \mathcal{T} \cap \mathcal{T}_f'. \quad (3.78)$$

3.3 Case Study Setup

3.3.1 Test System

The performance of the proposed model is validated through a case study using the modified single-area IEEE RTS-96 system [32] for its transmission network, alongside a standard 33-bus radial distribution network [45] representing each connected distribution system. While our model could be extended to include real transmission [46] or distribution [47] networks, this aspect is deferred to future work. It's worth noting that in studies modelling both transmission and distribution networks, it is common to use test systems for at least one network level, as observed in [48]. The acquisition of detailed data for a real transmission network and all its downstream connected networks is a significant challenge, as such data are rarely readily available.

Three grid-connected MGs are positioned within the distribution network at the specified bus locations shown in Figure3.2, while their corresponding locations in the transmission network are shown in Figure 3.3. These MGs, located at Distribution Nodes 13, 18, and 30, are equipped with BESS with energy/power ratios of 17.2kWh/14.4kW, 25.9kWh/21.6kW, and 134.9kWh/111.76kW, respectively. Comprehensive data are available online in the "TSO-DSO coordination" folder[1] of the openTEPES model repository [5]. At each transmission node with a connection point to a distribution network, 10 standard distribution networks were assumed to be connected. Thus, a total of 80 distribution networks and 240 grid-connected MGs were considered throughout the system. The projected system load is 6783.37 MW, with 10% of this load distributed between the distribution networks and the grid-connected MGs. Notably, both system load and generation capacity were scaled up by a factor of 2.38 compared to the original data, facilitating the use of the test system for transmission expansion planning purposes. The existing transmission network consists of 33 lines and 5 power transformers, and the candidate network investments include the duplication of all network lines and transformers, the cost of which depends on the system. The flexibility activation period is from 16:00 to 20:00, which is in line with the activation periods requested by small to medium-sized companies offering flexibility [49].

[1]https://github.com/IIT-EnergySystemModels/openTEPES/tree/master/cases/TSO-DSO_coordination/RTS24a
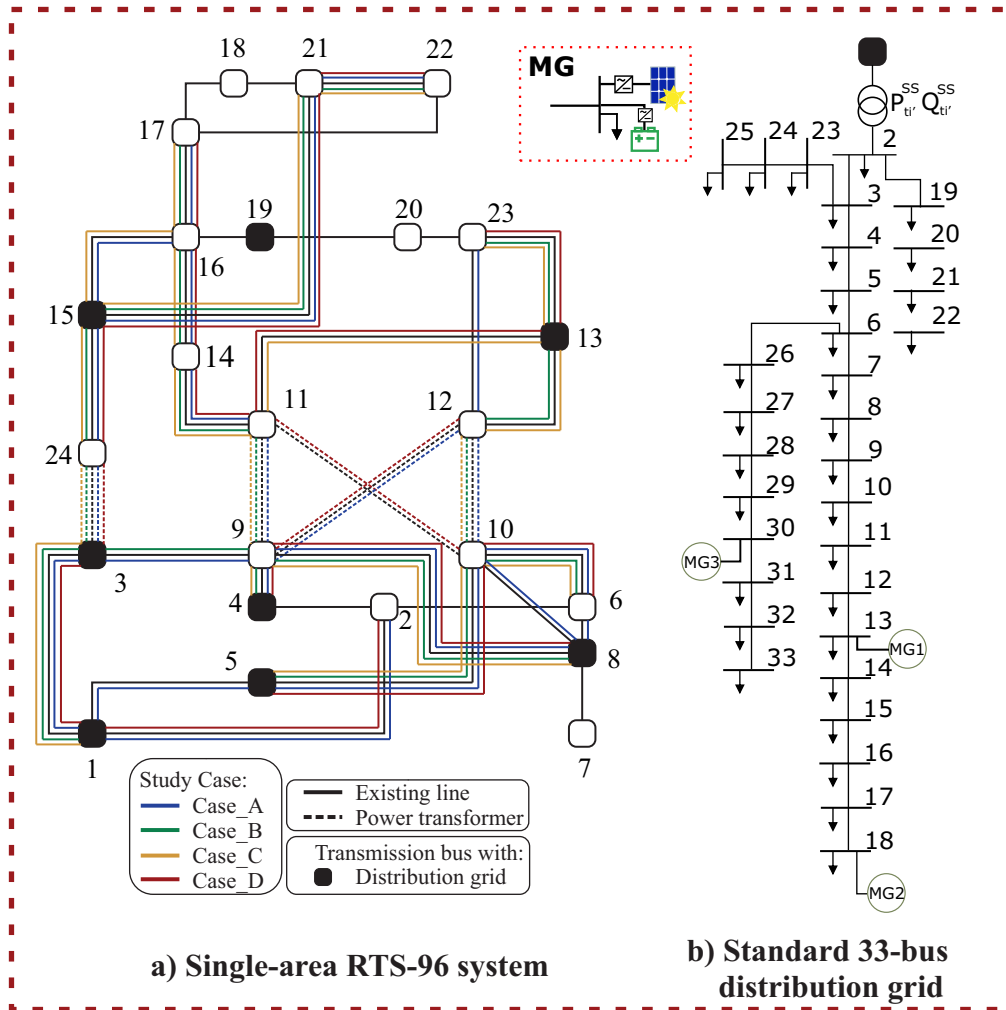
Fig. 3.2.: Representation of the network topology with single-line diagrams: a) for the RTS network, including investments per cases featuring FS-C; and b) for the modified 33-bus network with three grid-connected MGs. [Source: Author's own illustration]

Microgrid	Distribution Node	Distribution Grid	Transmission Node	Microgrid	Distribution Node	Distribution Grid	Transmission Node
MG1	13	DistGrid-1	1	MG13	13	DistGrid-5	8
MG2	18	DistGrid-1	1	MG14	18	DistGrid-5	8
MG3	30	DistGrid-1	1	MG15	30	DistGrid-5	8
MG4	13	DistGrid-2	3	MG16	13	DistGrid-6	13
MG5	18	DistGrid-2	3	MG17	18	DistGrid-6	13
MG6	30	DistGrid-2	3	MG18	30	DistGrid-6	13
MG7	13	DistGrid-3	4	MG19	13	DistGrid-7	15
MG8	18	DistGrid-3	4	MG20	18	DistGrid-7	15
MG9	30	DistGrid-3	4	MG21	30	DistGrid-7	15
MG10	13	DistGrid-4	5	MG22	13	DistGrid-8	19
MG11	18	DistGrid-4	5	MG23	18	DistGrid-8	19
MG12	30	DistGrid-4	5	MG24	30	DistGrid-8	19

Fig. 3.3.: Location of grid-connected MGs and distribution networks.

3.3.2 Cases

To address the research questions outlined in Section 3.1, four test cases have been established, each representing different configurations of the overall expansion and operation problem, as shown in Figure 3.4. The results obtained from these cases are compared to evaluate the influence of TSO-DSO coordination model selection and the provision of local flexibility on system expansion, operation, and associated costs. The provision of local flexibility through FSs is only considered in Case B and Case D. These two cases aim to investigate the relationship between the level of the flexibility price and the amount of local flexibility mobilised. In Case B, power exchanges between the TSO and the DSO networks are optimised, indicating efficient coordination between the operation and expansion of the transmission system and distribution operations, a concept called TSO-DSO coordination. However, in Case D, TSO-DSO power exchanges are determined solely based on decisions made at the distribution and MG levels, resulting in a lack of coordination between transmission expansion/operation and distribution operation, referred to as no TSO-DSO coordination. This is followed by a detailed description of the objectives and characteristics of each case, along with the mathematical formulation of the respective optimisation problems.

Case A

This case does not include BESS. Consequently, there are no dispatchable DERs or active MGs connected to the distribution grids. The power exchange at each interface between grids is determined solely by the downstream net load demand (including solar photovoltaic (PV) generation). Therefore, the power exchange at the boundary nodes between transmission and distribution, denoted as $p_{ni'}^{SS}$, is introduced as a parameter in the TEP problem (3.1) subject to constraints (3.2)–(3.10), facilitating the calculation of transmission expansion and operation along with associated costs, as illustrated in Figure 3.4.

Case B

In this case, the operation of the TSO's network, the DSO's networks and the MGs are jointly optimised and coordinated with the expansion of the TSO network. This optimisation takes into account the provision of local flexibility at the MG level. In particular, the objective function of the TSO problem is modified to incorporate the cost of flexibility.

$$\min \sum_{ijc \in \mathcal{L}^c} C_{ijc}^t \alpha_{ijc}^t + \sum_{ng} \Delta t C V_g p_{ng}^{tg} + \sum_{ni} \Delta t C^{shed} l_{ni}^{ens} + c^{flex}, \tag{3.79}$$

Within this case, two sub-cases are distinguished based on the type of FSs provided. First, one sub-case considers only the provision of FS-C, while the second sub-case focuses only on the provision of FS-B.

- In the FS-C case, the flexibility price π_{flex}^{Cap}, and the operation of the whole system and expansion of the TSO grid, are computed by solving the bilevel optimisation problem (3.79) s.t. (3.2)–(3.10), (3.13)–(3.24), (3.29)–(3.52), (3.60)–(3.72), and (3.77)–(3.78).

- In the FS-B case, the flexibility prices $\pi_{flex}^{im}/\pi_{flex}^{ex}$, and the operation of the whole system and expansion of the TSO grid, are computed by solving (3.11) s.t. (3.13)–(3.21), (3.25)–(3.27), (3.29)–(3.49), and (3.53)–(3.76).

It's important to note that the formulation of the above two problems includes the CS conditions of the LL inequality constraints.

Fig. 3.4.: Case studies considered to investigate the value of local flexibility and its impact on the transmission investments. [Source: Author's own illustration]

Case C

In this case, each MG optimises its energy dispatch without considering the provision of FSs, resulting in a modified MG's objective function:

$$\min f_m^{LL} = c_m^{im} - r_m^{ex}, \tag{3.80}$$

subject to constraints (3.29)–(3.49), not considering the CS conditions.

Solving each MG's problem yields the power exchange profile with the distribution network $(p_{nm}^{MG,ex} - p_{nm}^{MG,im})$. These profiles are used as input parameters in the distribution grid's power flow problem to compute the values of $p_{ni'}^{SS}$, $\forall i' \in \mathcal{B}_i^d$, as shown in Figure 3.4. Subsequently, these values serve as input parameters in the TEP problem, where transmission expansion and operation, along with associated costs, are determined. In particular, no coordination of network operation is considered at the interfaces between DSOs and MGs, or between TSO and DSOs.

Case D

In this case, the DSO coordinates with the MGs to jointly optimise the provision of local flexibility within the MGs. The goal is to reduce the DSO's peak power costs while minimising the net cost to each MG (see Figure 3.4). Two sub-cases are considered within this case:

- In the first one, only the FS-C is mobilised. Then, the flexibility price π_{flex}^{Cap}, and the operation of the DSO grid and MGs, are computed by solving the bilevel optimisation problem (3.11) s.t. (3.12)–(3.24) and (3.29)–(3.52), (3.60)–(3.72), and (3.77)–(3.78). In the second sub-case, only the mobilisation of the FS-B is considered.

- In the second sub-case, only the mobilisation of the FS-B is considered. Then, the flexibility prices $\pi_{flex}^{im}/\pi_{flex}^{ex}$, and the operation of the DSO grid and MGs, are computed by solving (3.11) s.t. (3.12)–(3.21), (3.25)–(3.27), (3.29)–(3.49), and (3.53)–(3.76).

The above problem formulations include the CS conditions of the LL inequality constraints. After solving them, $p_{ni'}^{SS}$ are computed for all $i' \in \mathcal{B}_i^d$. These values are then used as input parameters in the TSO expansion and operation problem (3.1) s.t. (3.2)–(3.10), facilitating the calculation of investment and operating costs corresponding to the mobilisation of the respective FS.

3.4 Simulation Results

This section discusses the results computed for the four test cases simulated using the test system described in Section 3.3. As mentioned above, for Case B and Case D, which consider FSs, the simulations were performed considering the mobilisation of FS-B and FS-C separately in two different sub-cases. The analysis of the results addresses the research questions stated in section 3.1. In particular, the comparison of the investment plan and the system costs for cases A & B allows us to answer the second and third research questions. In addition, the comparison of the BESS dispatch of the MGs in Cases B, C, & D allows us to answer the first research question.

3.4.1 The Role of the TSO-DSO Operation Coordination Model in the Dispatch of Local Flexibility Resources

This section discusses the management of MGs' energy resources and how this can be affected by flexibility dispatch. Figure 3.5 provides an example illustrating the difference in BESS' dispatch within MG20 between Case B and Case D, when it provides FS-C, w.r.t. that in Case C, where no flexibility service is provided (see Figure 3.5-c). In Cases B & D, the last discharge half-cycle of MG20's BESS occurs earlier during the flexibility activation period to provide flexibility to upstream connected systems. It's worth noting that flexibility is dispatched at 19:00-20:00 in Case B and at 18:00-19:00 in Case D (see Figure 3.5-a and Figure 3.5-b). This illustrates how the implementation of a TSO-DSO coordination scheme can change the output profile of flexibility resources to meet the specific needs of the transmission system.
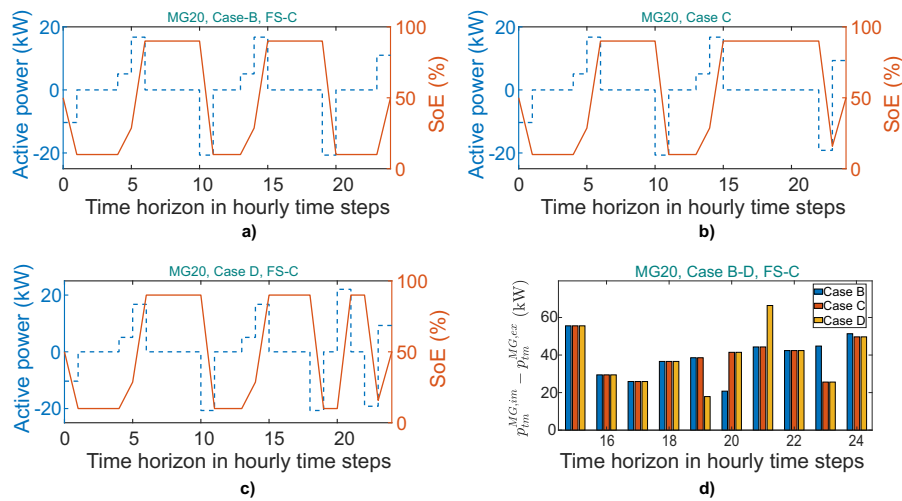
Fig. 3.5.: The BES dispatch of MG20: a) for Case B with FS-C, b) for Case C, c) for Case D with FS-C; and d) the MG's import power in Cases B-D. [Source: Author's own illustration]

In addition, Figure 3.5-d shows the change in the imported power of MG20 in Cases B & D. Right after the flexibility period in Case D, there is large increase in the imported power, as the earlier dispatch of flexibility leaves time for one more BESS cycle before the end of the day, which allows the MG to benefit from energy arbitrage. It should be noted, however, that having more frequent cycling of BESS can have a long-term cost related to the further degradation of these facilities, decreasing their lifetime.

3.4.2 The Impact of the Coordination Scheme on the Allocation, Amount, and Value of Local Flexibility

Table 3.1 shows the locations of the microgrids (MGs) that provide the flexibility service FS-C to the TSO in Case B. It is observed that all MGs located downstream of a transmission bus that requires additional flexibility provide FS-C.

Tab. 3.1.: Allocation of flexibility dispatch (Case B, FS-C).

Microgrid	kW	Distribution Node	Transmission Node
MG4	14	13	
MG5	21	18	3
MG6	107	30	
MG19	14	13	
MG20	21	18	15
MG21	107	30	
MG22	14	13	
MG23	21	18	19
MG24	107	30	

In contrast to Case B, where the TSO procures flexibility, in Case D, all DSOs utilise the flexibility provided by all MGs connected to their grids. The amount of flexibility each MG provides in either Case B or Case D, as shown in the table 3.1, depends solely on its location within the distribution system. In the considered case study, the local FSPs did not benefit from the provision of FS-B. Similarly, DSOs did not benefit from FS-B, as in Case D, no flexibility was procured from them and their operating costs were the same as in Case C However, in Case B, the dispatch of resources within some MGs changed with FS-B, although their costs remained unchanged compared to Case C. This adjustment in the dispatch of the MGs' BESS was aimed at supporting the TSO with local flexibility, without incurring additional costs or generating profit for the MGs. Therefore, while FS-B did not directly add economic value to the day-to-day operations of the MGs or the DSOs, it did benefit the investment costs and operations of the transmission system.

The flexibility value of FS-C depends on the choice of P_m^{Cap}, which is affected by the configuration of all connected grids. It should, therefore, be customised for each specific test system. In the bilevel formulation, these parameters are eliminated. Therefore, FS-C has been implemented as an addition of a penalty to the objective function (OF) of the FSPs and an income from the payment of this penalty to the OF of the TSO in Case B or the DSO in Case D. To understand this, set $P_m^{Cap} = 0$ to (3.22) and (3.50).

Furthermore, a sensitivity analysis performed on P_m^{Cap} only for Case D showed that when P_m^{Cap} was set equal to 25% of the capacity at the MG's connection points, the DSO and all MGs connected at nodes 13 & 18 had a daily economic value of flexibility of 0.2%, 0.8% and 1.8% of their total daily operating costs, respectively. However, the MGs at node 30 had higher costs. Considering that the installed BESS capacity at each distribution network corresponded to a conservative future scenario of BESS deployment, it is possible that with the integration of more BESS, this FS-C could provide an even higher economic value and potentially benefit all connected systems.

3.4.3 Impact of the Provision of Local FSs on the TEP

The performance of Cases A & B is assessed by comparing the total system operating and expansion costs for each case, as shown in Figure 3.6. In Case A, where neither MGs nor FSs are considered, the total system cost is significantly higher compared to all other cases.

Conversely, Case B emerges as the most cost-efficient option. In particular, Case B achieves a reduction in total system costs of 12% and 21%, respectively, compared to Case A when FS-B and FS-C are implemented. It's important to note that the RTS test system was deliberately stressed to incentivise investment by increasing electricity demand and generation while maintaining transmission capacity. The differences observed in the total system costs are mainly due to the avoidance of production from high-cost generation sources located close to the loads and to the reduction in the utilisation of congested lines, thus changing the power flows.
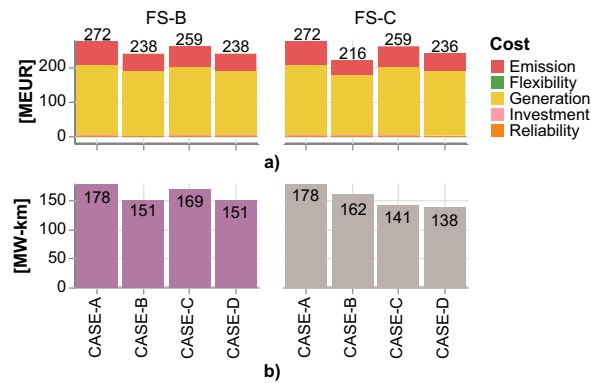
Fig. 3.6.: Expansion plans corresponding to each case: a) related to total expansion cost, and b) related to the total capacity per kilometer deployed. [Source: Author's own illustration]

Figure 3.7 shows the differences in the aggregated net distribution load per transmission node and hour of the day between Case A and Case B when FS-C is mobilised. The
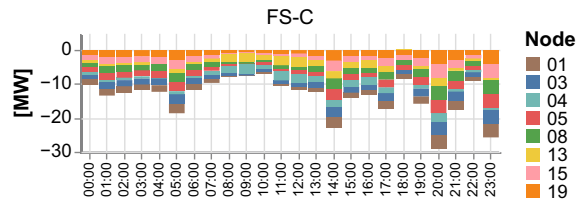
Fig. 3.7.: Comparison of load aggregated and power exchange per node in hourly time steps between Case A and Case B with FS-C, where the net load of Case A is subtracted by the net load of Case B. [Source: Author's own illustration]

comparison of these two cases shows a notable difference in the amount of net load at transmission nodes 1, 3, 5 and 8, where these differences amount 1.79 MW, 1.87 MW, 1.88 MW and 1.85 MW respectively. Interestingly, there are relevant network investments associated with these nodes, affecting lines 1-3, 3-24, 5-10 and 8-9, as shown in Figure 3.2-a. The pattern of changes in net demand due to the provision of local flexibility can be divided into two groups of nodes. In some transmission nodes, such as 4 and 13, the net load changes occur during the midday hours (10:00-12:00), while in others, such as 1, 3 and 5, the changes occur outside the midday hours. These patterns are related to the location of each node and the distribution of generation. Most of the low-cost generation is located in the northern area (i.e. nodes 11-24) of the transmission network, and the energy it produces is transported through large corridors to the southern area (i.e. nodes 1-10) via lines 21-22 and 9-11.

3.5 Conclusion

This chapter presents an optimisation model for the coordination framework of transmission system expansion, the operation of resources at the transmission and distribution levels, and the provision of local FSs. Two types of local FSs are modelled: 1) the baseline FS-B and 2) the capacity-constrained FS-C. The FSPs are grid-connected MGs at the distribution system level, and their interaction with the upper system levels is formulated as a bilevel optimisation problem. Based on the resulting formulation, four case studies were configured to address Research Question 3 (RSQ-3) presented in section 1.2 by investigating the value of local flexibility provided by DERs and the impact of this provision on transmission expansion planning.

The calculated results show that the mobilisation of both FSs leads to a reduction in transmission investment costs. The provision of FS-C was found to reduce the costs faced by the TSO to a greater extent than the provision of FS-B. It was also found that the provision of local FSs reduced transmission costs even in the absence of TSO-DSO coordination, as long as the required local flexibility was procured by the DSOs to support distribution system operations. Regarding the economic value of flexibility, it was shown that FS-B only benefited the TSO, while the costs of the DSO and the MGs remained unaffected under this FS. The economic value of FS-C is not straightforward as it depends on the choice of the capacity limit and the configuration of the connected networks and their resources.

In addition, the inclusion of local flexibility increases system efficiency by optimising the use of existing infrastructure and reducing congestion on the transmission system. The use of DERs allows for more efficient use of resources, such as avoiding the production of high-cost generation and reducing the use of congested lines. In addition, including DERs in transmission expansion planning promotes resiliency and reliability by decentralising generation and providing localised support in the event of grid disturbances.

In terms of planning outcomes, incorporating local flexibility not only reduces transmission investment costs, but also increases overall system resilience and efficiency. It allows the system to better accommodate fluctuations in demand and generation, reducing the need for costly infrastructure upgrades. In addition, by harnessing the capabilities of DERs, transmission expansion planning can become more flexible and responsive to evolving energy needs and technological advances.

Overall, accounting for local flexibility, particularly from DERs, adds significant value to transmission expansion planning by improving system efficiency, resiliency, and planning outcomes. It represents a paradigm shift toward a more integrated and sustainable energy system that leverages distributed resources to optimise grid operations and planning.

The Role of Utility-Scale Storage in the Optimal Flexibility Mix

<div style="text-align: right">4</div>

> *Users do not care about what is inside the box, as long as the box does what they need done*
>
> — **Jef Raskin**
> about Human Computer Interfaces

Declaration

This chapter is based on an unpublished work.

Declaration

I carried out all study elements and authored the initial draft. Co-authors edited and reviewed paragraphs, and validated some results.

4.1 Introduction and Literature Review

The ongoing energy transition, driven by the need to address climate change and integrate renewable energy sources (RES), is reshaping power systems worldwide. In this dynamic context, transmission expansion planning (TEP) has emerged as a critical component for ensuring the adequacy and efficiency of system operations. Unlike generation expansion planning, which is traditionally managed by generation companies (GENCOs) that invest in generation capacity for profit, TEP focuses on the efficient, sustainable and cost-effective supply of electricity and the seamless integration of RES into the grid. Integrating RES into power systems poses unique challenges due to their intermittent, stochastic nature; it requires robust and flexible transmission infrastructures for optimal power management in both spatial and temporal dimensions. To address these challenges, the authors in [50] proposed a robust optimisation approach for TEP that considers long- (5-10 years) and short-term (< 1 year) uncertainties to facilitate power flows from regions with excess generation to those with deficits. Similarly, the authors of [51] highlight the critical need for flexible transmission expansion planning systems to increase system flexibility and manage the dynamic characteristics of RES investments. They argue that traditional static planning

models are inadequate for modern needs and emphasise the importance of adopting more adaptive and responsive planning methods. Traditional TEP approaches have focused primarily on static demand forecasts and established generation patterns, often underestimating the transformative potential of modern solutions such as energy storage systems (ESS) and demand side management (DSM). These solutions are starting to play a vital role in addressing the challenges posed by the intermittent nature of RES. By storing excess energy or increasing consumption during periods of high generation and releasing or reducing the energy consumption during periods of high demand, ESS and DSM help to balance supply and demand, maintain frequency stability, and reduce the need for expensive and polluting peak load power plants, as well as reducing the needs for transmission capacity [52, 53].

However, in order to implement solutions that include an efficient mix of flexible technologies, it is important to determine the role of each in order to optimise their use and maximise RES generation. In this respect, determining the optimal size and location of ESS, such as batteries to be invested in by GENCOs, is critical. This depends on how much energy can be shifted through the application of DSM and the reinforcement and expansion of the transmission system. By considering these factors and optimally siting batteries, it is possible to improve system resiliency, reduce congestion, and increase overall system efficiency. As the authors of [54] show, DSM complements the operation of batteries, reduces the investment required of them and helps with their optimal placement and sizing, as demonstrated in a case study based on the Lombok electrical system in Indonesia. In addition, they found out that battery integration could help reduce total daily operation costs by up to 18.27% by avoiding curtailment of renewable energy, provided a significant number of batteries are located near large power generation centres or near residential areas with high electricity demand. Total costs over the weekend could be reduced by up to 33.63% through efficient battery placement.

In addition, Loschan et al. [55] examine the synergies and competition between various flexibility options, with a focus on Austria and Germany. The assessment covers several technologies contributing flexibility, including ESS such as batteries, DSM, and the use of hydrogen as an ESS. The study highlights the role of DSM in providing fast and cost-effective flexibility. However, its effectiveness largely depends on consumer behaviour, willingness to engage in collective management, and the availability of incentives for participation in DSM. Despite their high investment costs, which are likely to be reduced by economies of scale, batteries are essential for short-term storage, offering rapid dispatch capabilities to manage short-term grid flow fluctuations and aid DSM flexibility, especially on an inter-day basis. For weekly flexibility, they compete directly with the hydrogen sector coupling development, which involves the production, storage, and subsequent use of hydrogen as a primary resource for power generation[1].

Competitive dynamics between other flexibility elements like storage and transmission expansion emerge not only over time but also across regions. What is more, the synergies created between these elements increase socioeconomic welfare by reducing congestion,

---

[1]Note that this hydrogen production is decoupled from the hydrogen demand with potential use in other sectors.

individual stakeholder benefits, CO2 emissions, and renewable curtailment. Previous studies, such as [56], have quantified the individual benefits of energy storage and transmission investments. However, these benefits are affected by several factors, including investment, operating, and maintenance costs. The analysis is further complicated by the need to consider additional factors, such as the need to consider potential correlations, including negative ones, between the availability of flexibility from certain sources, such as the level of DSM participation in each country, and the availability of renewable resources (such as solar PV, wind, and hydro) in the countries. To address these additional complicating factors, this work considers a European scale system, considering multiple regions within countries with their respective profiles for renewable resources output.

In addition, the integration of batteries and H2 subsystems (such as electrolysers, hydrogen storage caverns, and H2 gas turbines) into transmission expansion planning introduces significant complexity and potentially impacts the synergies between these technologies due to their responsiveness and storage capacity. This study addresses this issue by examining the role of utility-scale storage solutions, including batteries and H2 subsystems. By reformulating a transmission expansion planning problem to include energy storage systems as investment options, this study seeks to determine the optimal mix of flexible resources to improve the overall system efficiency.

Moreover, this study also provides a comparative framework for conducting a quantitative analysis that assesses how the incremental and marginal value of the flexibility provided by each technology varies according to the system features, which are varied over a wide range of scenarios. Factors considered for scenario generation include the incremental deviation from the expected electricity demand, the DSM rates, and the pathway of maximum capacity additions for transmission and storage expansion (battery and H2 subsystems). This approach differs from previous studies in that it takes a more comprehensive approach to DSM modelling based on recent proposals and includes H2 subsystems. This results in a more thorough optimisation model that facilitates the assessment of the roles of batteries, hydrogen, and transmission lines. Furthermore, this comparative framework is applied at both national and European levels.

The expansion of the storage and transmission network and the operation of the system are formulated as a Mixed Integer Linear Programming (MILP) problem, considering investment decisions, commitment, start-up and shutdown of thermal generation units with binary variables. In line with previous studies, [55], this formulation considers the DC power flow model and various flexibility sources such as batteries, DSM, pumped storage, H2 subsystems, and transmission lines. The main research questions addressed in the work reported on here follow:

1. How does the combined value of these flexibility resources compare to that of the stand-alone deployment of storage, or other flexible technologies? Are stand-alone deployment scenarios feasible?

2. How does the integration of DSM, batteries, and H2 subsystems affect the optimal mix of flexible resources within transmission expansion planning?

3. How can the mathematical formulation of this problem be enhanced to consider the calculation of the value of storage, including factors such as its capacity and energy supply cost (price) arbitrage potential, within the transmission expansion planning framework?

The main contributions of this work are described below.

- A novel MILP optimisation model to address the TEP problem considering storage deployment. This model includes the sizing and computation of the optimal location of the batteries and H2 subsystems. This approach allows us to assess the flexibility of the system for each set of technologies available and the impact of the latter on both the required set of transmission upgrades and the overall system operation.
- A comprehensive analysis of the optimal flexibility provided by key technologies - such as transmission lines, batteries, DSM and H2 subsystems - through system expansion and operational comparisons under different scenarios. This includes an evaluation of utility-scale storage solutions within transmission expansion planning, focusing on the batteries and H2 subsystems, to determine their value and contribution to improving system flexibility and operational efficiency.

4.2 Model Formulation

The existing openTEPES model [5] has been modified to develop a new formulation that incorporates improvements in (a) system expansion and operation, (b) demand management, and (c) H2 subsystems. This new formulation adopts a static planning approach with 2030 as the target year. While a dynamic (multi-year) planning approach is conceptually straightforward, the model is constrained to a single target year due to the large size of the case study. Our investment planning problem considers both long and short-term uncertainties, which are critical and can be addressed using several techniques, such as robust optimisation or stochastic programming. These methods are essential to accurately represent various uncertainties affecting renewable energy production, policy decisions, fuel prices, demand forecasts, and sector coupling developments. However, accounting for these uncertainties is beyond the scope of this work.

This study focuses on determining the role, value, and impact of utility-scale storage, specifically batteries, and the use of hydrogen as an ESS, within the transmission expansion planning problem. The formulation developed considers an outline of the electricity system as that shown in Fig. 4.1, which includes both RES and thermal generation units. The thermal units represented may correspond to technologies such as nuclear, coal, oil, OCGT, and CCGT. As shown in the figure, this formulation also considers the existence and deployment of utility-scale batteries and CAES connected near demand centres, H2 subsystems consisting of electrolysers (power to H2) for hydrogen production, hydrogen storage, power plants that use H2 as fuel (H2 to power), and demand side management.

The formulation of each component of the overall model is described separately in this section. The detailed problem formulation for each test case, representing a specific coordination paradigm, is given in section 4.3.
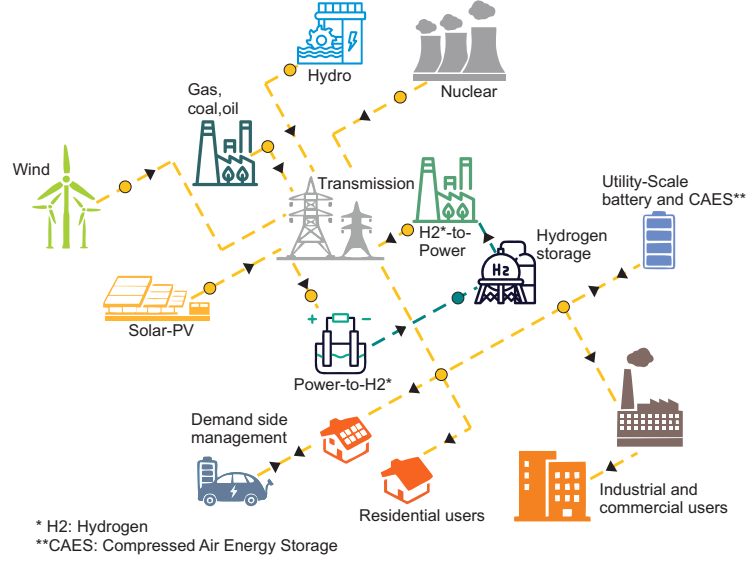
Fig. 4.1.: Representation of the electricity system architecture considered in the model formulation. [Source: Author's own illustration]

4.2.1 TEP Problem

The proposed formulation for the transmission planning problem is consistent with the basic TEP formulation presented in section 2.2. In this approach, network investment decisions are computed for future years, considering an hourly resolution for the expected system operation. User-defined candidate lines are specified in advance, allowing the model to determine optimal investment decisions from these predefined options using a DC-OPF linearized approximation. The detailed formulation of the TEP problem is described by the objective function in (4.1)-(4.2), subject to the constraints (4.3)–(4.25).

Objective Function

The objective in the problem formulated is to minimize the total cost, as expressed in (4.1). This includes both the investment costs (first term) and the operation costs associated with generation dispatch and load shedding (last two terms).

$$\min \sum_{ijc \in \mathcal{L}^c} C_{ijc}^t \alpha_{ijc}^t + \Delta t \left(\sum_n C_n^{gen} + C_n^{con} + C_n^{CO2} + C_n^{ens} \right). \tag{4.1}$$

$$C_n^{gen} = \sum_{g \in \mathcal{G}_i} (CV_g p_{ng}^{tg} + CF_g uc_{ng}) + C_g^{su} su_{ng} + C_g^{sd} sd_{ng}, \qquad : \forall n, \tag{4.2a}$$

$$C_n^{con} = \sum_{e \in \mathcal{G}_i} CV_e p_{ne}^{tc}, \qquad : \forall n, \tag{4.2b}$$

$$C_n^{CO2} = \sum_{g \in \mathcal{G}_i} P^{co2} E_g^{co2} p_{ng}^{tg}, \qquad : \forall n, \tag{4.2c}$$

$$C_n^{ens} = \sum_{i \in \mathcal{B}^t} C^{shed} l_{ni}^{ens} P_{ni}^d, \qquad : \forall n, \tag{4.2d}$$

The parameters C_{ijc}^t, CV_g, P^{co2}, E_g^{co2}, and C^{shed} denote the annualized fixed cost of a candidate line, the variable cost of electricity generation, the CO2 price, the CO2 emission rate associated with electricity generation, and the cost of unserved energy, respectively. Variable costs include fuel and operation and maintenance (O&M) costs. In addition, Δt represents the duration of the time discretisation step. The variables l_{ni}^{ens}, p_{ne}^{tc}, p_{ng}^{tg}, and the binary variable α_{ijc}^t represent load shedding, power consumption, power generation, and the decision to install candidate lines, respectively.

Constraints

Power Balance
The balance between generation and demand at each node, ignoring ohmic losses, is expressed in (4.3),

$$\sum_{g \in \mathcal{G}_i} p_{ng}^{tg} - \sum_{e \in \mathcal{G}_i} p_{ne}^{tc} - P_{ni}^d - l_{ni}^{ens} - \sum_{ijc \in \mathcal{L}} f_{nijc}^P + \sum_{jic \in \mathcal{L}} f_{njic}^P = 0, \qquad \forall ni, \; (4.3)$$

where the parameter P_{ni}^d represents the electricity demand, and the variable f_{nijc}^P represent the power flow on each line, respectively.

Power Flow Representation
The DC power flow equations for existing and candidate lines (following Kirchhoff's second law) are represented in (4.4).

$$\frac{f_{nijc}^P}{\overline{S}_{ijc}} = (\theta_{ni} - \theta_{nj}) B_{ijc} \frac{S_B}{\overline{S}_{ijc}}, \qquad \forall nijc, ijc \in \mathcal{L}^e \; (4.4)$$

The transfer capacity of candidate transmission lines conditioned by the investment decisions on these is represented in (4.5).

$$\left| \frac{f_{nijc}^P}{\overline{S}_{ijc}} - (\theta_{ni} - \theta_{nj}) B_{ijc} \frac{S_B}{\overline{S}_{ijc}} \right| \leq 1 - \alpha_{ijc}^t, \qquad \forall nijc, ijc \in \mathcal{L}^c \; (4.5)$$

$$- \alpha_{ijc}^t \leq \frac{f_{nijc}^P}{\overline{S}_{ijc}} \leq \alpha_{ijc}^t, \qquad \forall nijc, ijc \in \mathcal{L}^c \; (4.6)$$

Where $\overline{S}_{ijc}$ is the total transfer capacity of the line, and θ_{ni} and B_{ijc} represent the corresponding bus voltage angle and the susceptance of the line in per unit (p.u.), respectively. $\overline{S}_{ijc}$ corresponds to the big M value employed to represent the disjunctive constraint affecting the relationship between the voltage angles on the two ends of a candidate line and its flow depending on the investment decision made for it.

Power Generation Constraints
Electricity generation $p_{ng}^{tg}, \forall ng$ is classified into three types for modelling purposes, based on the primary resource used by it: variable renewable energy generation (VRE) (solar PV and wind), hydro, and thermal generation units. The electricity production of VRE units is limited by the maximum amount of primary resource available, which varies over time.

This is represented by considering the maximum amount of power generation allowed $\overline{P}_{ng}$ varying over time, and, therefore, depending on the operation hour (time step) considered and the generation unit concerned, as shown in (4.17).

Hydro units are further categorized into three types: run-of-river, reservoir, and pumped storage (PSH). Run-of-river hydro units are modelled similarly to VRE units, with water energy inflows limiting the maximum generation allowed for them. For reservoir hydro units, on the other hand, an energy storage site is considered, whose management requires accounting for inflows (rain) ei_{ne}, discharging p_{ng}^{tg}, and spillage s_{ne} variables. In this formulation, the amount of energy stored is quantified in terms of MWh of electricity rather than volumes of water for simplicity. PSH units are modelled similarly to reservoir units, but considering also a charging variable p_{ne}^{tc} representing the electricity consumption of the corresponding PSH unit when storing energy. The amount of energy stored in the reservoir for its later use is affected by the efficiency rate of the unit η_e.

Therefore, this charging variable is also included in the power balance constraint (4.3) and the objective function to take into account the O&M costs associated with the pumping activity. Thus, the general equation representing the management of energy for hydro units is defined in (4.7).

$$y_{n-\tau_e,e} - y_{ne} + s_{ne} + \sum_{n'=n-1}^{n} \Delta t' \left(ei_{n'e} - p_{n'e}^{tg} + \eta_e p_{n'e}^{tc} \right) = 0, \qquad : \forall ne, \quad (4.7)$$

The variable y represents the energy storage level of the hydro reservoir or PSH unit. The interval at which the storage level is checked and reported is one hour.

In addition, I impose the constraint that the storage site of a PSH unit cannot be charged and discharged at the same time. Traditionally, this is avoided using a binary variable for the operation of the storage. However, this could lead to a more complex formulation and result in higher computation times. Thus, this formulation considers a continuous storage model, according to equation (2.19c), which is based on [22], to separately consider charge and discharge variables and capacities, which are related to (4.8).

$$\frac{p_{ne}^{tg}}{\overline{P}_e} + \frac{p_{ne}^{tc}}{\overline{P}_e^c} \leq 1, \qquad : \forall ne, \quad (4.8)$$

Where $\overline{P}_e^c$ is the maximum power consumption of a PSH unit corresponding to the maximum pumping capacity.

The thermal generation units are represented considering their commitment and the energy block approach. Variable and fixed energy blocks are defined. The variable energy block is represented by the variable p_{ng}^{sg} affecting the electricity production variable p_{ng}^{tg}, which is computed in (4.9)-(4.11).

$$\frac{p_{ng}^{sg}}{\overline{P}_g - \underline{P}_g} \geq 0, \qquad : \forall ng, \quad (4.9)$$

$$\frac{\overline{p_{ng}^{sg}}}{\overline{P}_g - \underline{P}_g} \leq uc_{ng}, \qquad\qquad\qquad : \forall ng, \text{ (4.10)}$$

$$\frac{p_{ng}^{tg}}{\underline{P}_g} = uc_{ng} + \frac{p_{ng}^{sg}}{\underline{P}_g}. \qquad\qquad\qquad : \forall ng, \text{ (4.11)}$$

On the other hand, the logic applied to determine the unit commitment state of the thermal generation units involves considering the coupling uc_{ng}, start-up su_{ng}, and shut-down sd_{ng} variables, which are related through (4.12).

$$uc_{ng} - uc_{n-1,g} = su_{ng} - sd_{ng}. \qquad\qquad\qquad : \forall ng, \text{ (4.12)}$$

In addition, limits are imposed on the up and down ramps of the output of these units, taking into account their unit commitment state. These are expressed in (4.13)-(4.14).

$$\frac{-p_{n-1,g}^{sg} + p_{ng}^{sg}}{\Delta t R_{ng}^u} \leq uc_{ng} - su_{ng}, \qquad\qquad\qquad : \forall ng, \text{ (4.13)}$$

$$\frac{-p_{n-1,g}^{sg} + p_{ng}^{sg}}{\Delta t R_{ng}^d} \geq -uc_{n-1,g} + sd_{ng}, \qquad\qquad\qquad : \forall ng, \text{ (4.14)}$$

And, the minimum up and down time constraints for each committed unit are enforced according to (4.15)-(4.16).

$$\sum_{n'=n+1-T_g^u}^{n} su_{n'g} \leq uc_{ng}, \qquad\qquad\qquad : \forall ng, \text{ (4.15)}$$

$$\sum_{n'=n+1-T_g^d}^{n} sd_{n'g} \leq 1 - uc_{ng}. \qquad\qquad\qquad : \forall ng, \text{ (4.16)}$$

Note that equations (4.9)–(4.16) are a modified version of the set of equations (2.20) derived in section 2.3. This is needed due to the fact that the operating reserves are not considered in this formulation.

Compressed Air Energy Storage

Compressed Air Energy Storage (CAES) systems are modelled similarly to PSH units, representing their charging and discharging processes, and considering their storage capacity, and efficiency. In a CAES system, electrical energy is used to compress air and store it in an underground cavern or above-ground tank. During periods of high electricity demand, the compressed air is released, heated, and expanded in a turbine to generate electricity. The primary components of this include a compression system, a storage tank, an expansion system, and a heat management system. The energy required to charge the storage site p_{ne}^{tc} (compression) and the energy produced when discharging it p_{ne}^{tg} (expansion) can be computed by making use of efficiency-adjusted equations. The total round-trip efficiency of these devices η_e, which typically ranges from 40-70%, is the product of the compression and expansion efficiencies. In addition, the state of energy charge constraints (4.26) and the charge and discharge power limits (4.17)-(4.19) must be met to accurately represent

the operation of these resources. Considering these constraints and factors, the operation of CAES devices can be modelled within the energy storage and optimisation frameworks. These devices provide valuable flexibility and achieve an increase in the adequacy of the system. New CAES devices are not deemed to be deployed within the expansion computed here. The CAES devices considered across Europe must be an input in the problem.

Generation System Bounds

The bounds related to the generation and storage units are defined in (4.17)-(4.21).

$$\underline{P}_g \leq p_{ng}^{tg} \leq \overline{P}_g \qquad\qquad \forall ng, \ (4.17)$$

$$0 \leq p_{ne}^{tc} \leq \overline{P}_e^c \qquad\qquad : \forall ne, \ (4.18)$$

$$0 \leq y_{ne} \leq \Psi_e \qquad\qquad : \forall ne, \ (4.19)$$

$$0 \leq s_{ne} \qquad\qquad : \forall ne, \ (4.20)$$

$$uc_{ng}, su_{ng}, sd_{ng} \in \{0,1\}, \qquad\qquad \forall ng, \ (4.21)$$

Transmission System Bounds

The bounds on load shedding, transmission network transfer capacity, and the decision variables for line installation are defined in (4.22)-(4.24).

$$0 \leq l_{ni}^{ens} \leq P_{ni}^d, \qquad\qquad \forall ni, \ (4.22)$$

$$-\overline{S}_{ijc} \leq f_{nijc}^P \leq \overline{S}_{ijc}, \qquad\qquad \forall nijc, ijc \in \mathcal{L}^e, \ (4.23)$$

$$\alpha_{ijc}^t \in \{0,1\}, \qquad\qquad \forall ijc, ijc \in \mathcal{L}^c. \ (4.24)$$

Where $\underline{P}_g$ and $\overline{P}_g$ represent the minimum load and maximum power of each generator, respectively, while $\overline{S}_{ijc}$ is the maximum transfer capacity of a line. Additionally, the voltage angle of the reference node is set to 0 for each time step according to (4.25).

$$\theta_{n,node_{ref}} = 0. \qquad\qquad \forall n. \ (4.25)$$

4.2.2 Batteries and H2 Subsystems

Batteries Energy Storage Systems

Utility-scale battery energy storage (BESS) in this formulation is represented similarly to PSH, with the primary difference being that BESS do not have external energy inputs, such as hydro inflows, nor do they experience energy spillages. When BESS are considered as an investment option, the objective function must be modified accordingly. The following equations represent the operation of batteries:

$$y_{n-\tau_e,e} - y_{ne} + \sum_{n'=n-1}^{n} \Delta t' \left(\eta_e p_{n'e}^{tc} - p_{n'e}^{tg} \right) = 0, \qquad\qquad : \forall ne, \ (4.26)$$

Where the variables y_{ne}, p_{ne}^{tc}, and p_{ne}^{tg} represent the state of charge, the charging, and the discharging of the BESS, respectively. The parameter η_e denotes the efficiency of the system. The bounds for these variables are similar to those in equations (4.17), (4.18), and (4.19).

The energy balance is enforced as defined in (4.3), but the objective function (4.1) is modified as follows:

$$\min \sum_{e \in \mathcal{E}_i^c} C_e^{sto} \alpha_e^e + \sum_{ijc \in \mathcal{L}^c} C_{ijc}^t \alpha_{ijc}^t + \Delta t \left(\sum_n C_n^{gen} + C_n^{con} + C_n^{CO2} + C_n^{ens} \right). \tag{4.27}$$

Where the parameter C_e^{sto} represents the investment cost of a Battery Energy Storage System (BESS), while α_e^e is the binary variable representing the investment decision for a BESS. The objective function originally considers simultaneous investments in both BESS and transmission lines. However, if investments are limited to BESS, the expression of the objective function should be:

$$\min \sum_{e \in \mathcal{E}_i^c} C_e^{sto} \alpha_e^e + \Delta t \left(\sum_n C_n^{gen} + C_n^{con} + C_n^{CO2} + C_n^{ens} \right). \tag{4.28}$$

In addition, the following constraints must be enforced to represent the operation of the BESS units deployed in certain scenarios:

$$\frac{p_{ne}^{tg}}{\overline{P}_e} \le \alpha_e^e \qquad\qquad\qquad : \forall ne | e \in \mathcal{E}_i^c, \tag{4.29a}$$

$$\frac{p_{ne}^{tc}}{\overline{P}_e^c} \le \alpha_e^e \qquad\qquad\qquad : \forall ne | e \in \mathcal{E}_i^c, \tag{4.29b}$$

Where $\overline{P}_e$ and $\overline{P}_e^c$ are the maximum discharge and charge capacity of the BESS, respectively.

H2 subsystems

H2 subsystems, commonly known as Power-to-Hydrogen (P2H) or Hydrogen-to-Power (H2P), as shown in Fig. 4.1, are employed to produce hydrogen via electrolysis making use of excess electrical energy. This hydrogen can later be burned to produce electricity. This process is, thus, an alternative for energy storage considered in the proposed formulation. The primary devices involved in this process are electrolysers, hydrogen storage sites, and fuel cells or combustion turbines for the subsequent production of electricity. In the P2H phase, electricity is used to divide water into hydrogen and oxygen within electrolysers. The hydrogen produced can be stored in various forms, including compressed gas, liquid, or chemically bound materials. I assume that the amounts of electricity consumed and hydrogen produced in this process are linked through the production function below.

$$h_{nz}^{tg} = PF_z^P p_{nz}^{tc}, \qquad\qquad\qquad \forall nz, \tag{4.30}$$

Where z denotes the index of an electrolyser unit, which belongs to the set H_i, representing all the hydrogen units. The electricity consumption level of the electrolyser at the time step n is represented by the variable p_{nz}^{tc}, and the hydrogen production level is represented by h_{nz}^{tg}. The production function, denoted by PF_z^P in kWh/kgH2, varies according to the type of electrolyser employed.

On the other hand, when electricity demand is high, within the H2P process, the stored hydrogen is used to produce electricity using fuel cells [57] or gas turbines. Fuel cells

generally have higher efficiencies than gas turbines, especially in configurations that use waste heat. However, for simplicity, within this formulation, only gas turbines are considered to produce electricity from hydrogen. This is represented in (4.31).

$$p_{nx}^{tg} = PF_x^H h_{nx}^{tc}, \qquad \forall nx, \text{ (4.31)}$$

The hydrogen consumption of the gas turbine x ($x \in H_i$) is represented by the variable h_{nx}^{tc}, while the electricity production is given by p_{nx}^{tg}. The production function, denoted by PF_x^H in kgH2/kWh, varies according to the type of gas turbine used. As mentioned above, hydrogen is stored using tanks or caverns. These caverns are designed to feature a specific storage capacity, which is determined by certain parameters such as the allowed pressure inside and their efficiency. The efficiency of the storage system is given by η_e, where $e \in H_i$ represents the index of the H2 tank within the hydrogen units in the set H_i. The representation made of the storage and management of hydrogen in these tanks is similar to the representation made of the management of BESS in equation (4.26). In both cases, the management process represented involves monitoring and controlling the input and output of energy into and out of this site to ensure optimal performance and efficiency. The state of energy charge (SoE) of the hydrogen tank is denoted by $y_{ne}, \forall e \in H_i$, the energy charging (hydrogen consumption) variable of the tank by h_{ne}^{tc}, and the discharging variable by h_{ne}^{tg}. Then, the management of energy is given by (4.32).

$$y_{n-\tau_e,e} - y_{ne} + \sum_{n'=n-1}^{n} \Delta t' \left(\eta_e h_{n'e}^{tc} - h_{n'e}^{tg} \right) = 0, \qquad : \forall ne, \text{ (4.32)}$$

In addition to the previous equations, to complete the representation of the management of H2 subsystems in this formulation, it is important to redefine the energy balance equation to include the electricity consumption by the electrolyser and the electricity production of the turbines. This new equation is a modified version of the electricity balance in (4.3), and it is shown in (4.33).

$$\sum_{g \in \mathcal{G}_i} p_{ng}^{tg} + \sum_{x \in H_i} p_{nx}^{tg} - \sum_{e \in \mathcal{G}_i} p_{ne}^{tc} - \sum_{z \in H_i} p_{nz}^{tc} - P_{ni}^d - l_{ni}^{ens} - \sum_{ijc \in \mathcal{L}} f_{nijc}^P + \sum_{jic \in \mathcal{L}} f_{njic}^P = 0, \quad \forall ni, \text{ (4.33)}$$

And the hydrogen balance is given by (4.34).

$$\sum_{z \in H_i} h_{nz}^{tg} - \sum_{e \in H_i} h_{ne}^{tc} - \sum_{ijc \in P} f_{nijc}^H + \sum_{jic \in P} f_{njic}^H = 0, \qquad \forall ni, \text{ (4.34)}$$

The hydrogen balance includes several key components: the production of hydrogen by the electrolyser, the processes of storing into and extracting hydrogen from caverns, and the transportation of hydrogen f_{nijc}^H through a designated pipeline c. This pipeline connects nodes i and j, allowing the transportation of hydrogen both from the electrolyser to the cavern and from the tank to the turbine.

Furthermore, investments in H2 subsystems need to be represented. These investments are represented by making use of an investment decision variable α_n^e and an associated cost C_e^{sto}. These costs include investments in critical infrastructure, including the electrolyser, the preparation of caverns for storage, and a turbine. Both the investment decisions and their associated costs are included in the modified objective function in (4.27) if investments in

transmission lines and/or BESS are considered; otherwise the objective function to consider should be (4.28) still having the possibility to consider or not investments in BESS. In addition, the relationships between investment decisions and operation variables defined in (4.29) should be enforced.

4.2.3 Demand Side Management

Demand-side management (DSM) involves the implementation of strategies and the use of technologies to optimise energy use by adjusting electricity demand rather than changing supply. DSM results in an increase of energy efficiency, a reduction of peak demand, and contributes to the adequacy of the electric grid. However, only some consumers can manage their demand, as shown in Fig. 4.1.

DSM encompasses various methods aimed at optimising energy consumption patterns. These methods include demand response programs and the implementation of energy efficiency measures. DSM programs encourage consumers to reduce or shift their energy use during peak periods, often through dynamic pricing or direct control of appliances and equipment. This work focuses on the application of load-shifting techniques as the primary demand response strategy within DSM.

Load-shifting techniques aim to shift energy-intensive activities to off-peak hours, thereby smoothing demand fluctuations.

As proposed by the authors in [53, 55], the DSM is modelled by making use of a BESS. The charging capacity of this BESS depends on the demand profiles and the percentage of demand participating in the DSM program. Thus, the implementation of DSM is represented with the same equation as a BESS in (4.26). However, in this case, the upper bound ($\overline{P}_{ne}^c$) of the charging variable depends on the level of DSM participation (percentage of the demand involved in load shifting) as given by (4.35):

$$0 \leq p_{ne}^{tc} \leq \overline{P}_{ne}^c \qquad\qquad : \forall ne, \text{ (4.35)}$$

where $\overline{P}_{ne}^c$ is a percentage of the electricity demand P_{ni}^d at time step n. Note that the BESS e used to represent DSM is considered to be located at the same node as the corresponding demand.

The storage capacity of the BESS considered for DSM representation also varies over time and depends on the sum of the level of DSM participation in the corresponding hour and the several subsequent hours where energy consumption can be shifted to others. For example, the storage capacity in hour 1 would be the sum of the level of DSM participation (energy amount) in hour 1 plus the amount for this in hours 2, 3, and 4 if only energy consumption in these 4 hours can be jointly shifted to others. Thus, the upper bound (Ψ_{ne}) of the SoE of the BESS is limiting the amount of energy shifted and it is shown in (4.36).

$$0 \leq y_{ne} \leq \Psi_{ne} \qquad\qquad : \forall ne, \text{ (4.36)}$$

The storage capacity is calculated as follows: $\Psi_{ne} = \delta \sum_{n'=n+\sigma} P_{n'e}^d$, where δ is the percentage of the demand participating in DSM and σ is the number of shifting hours (for which energy can be jointly shifted to others).

In addition, any decrease in electricity consumption during a given day must be offset by the same increase in consumption within the same day. This ensures that the total daily electricity demand remains constant and prevents a decrease in the level of energy usage. This principle is enforced through (4.37).

$$\sum_{i=0}^{23} p_{n+i,e}^{tg} - p_{n+i,e}^{tc} = 0 \qquad : \forall ne|n \bmod 24, \quad (4.37)$$

4.3 Cases, Assumptions and Parameters Considered

This section describes the test system, the study cases and the assumptions used in: 1) the simulations to validate the performance of the proposed model, and 2) the comprehensive analysis of the optimal flexibility provided by transmission lines, batteries, DSM and H2 subsystems. The optimisation problems were formulated and solved using Gurobi 11.0.2, a commercial mixed integer programming (MIP) solver. The computations were performed on a computer equipped with a 3.40 GHz Intel Core i7-10875H processor and 64 GB of RAM. The simulation environment was set up using Python 3.12.3, with Pyomo 6.7.2 used to develop and solve the models.

4.3.1 Test System

The soundness of the proposed formulation is validated through its application to analyse a case study involving a European-scale transmission network with 84 nodes. The network nodes are derived from a clustering analysis performed as part of the e-highways2050 project[2]. This analysis involved classifying NUTS3 regions according to the NUTS 2021 classification[3] and combining similar regions into coherent groups. Data from the e-highways2050 database was used to develop the European-scale transmission network shown in Fig.4.2. This figure illustrates the existing network, which serves as the baseline for the network expansion planning analysis. The expansion planning is carried out for the year 2030, using a static planning approach and considering four representative weeks at an hourly resolution.

The expansion candidate line set consists of high-voltage alternating current (HVAC) and high-voltage direct current (HVDC) lines that connect different pairs of nodes in the European grid. These lines are predefined using the candidate discovery algorithm proposed in [58], which is described in the algorithm 1, depicted here. This algorithm identifies promising candidates by analyzing differences in marginal supply costs between network nodes and their respective distances. For the selected expansion candidates, the following characteristics are taken into account: line length, line capacity, resistance, reactance, voltage level, and investment cost. The set of expansion candidates is common to all the executions within the case study.

---

[2]See: https://docs.entsoe.eu/baltic-conf/bites/www.e-highway2050.eu/e-highway2050/
[3]See: https://ec.europa.eu/eurostat/web/nuts/background
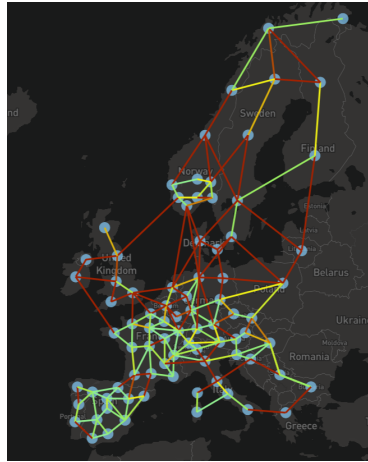
Fig. 4.2.: European-scaled transmission network. [Source: Author's own illustration]

Algorithm 1 Candidate discovery algorithm

Data: Existing transmission network

Result: Reduced set of candidate lines

Initialization: The set of candidate lines preliminarily selected for their installation is initialized to the empty set (LC=0) The set of candidates preliminarily chosen for their installation in the previous iteration (PCI) is initialized to any non-empty set, just to allow the algorithm to start running

While The PCI set is not empty ($PCI > 0$) **do**

1. Set all the candidates included within LC as existing lines (LC)

2. Solve the economic dispatch (ED) problem for the updated network topology just defined

3. Search for additional promising candidates as shown in [58]

4. Solve the relaxed expansion planning problem (LP) considering as candidates all the promising ones identified in the previous step and as already existing lines all those lines already included in set LC

5. Solve the discrete reduced problem (MIP)

   • Considering as candidates the promising ones that were deployed, at least for a certain fraction of their capacity, in the previous step, and all those already included in set LC as existing lines

6. Make the set PCI equal to the set of promising candidates who are deployed in the previous step

7. Add the PCI set to the set of candidate lines already chosen preliminarily for their installation: LC = LC + PCI

Solve the complete, discrete, problem considering as candidates all those preliminarily chosen for their installation (those within set LC) to compute the expansion of the grid.

The electricity generation capacity by technology and region for 2030 is drawn from the results included within the Techno-Friendly Pathway developed by the GENESyS-Model [59], available at this URL: `https://zenodo.org/doi/10.5281/zenodo.7997297`. The charging and discharging capacities of BESS are also data drawn from this pathway. Their storage capacity is determined by multiplying the charging capacity of each specific BESS by 4, corresponding to the number of full storage hours assumed for BESS. This amount has been set to consider BESS devices that could provide the same type of flexibility (short-term) as DSM, since this study considers a 4-hour DSM shift. For the H2 subsystems, their hydrogen and electricity production capacities are also drawn from data included within the same pathway. The hydrogen storage capacity is calculated by multiplying the hydrogen production capacity by 168 hours (one week). This amount of hours of storage capacity has been set to consider hydrogen storage providing flexibility in the same time range as water storage and PSH. The full data set considered is also available online at the following URL `https://zenodo.org/doi/10.5281/zenodo.8065982`.

4.3.2 Expansion Pathways

To address the first and second research questions outlined in section 4.1, fifteen transmission and storage expansion pathways are considered in the context of the overall expansion and operation problem. Results are computed for all the pathways and compared to assess the impact of the pathway selection on the system expansion, operation, and the associated costs. Besides, different sets of results are computed for different combinations of flexible technologies available for the deployment, to assess the impact of the set of flexible technologies on the expansion, operation and cost results.

Table 4.1 summarizes the features of the different pathways based on the types of investments allowed within them, where options include international and/or national transmission lines, BESS, and H2 subsystems. Each pathway represents a unique strategy for expanding and optimising the energy system. The pathways differ in their focus on individual or combined investment options potentially including transmission infrastructure, BESS, and H2 subsystems. For transmission investments, the sets of candidate transmission lines considered play a critical role in shaping the pathways' results. By evaluating different combinations of investment options related to national and international lines or interconnections, the impact of different infrastructure development strategies on the energy system development and operation can be assessed.

National network investments make it possible to strengthen the internal grid, improving its adequacy, and facilitating the integration of renewable energy sources within the country. New international lines enable an increase in cross-border electricity exchanges, which can enhance energy security, optimise resource utilization, and reduce costs by increasing the level up to which infrastructure is shared. Exploring these configurations helps one to identify the most effective strategies for meeting future energy needs and achieving sustainability goals.

Tab. 4.1.: Expansion pathways.

| Pathway | Investment type | | | |
	National Line	International Line	BESS	H2 subsystem
1	✓	-	-	-
2	-	✓	-	-
3	✓	✓	-	-
4	-	-	✓	-
5	-	-	-	✓
6	-	-	✓	✓
7	✓	-	-	✓
8	-	✓	-	✓
9	✓	✓	-	✓
10	✓	-	✓	-
11	-	✓	✓	-
12	✓	✓	✓	-
13	✓	-	✓	✓
14	-	✓	✓	✓
15	✓	✓	✓	✓

For all the pathways, I consider the deployment of additional flexibility, but only for four of them (Pathways 1, 2, 4, and 5) I do not allow the joint deployment of several flexible technologies to assess the potential synergies among them and compute the optimal amount of flexibility to be mobilized by each through the appropriate amount of capacity for this being deployed. For example, Pathway 15 uniquely optimises the size and location of transmission and storage investments simultaneously, ensuring the efficient coordination of the expansion of transmission, BESS and H2 subsystems. This integrated approach is referred to as TEP-SEP coordination.

In contrast, pathways 1, 2, 4 and 5 follow a decoupled TEP-SEP approach whereby investments in transmission lines, BESS, and H2 subsystems are determined independently. These may lead to suboptimal results due to a lack of coordination in the expansion planning for several technologies. These may lead to a reduction of adequacy levels or may result in higher costs and lower operational efficiency compared to the integrated approach in Pathway 15.

The analysis of these pathways provides valuable insights into how different approaches to providing flexibility and coordinating investments affect the overall efficiency, adequacy, and cost-efficiency of the system. The integrated approach in Pathway 15 is expected to deliver superior results by reducing overall system costs, increasing operational flexibility, and ensuring better resource allocation through simultaneous optimisation. This pathway highlights the importance of implementing coordinated investment strategies to achieve a more resilient and economically efficient energy system.

In addition, the comparison carried out highlights the advantages and trade-offs associated with each planning strategy. For example, pathways that focus solely on BESS or H2 subsystems deployment (such as paths 4 and 5) may lead to low-adequacy levels or may have specific advantages in terms of the provisioning of targeted flexibility, but may miss out on the synergistic benefits of integrated planning. Similarly, paths that include transmission investments (paths 7 to 15) provide insights into how transmission lines can complement

storage solutions to increase system flexibility. A detailed description of the goal and characteristics of each path is provided next, along with the mathematical formulation of the associated optimisation problems.

Pathways 1-3

This pathway illustrates the traditional approach to transmission expansion planning, which does not consider investments in BESS or H2 subsystems. The goal is to develop an optimal transmission investment plan without considering these complementary flexible solutions. The problem is formulated mathematically as (4.1) subject to the constraints (4.2)–(4.25).

Pathway 4

This pathway does not include additional investments in transmission lines or H2 subsystems. Therefore, BESS are the only investment candidates. The transmission network and generation capacities are assumed to be those computed by GENESyS-Mod [59]. Thus, the optimisation problem is defined by the objective function within equation (4.28) subject to the constraints (4.2)–(4.4), (4.7)–(4.25), (4.26) and (4.29) to calculate the expansion of storage, the system operation, and the associated costs.

Pathways 5-6

These pathways share a common limitation: additional transmission investments are not allowed. The main distinctive pathway is number 6, where additional investments in BESS are allowed. The formulation of equation (4.26) is quite similar to that of (4.32), except for the fact that the parameters and variables are represented differently for BESS and H2 management. Consequently, for both paths, the same problem formulation is considered, comprising the objection function in equation (4.28), subject to constraints (4.2), (4.4), (4.7)–(4.25), (4.29) and (4.30)–(4.34).

Pathways 10-12

These pathways are similar to pathways 1-3, with one key difference: the inclusion in the former of transmission lines as potential investment candidates. This strategy allows the system to achieve better coordination and larger synergies between investments in transmission and BESS. The problem is formulated as the objective function in (4.27), subject to (4.2)–(4.25), (4.26) and (4.29). This formulation supports the coordinated development and operation of the transmission and storage systems to minimize the system costs.

Tab. 4.2.: Electricity demand increases and DSM participation levels considered in each of the scenarios defined

| Scenario | Scenario denominations | |
	Demand Increase [%]	DSM Participation [%]
1	0	0
2	0	10
3	0	20
4	2.5	0
5	2.5	10
6	2.5	20
7	5	0
...	...	...
12	7.5	20

Pathways 7-9 and 13-15

These pathways are analogous to pathways 5 and 6, respectively, with the main difference between the two sets being the inclusion of additional transmission investments as candidates in the former. This facilitates the coordination between TEP and SEP. This coordination problem can be addressed taking (4.27) as the objective function, subject to the constraints (4.2)–(4.25), (4.29), and (4.30)–(4.34). This integrated approach improves the level of coordination between the expansion of the capacity of these technologies and leverages larger synergies between transmission and storage investments.

4.3.3 Scenarios

Within the pathways, several scenarios were developed to illustrate different potential outcomes for different possible combinations of two key factors: demand growth and DSM participation. These factors play a critical role in shaping the system needs and functioning. DSM is a key strategy for increasing the flexibility of the power system, while demand increases increase the system expansion needs and affect the system operation. These factors affect the potential contribution of key technologies, making this more or less relevant depending on the scenario. Understanding these variations is essential for strategic planning, as this guides the evaluation and selection of technologies under different technological and socio-economic conditions.

To accurately model the impact of varying demand and DSM participation on strategic decisions under different techno and socio-economic conditions, scaling factors are applied to both the baseline DSM and demand values. Specifically, electricity demand is adjusted using scaling factors of 0%, 2.5%, 5%, and 7.5%, based on [53], while DSM participation is adjusted applying factors of 0%, 10%, and 20%, as shown in Table 4.2. The approach followed has allowed me to comprehensively analyse how changes in electricity demand and DSM participation affect strategic planning.

The impact of the scenario features on the development and operation of the energy system is multifaceted. Higher electricity demand typically requires more capacity of both generation and transmission infrastructure, potentially increasing costs and requiring greater investment in these technologies. Conversely, increased DSM participation can relieve some
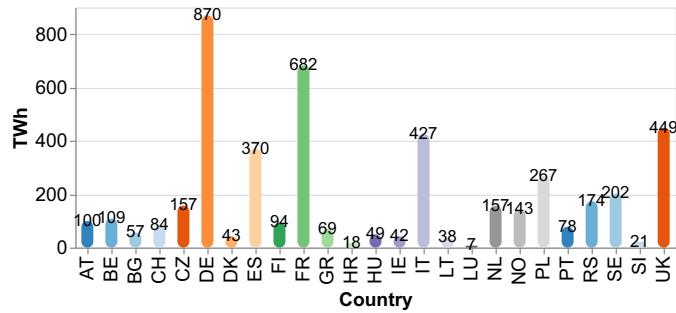
Fig. 4.3.: Baseline electricity demand in TWh/year per country in the year 2030. The total system demand is 4538 TWh/year. [Source: Author's own illustration]

of the pressure on the system by smoothing peak demand and allowing a more efficient use of existing resources to take place. This can reduce operation costs and defer investments in new capacity.

The baseline values for electricity demand in 2030 come from the dataset available at this URL: `https://zenodo.org/doi/10.5281/zenodo.7997297`. These values, shown in Figure 4.3, represent the annual aggregated electricity demand projections of the European system for 2030. These figures also affect the potential impact that DSM participation could have on the coordinated expansion planning and operation of the European system, given the relative distribution of electricity demand across countries. These baseline values serve as the reference point for modelling demand growth and calculating DSM participation. DSM participation, including the size of it, is modelled in equations (4.35) and (4.37). Demand shifts are assumed to take place over a 4-hour period.

As a result, 12 different scenarios have been defined. Together with the pathways defined, these result in a total of 180 combinations of pathways and scenarios explored, which requires solving the 180 resulting optimisation problems representing the European power system, including its transmission network. This analysis covers a wide range of variations in the electricity demand and the DSM potential in the 2030 time horizon.

4.4 Simulation Results

This section provides and discusses the results of the 180 simulations performed for the European system described in section 4.3.1. As mentioned above, simulations for pathways 4-6, excluding candidate lines, have been run separately. For all the remaining pathways, all 36 scenarios have been evaluated preliminarily. The scenarios further explored have been further reduced to those that yield feasible solutions, i.e. those for which non-served energy (NSE) levels are zero. Scenarios considering insufficient options or investment candidates to meet future system needs have been labelled accordingly. Figure 4.4 shows a heat map indicating that scenarios that exclude international lines as candidates result in relevant amounts of unserved energy. For example, stand-alone scenarios where network investments only include national lines, BESS, or H2 subsystems as candidates result in large amounts of NSE. Similarly, scenarios featuring only national lines + H2 subsystems

Electricity Unserved

Demand and DSM Increase [%]	2. LineInt	3. Line	8. LineInt-H2	9. Line-H2	11. BESS-LineInt	12. BESS-Line	14. BESS-LineInt-H2	15. BESS-Line-H2	10. BESS-LineNat	13. BESS-LineNat-H2	1. LineNat	7. LineNat-H2	4. BESS	6. BESS-H2	5. H2
0.0-0.0	0	0	0	0	0	0	0	0	2	2	15	14	15	15	31
0.0-10.0	0	0	0	0	0	0	0	0	1	1	11	11	14	14	28
0.0-20.0	0	0	0	0	0	0	0	0	1	1	9	9	13	13	25
2.5-0.0	0	0	0	0	0	0	0	0	3	3	20	19	24	24	44
2.5-10.0	0	0	0	0	0	0	0	0	2	2	16	15	23	23	41
2.5-20.0	0	0	0	0	0	0	0	0	2	1	13	12	23	23	39
5.0-0.0	0	0	0	0	0	0	0	0	5	5	27	26	33	33	59
5.0-10.0	0	0	0	0	0	0	0	0	4	4	23	22	33	33	55
5.0-20.0	0	0	0	0	0	0	0	0	3	3	20	19	32	32	52
7.5-0.0	0	0	0	0	0	0	0	0	9	9	39	37	43	43	81
7.5-10.0	0	0	0	0	0	0	0	0	7	7	32	30	42	42	75
7.5-20.0	0	0	0	0	0	0	0	0	6	6	28	27	42	42	70

TWh (color scale: 0 – 20 – 40 – 60 – 80)

Investment options

Fig. 4.4.: Electric energy non served in TWh/year. [Source: Author's own illustration]

or BESS + H2 subsystems as investment options result in large amounts of NSE as well. Those scenarios featuring national lines + BESS or national lines + BESS + H2 subsystems as investment candidates result in small amounts of NSE for some regions and hours, but they are still discarded from the analysis for security of supply reasons. Consequently, the 180 combinations of pathways and scenarios originally defined to be explored, leading to 180 simulations, have been reduced to 96, in all of which at least international lines are considered as investment options. These combinations do not result in relevant levels of non-supplied electricity.

In addition, two observations can be made regarding the impact of demand on the amount of NSE. First, increasing the DSM participation levels to larger ones, 10% or 20%, leads to slightly lower levels of unserved energy in those scenarios where this is present. Second, the increase in the level of demand contributes significantly to the increase in unserved energy. For example, in the pathway where only H2 subsystems are considered as candidates, there is 31 TWh of unserved energy for the reference demand level and 0% DSM participation, which increases to 81 TWh with a 7.5% increase in demand, other features being equal.

The results for the several pathways and scenarios are analyzed using a comparative framework to address the first two research questions defined in Section 4.1. This analysis is conducted for the 96 simulations, which include the following expansion pathways, characterized by the technologies considered for expansion in them:

- 2. International lines
- 3. International and national lines
- 8. International lines + H2 subsystems

- 9. International and national lines + H2 subsystems
- 11. International lines + BESS
- 12. International and national lines + BESS
- 14. International lines + BESS + H2 subsystems
- 15. International and national lines + BESS + H2 subsystems

The framework used to assess each pathway includes several metrics, classified into annual cost comparisons, individual key performance indicators (KPIs), and comparative KPIs, as shown in Table 4.3. These KPIs refer to the achievement of specific objectives. They allow one to assess the magnitude and duration of the impact of the deployment of DSM, BESS, and H2 subsystems, thereby addressing the first research question (RSQ1). In addition, these KPIs are used to evaluate the economic value and functional performance of each flexibility asset (BESS, H2 subsystems, and lines), which is the focus of the second research question (RSQ2).

Tab. 4.3.: Types of metrics/KPI and their assessment objectives.

	Impact (RSQ1)	Value (RSQ2)	
	Magnitude	Economic	Function
Metric	✓	✓	✓
Individual KPI	✓	-	-
Comparative KPI	✓	✓	-

In this sense, the following subsections provide an in-depth analysis of the contributions of flexibility technologies to the energy system. Section 4.4.1 examines the impact of DSM, BESS and H2 subsystems on key system performance metrics such as additional storage and grid capacity, renewable integration and grid reinforcement needs. Section 4.4.2 shifts the focus to the economic value of these technologies, highlighting their cost-effectiveness, operational benefits and role in optimising system investments under different scenarios. Together, these sections aim to highlight the strategic importance of these technologies in achieving a resilient and efficient energy system.

4.4.1 Impact of the DSM, BESS and H2 Subsystems

This section presents the results of an analysis aimed at determining the impact of various flexible technologies- namely DSM, BESS, and H2 subsystems-on the optimal mix of flexibility resources and the generation unit dispatch. The analysis is organized into subsections, each focusing on the specific impacts of DSM, BESS, and H2 subsystems for different demand scenarios, DSM deployment rates, and pathways. Table 4.4 shows the metrics and key performance indicators (KPIs) used in this assessment.

These KPIs are divided into individual and comparative metrics at both European and national levels. Individual KPIs are used to separately assess each expansion pathway, while comparative KPIs highlight the differences and similarities among the expansion pathways. M-1, M-2 and KPI-3 are used to determine the impact of DSM, while the remaining metrics and KPIs assess the impact of the BESS and H2 subsystems.

Tab. 4.4.: Individual and comparative KPIs at European and national levels to measure the impact of technologies providing flexibility.

Index	Metrics/KPI	Individual		Comparative	
		European	National	European	National
M-1	Total additional storage capacity[1]	✓	✓	-	-
M-2	Total additional grid capacity[2]	✓	✓	-	-
KPI-3	Total additional grid capacity/total additional storage capacity[1]	✓	-	-	-
M-4	Reduction in the network capacity needs due to storage deployment	-	-	✓	✓
M-5	Variable renewable generation[3]/total generation (minus DSM)	-	-	✓	✓
KPI-6	RES curtailment reduction/Total additional storage capacity[1]	-	-	-	✓
KPI-7	Grid investment reduction[4]/Total additional storage capacity[1]	-	-	✓	✓
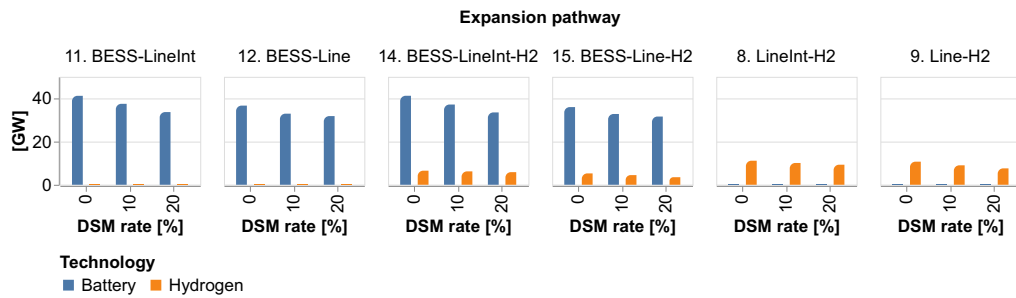
Fig. 4.5.: M-1: Total additional storage capacity deployed per technology for each pathway and DSM rate. [Source: Author's own illustration]
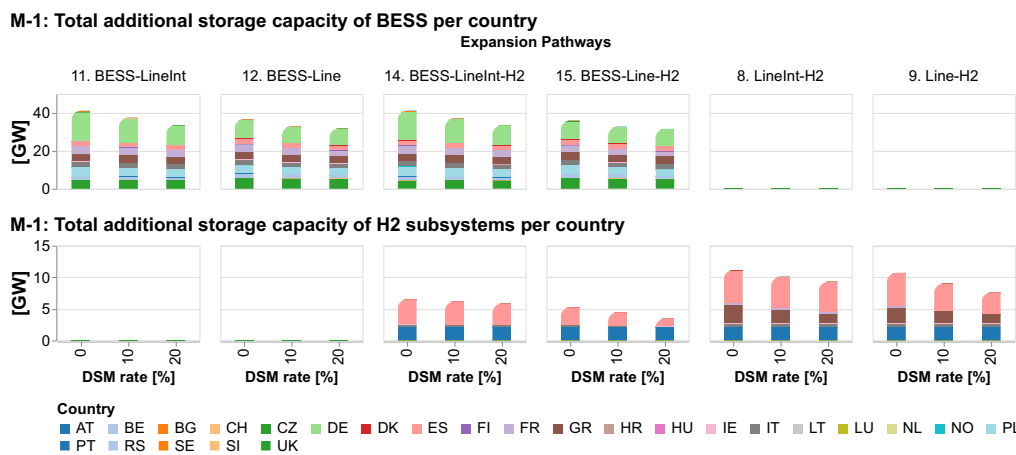
Fig. 4.6.: M-1: Total additional storage capacity per technology and country for each pathway and DSM rate. [Source: Author's own illustration]

Impact of the DSM

The impact of DSM is evaluated using M-1, M-2, and KPI-3. Figure 4.5 shows the values for M-1 across different technologies, DSM rates, and expansion pathways. The increases in the demand domain are aggregated into the average value in order to focus on the impact of DSM. Then, it is observed that increases in DSM participation rates, from 0% to 20%, lead to reductions in the level of storage deployment, ranging from 6% to 14% for BESS and 5% to 12% for H2 subsystems. These differences are consistent across all the pathways, with a more pronounced effect for BESS.
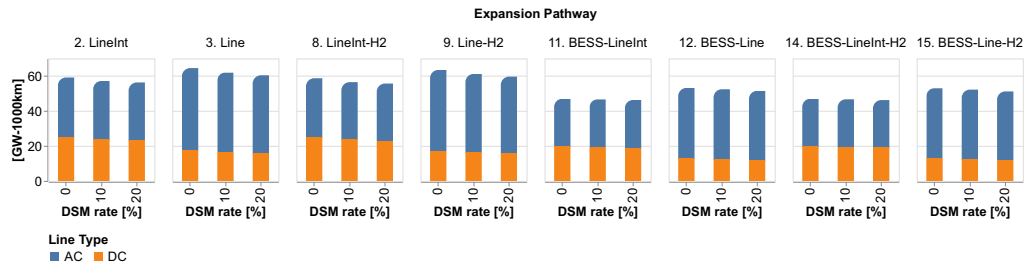
Fig. 4.7.: M-2: Total additional grid capacity per technology. [Source: Author's own illustration]

Figure 4.6 shows the distribution of investments by country per pathway and DSM rate. Battery investments are mainly concentrated in Germany (DE), Spain (ES), France (FR), Greece (GR), Italy (IT), Poland (PL), Serbia (RS) and the United Kingdom (UK). In contrast, new H2 subsystems are mainly deployed in Spain and Portugal (PT), with a smaller presence in Italy. This trend is related to the geographical position of Spain and Portugal in Europe and their potential for local storage deployment, as an alternative to importing energy from Central Europe. The impact of DSM is evident, with higher DSM rates leading to lower investment levels. For example, new battery capacity deployed in Germany decreases by 30%, while H2 subsystem capacity deployed in Greece decreases by 40%, with an increase from 0% to 20% in the DSM rate.

Figure 4.7 shows the total additional grid capacity required (in GW-1000 km) for each path and DSM rate. The figure shows that the DSM rate has a minimal effect on the required grid capacity, in contrast to its significant effect on the deployment of additional storage capacity, as shown in Fig.4.5. Conversely, storage deployment has a significant impact on reducing the additional grid capacity required. The overall reduction in grid capacity can reach up to 5% when H2 subsystems are deployed alongside transmission lines and up to 30% when BESS is considered, as shown by comparing the bars for paths 3 and 12 in Fig.4.7. This observation holds regardless of whether the additional network capacity is allocated within AC or DC networks.

In light of this finding, Figures A.1 and A.2 in the appendix A.1 provide, not only the additional network capacity needed at the national and international levels, but also the allocation of this to AC and DC networks, averaged over demand growth. National grid investments in AC networks occur mainly in Spain (ES-ES), Italy (IT-IT) and, significantly, in the French AC network. For AC lines, additional capacity is mainly needed between Germany and Denmark (DE-DK), Germany and Poland (DE-PL) and Spain and France (ES-FR). For all pathways, a smaller amount of network investments are needed for higher DSM rates, with the amount of national AC network investments being most affected by the DSM rate.

Conversely, additional DC network capacity is needed at both international and national levels. At the national level, the required additional DC network capacity is mainly located

---

[1]Total additional storage capacity includes new capacity from BESS and H2 subsystem.

[2]Both international and national lines.

[3]It considers the electricity generation from the following technologies: Solar PV, Wind, and Hydro.

[4]Incremental grid investment is the difference when including BESS and H2 subsystems as options.
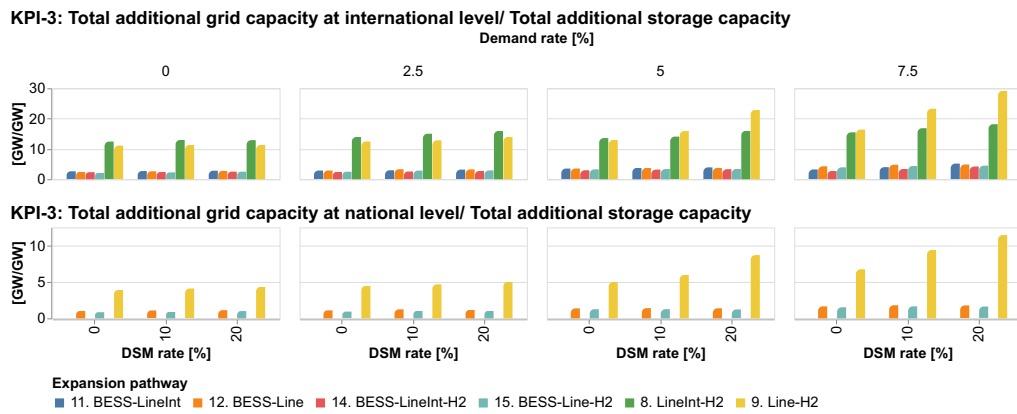
Fig. 4.8.: KPI-3: Amount of grid capacity required per unit of additional storage capacity deployed. [Source: Author's own illustration]

within Italy, Sweden (SE) and the United Kingdom (UK). At the international level, major DC network investments should take place on the lines between Spain and France (ES-FR), France and the United Kingdom (FR-UK), Norway and the United Kingdom (NO-UK), and Poland and Sweden (PL-SE). Investments in these lines are needed for all pathways and DSM rates, highlighting their critical role.

The impact of DSM on the amount of additional DC network capacity needed mirrors that of DSM on AC network development, with a reduction in the amount of required network capacity taking place as DSM rates increase.

Overall, the results computed point to the need to significantly reinforce the AC networks at the national level in Central Europe and the Iberian Peninsula, as well as further develop the DC networks in specific countries. In particular, the expansion of the line between France and the United Kingdom is required for all pathways and DSM rates, underlining its crucial role. Similarly, the lines between Poland and Sweden and between Norway and the UK are consistently identified as critically needed. Internationally, the need for substantial additional network capacity is clear, with some critical network investments concerning long-distance connections. This underlines the importance of strategic expansion planning and investments in both AC and DC networks to meet future demand and ensure a reliable energy supply across Europe. The results discussed so far do not concern the effect of considering different demand growth rates.

Figure 4.8 shows the additional network capacity required per unit of storage capacity deployed for each path, DSM rate and demand growth rate. The figure shows these requirements in absolute terms rather than relative to the scenarios that exclude the deployment of BESS and H2 subsystems. In contrast, Figure 4.9 shows the reductions in those requirements due to the deployment of BESS and H2-subsystems. Both figures highlight the impact of DSM rates on the additional capacity required for national lines and H2 subsystems.

Comparing paths 9, 12 and 15 in Fig. 4.8, the need for new network capacity is three times higher if only lines and H2 subsystems are deployed than if BESS is included. This highlights the critical role of BESS in reducing the need for network capacity, especially at demand

M-4: Considering investments in lines to reinforce the international grid

M-4: Considering investments in lines to reinforce the international and national grid

Expansion pathway
■ 11. BESS-LineInt ■ 12. BESS-Line ■ 14. BESS-LineInt-H2 ■ 15. BESS-Line-H2 ■ 8. LineInt-H2 ■ 9. Line-H2
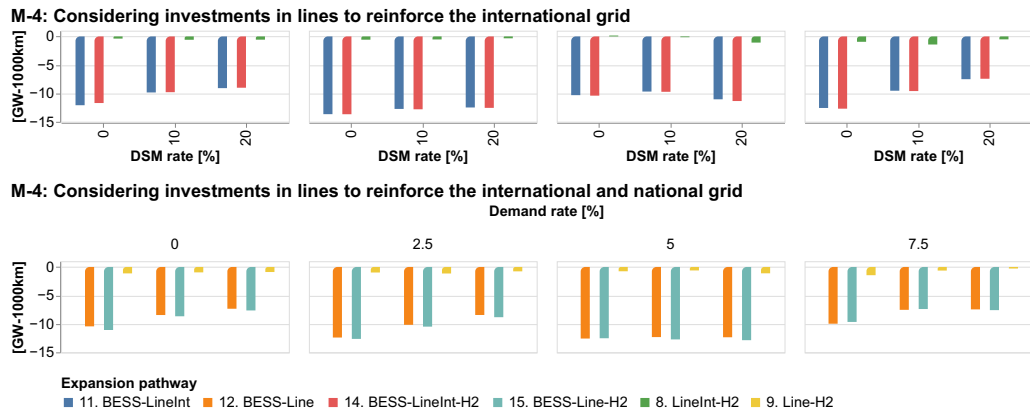
Fig. 4.9.: M-4: Reduction in the network capacity needs due to the inclusion of storage deployment. [Source: Author's own illustration]

Expansion Pathways
■ 2. LineInt ■ 3. Line ■ 8. LineInt-H2 ■ 9. Line-H2 ■ 11. BESS-LineInt ■ 12. BESS-Line ■ 14. BESS-LineInt-H2 ■ 15. BESS-Line-H2
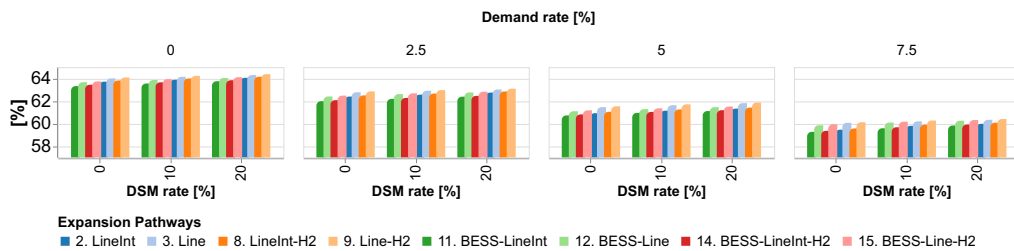
Fig. 4.10.: M-5: Annual RES share in the electricity generation. [Source: Author's own illustration]

growth rates of 5% and 7.5%. Conversely, DSM has little impact on this metric at demand growth rates below 5%. However, at a demand growth rate of 7.5%, DSM has a significant impact, particularly in pathways that exclude BESS deployment. Specifically, DSM rates of 20% can increase the need for new network capacity by up to 50% compared to scenarios with a 0% DSM rate.

This increase occurs because at higher DSM rates, while energy use is shifted to manage peaks, the absence of BESS means that the grid must absorb all of the increased load directly. Without BESS to absorb and redistribute energy, the grid needs additional capacity to manage these peaks and variations.

Figure 4.9 once again confirms the critical role of BESS. The figure also highlights the impact of DSM on the need for grid reinforcement, particularly at lower demand growth rates of 0% and 2.5%. At these low demand growth rates, DSM, although intended to reduce energy consumption during peak periods, actually increases the need for grid reinforcement. This counter-intuitive effect occurs because DSM alone does not significantly reduce total energy demand or eliminate peak loads, especially in a scenario where demand growth is minimal. As DSM participation rates increase, the potential reduction in the need for grid reinforcement is limited, with reductions up to 30%.

On the other hand, Figure 4.10 shows the share of RES in the generation mix for different expansion paths, demand growth rates and DSM rates. The figure shows that significant changes in the RES share occur mainly due to increases in demand growth rates. For

example, the RES share decreases from 64% at a 0% demand growth rate to 60% at a 7.5% demand growth rate. This decrease occurs because RES generation capacity remains static while demand increases and the additional energy demand must be met by other generation sources, such as fossil fuels or other non-RES options, that can handle the increased load.

DSM participation rates also affect the RES share, but their impact is less significant compared to demand growth rates. DSM strategies adjust consumption patterns to manage energy use, but they do not increase RES capacity. Therefore, while DSM can help shift energy use and reduce peak loads, it cannot compensate for static RES capacity as demand grows.

The impact of DSM is still more significant than the effect of the H2 subsystems, which have a relatively small impact on the RES share. This is because DSM affects energy consumption patterns, whereas H2 subsystems and the deployment of additional lines or BESS are more directly involved in managing energy supply and integrating RES into the system. Therefore, the main way to address the gap between increased demand and static RES capacity is to improve grid infrastructure and storage solutions.

In addition, the figure shows that the impact of DSM on RES shares is comparable to that of the consideration of reinforcements to national grids. For example, by comparing the results for paths 8 and 9, one can see that the increase in total RES shares occurring with an increase in the DSM level is comparable to that occurring when national grid reinforcements are added to the set of flexible technologies to be deployed. This suggests that DSM can play a significant role in RES deployment, similar in size to that of national grid extension.

Finally, this figure highlights the differences in RES shares taking place among different expansion pathways. As mentioned above, Pathways with higher DSM participation levels and lower demand growth rates tend to have higher RES shares, highlighting the importance of these factors (the demand growth rate being inversely proportional to the energy efficiency rate) in achieving higher RES penetration rates. Overall, the analysis underscores the critical role of demand management and strategic expansion planning in maximizing the renewable energy shares in the energy system.

Impact of BESS and H2 subsystems

The impact of the development of ESS (BESS and H2 subsystems) is assessed through comparative KPIs computed for both those scenarios with and without these ESS within different expansion pathways. For example, Figure 4.11 illustrates the variation in the relevant M-5 scenarios, which is used to measure the reduction in RES energy curtailment per additional capacity of storage of the BESS or H2 subsystems.

The reduction in RES curtailment is determined by the difference in the curtailment found in the expansion pathways (the ones shown in Table 4.1) 2 and 8 for the impact of H2 subsystems and the differences of 2 and 11 for the impact of BESS. Both differences consider paths that also comprise international lines as candidates as long as the storage ones. In a similar way, the reduction of RES curtailment is determined for those paths that also
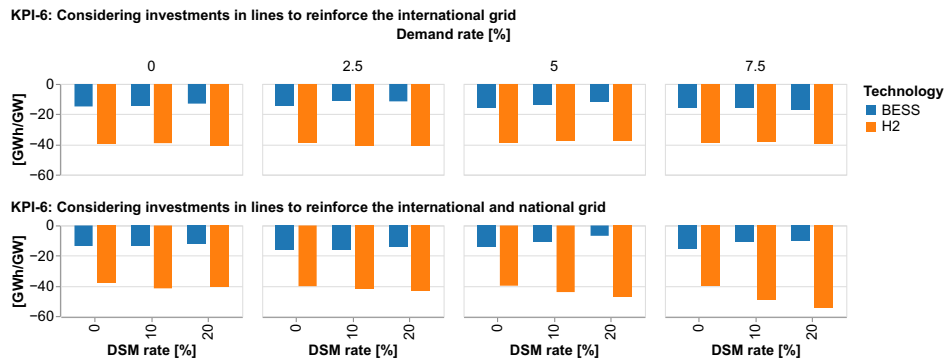
Fig. 4.11.: KPI-6: Reduction in RES curtailment per additional capacity in BESS or H2 subsystems. [Source: Author's own illustration]

comprise international and national lines. Where the differences, in this case, are between paths 3 and 9 for the impact of H2 subsystems and 3 and 12 for the impact of BESS.

On the other hand, the additional capacity is determined as the difference between the new storage capacity in the expansion pathways 2 to 8 and 3 to 9 for the impact of the H2 subsystems and the differences in the pathways 2 to 11 and 3 to 12 for the impact of BESS. This allows us to compute the impact of this added capacity on RES curtailment per demand growth increase and DSM rates, while also allowing investments in transmission lines to take place to improve either the international grid or both the international and national grids simultaneously. The ESS offer indirect benefits such as reducing the RES curtailment. This reduction is influenced by increased demand growth and DSM rates. However, it's important to interpret these results with caution, as they reflect the combined impact of both additional storage capacity and network investments.

In particular, the reductions in curtailment due to H2 subsystems are significantly larger than those due to BESS. When investments are made to strengthen only the international network, the reductions associated with H2 subsystems are larger, in the range of 1.2 to 3.7 times, than those associated with BESS. When considering investments that strengthen both international and national networks, the range changes from 1.4 to 4.2 times.

These results occur due to several key factors:

- *Synergy between storage and grid investments:* The reductions come from the combined use of ESS and increased grid capacity. The BESS and H2 subsystems help to manage the variability and intermittency of renewables by storing excess energy that would otherwise be curtailed. Meanwhile, network investments, such as reinforcing transmission lines, improve the grid's ability to transport electricity over longer distances and across borders. Together, these measures maximise the use of RES.

- *Higher impact of H2 subsystems:* H2 subsystems tend to provide more significant reductions than BESS because H2 storage can manage larger amounts of excess energy for longer periods of time. This is particularly beneficial when dealing with significant renewable energy surpluses or when integrating high levels of renewable energy into the grid.
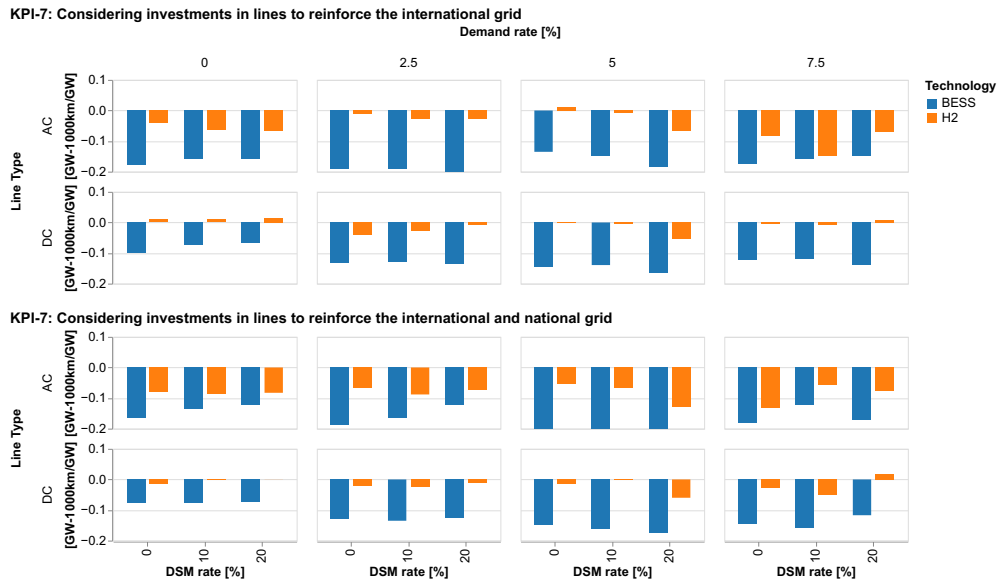
Fig. 4.12.: KPI-7: Reduction in grid capacity reinforcements per additional capacity in BESS or H2 subsystems. [Source: Author's own illustration]

- *Strengthening grid infrastructure:* The greater reductions in curtailment also observed with investment in international and national grid reinforcements suggest that reinforcing grid infrastructure allows for better distribution and balancing of energy over larger areas. This reduces congestion and allows a more flexible response to fluctuations in supply and demand, further minimising curtailment.

Similar to Figure 4.11, Figure 4.12 illustrates how the deployment of BESS or H2 subsystems reduces the optimal level of investment in network capacity, measured in GW-1000km. This reduction is observed when considering investments in either international transmission lines alone or a combination of international and national lines.

The reduction in the network capacity reinforcement per unit of additional ESS capacity is calculated by comparing the differences in network expansion paths with and without the specific ESS. This calculation involves dividing the change in expansion requirements by the additional capacity of the ESS. The methodology is similar to that used to determine the reduction in RES curtailment per unit of additional storage capacity.

In contrast to the greater impact of H2 subsystems on reducing the RES curtailment, BESS have a more significant impact on reducing the need for grid capacity reinforcement than H2 subsystems, as shown in Figure 4.12. This figure presents reductions as negative values and increases as positive values.

For investments in lines reinforcing the international network, BESS achieves larger reductions in network capacity reinforcements, ranging from 0.4 to 7 times those of H2 subsystems. This range changes to 0.8 to 9 times when considering investments in lines reinforcing both international and national networks.

In addition, the figure details the reductions based on line type - AC and DC. For international lines only, AC lines show an average reduction of 0.16 GW-1000 km/GW due to BESS deployment, taking into account all demand growth and DSM rates. In contrast, the average reduction for DC lines is 0.11 GW-1000km/GW. If both international and national lines are considered, the average reduction for AC lines remains at 0.16 GW-1000km/GW, while the average for DC lines increases slightly to 0.12 GW-1000km/GW.

The figure also shows some increases rather than decreases in network capacity requirements, mainly due to the introduction of H2 subsystems. These increases occur at demand growth rates of 0% and 5% when only international lines and storage are considered simultaneously as candidates.

From these results, the following findings can be summarised

- *Impact of BESS on grid reinforcements:* The results indicate that BESS is more effective in reducing the need for grid capacity reinforcements. This effectiveness is likely to be due to the faster response times and higher efficiency of BESS in managing energy storage and release. BESS can quickly absorb and release electricity, which helps to balance the grid and reduces the need for major grid expansions, especially during peak loads or sudden changes in demand.

- *Differences in line type impact:* The distinction between AC and DC lines shows that BESS has a greater impact on AC lines than on DC lines. This may be because AC lines are typically more widespread and used for regional and local distribution, where the rapid balancing capabilities of BESS are more advantageous. DC lines, which are often used for long-distance and high-capacity transmission, may not benefit as much from BESS, which focuses on short-term storage and local flexibility.

- *Impact of H2 subsystems on grid requirements:* The occasional increase in grid capacity requirements when deploying H2 subsystems, particularly at low demand growth rates (0% and 5%), suggests that H2 may not be as effective in scenarios where demand growth is minimal. This could be because H2 subsystems, while beneficial for large-scale and long-term energy storage, may not provide the immediate balancing capability required for networks operating under stable or low-growth conditions. Instead, the use of H2 subsystems in such contexts could increase the need for additional grid infrastructure to manage the production and distribution of hydrogen.

- *Broader implications:* These findings highlight the importance of selecting the right type of ESS based on specific grid needs and conditions. While H2 subsystems are advantageous for reducing RES curtailment and providing large-scale storage solutions, BESS is more effective in reducing immediate grid capacity reinforcement needs. This suggests a complementary role for both technologies, with BESS supporting grid stability and short-term balancing, and H2 subsystems addressing long-term storage and energy transport needs.

4.4.2 Value of DSM, BESS and H2 Subsystems

This section is divided into subsections, each focusing on the specific value of the DSM, BESS and H2 subsystems under different conditions. The conditions examined include different demand growth scenarios, DSM deployment rates and expansion pathways, providing a comprehensive assessment of the economic value and functional role of each flexibility source. By considering a wide range of scenarios, this analysis ensures a more informed understanding of how these technologies can contribute to grid stability and efficiency in different contexts. The assessment is based on various metrics/KPIs outlined in Table 4.5.

Tab. 4.5.: Individual and comparative metrics/KPIs employed at European and national levels to assess the value of the flexibility sources.

Index	Metric/KPI	Individual		Comparative	
		European	National	European	National
M-8	Total costs[1]	✓	-	-	-
KPI-9	Short-term marginal cost	✓	✓	-	-
KPI-10	Total system cost reduction[2]/Incremental total investment	-	-	✓	-
KPI-11	Incremental internal system rate of return[3]	-	-	✓	✓
M-12	ESS operation[4]	✓	✓	-	-

These KPIs are categorized into individual and comparative metrics used at both the European and national levels, allowing for a detailed analysis of how each flexibility source performs under different conditions. Specifically:

- M-8 and KPI-9 are aimed at computing the value of DSM.

- KPIs 10 and 11 are aimed at computing the value of the BESS and H2 subsystems.

- M-12 allows one to assess the functionality of BESS and H2 subsystems.

Economic value of DSM

The economic value of DSM is closely tied to its impact on the system development and operation, as discussed in Section 4.4.1. The primary metric used for assessing the economic value of DSM is the reduction this achieves in the total system costs, which include the investment costs, the generation (production) costs, and the emission costs. Figure 4.13 illustrates the variation of the corresponding metric, M-8, across scenarios with varying levels of DSM and demand growth rates. On average, investment costs represent 10% of total costs, production costs 66%, and emission costs 24%. This distribution underlines the significant share of variable production and emission costs in the total costs.

---

[1]Total investment, generation and emission costs.

[2]Computed as the difference between the level of these in those pathways with and without ESS.

[3]It is computed using the increases in the investment and operation cost savings in those pathways featuring ESS w.r.t. those without ESS.

[4]It allows one to identify the hours when the ESS is used for charging or discharging.
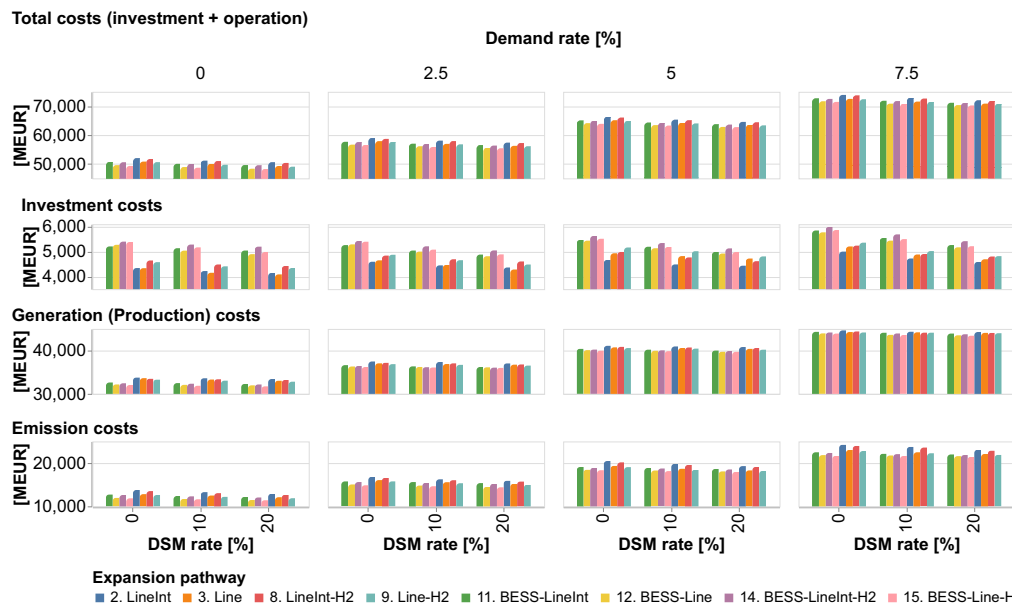
Fig. 4.13.: M-8: Annual total, investment and operation costs for the 96 simulations. [Source: Author's own illustration]

A closer look at Figure 4.13 shows an upward trend in total costs with the demand growth rate. This trend indicates the additional economic burden of serving larger amounts of energy demand and points out the larger relevance of implementing DSM to limit system costs for higher demand levels.

Investment costs are largely affected by the implementation of DSM, with savings in these costs achieved by DSM ranging from 1.8% to 7.8% depending on the DSM rate. These cost reductions underscore the effectiveness of DSM in lowering expenditures in infrastructure investment. By increasing the efficiency of the use of energy, for example, reducing peak demand, DSM enables a more efficient use of existing resources, thereby delaying, or even avoiding, the need for additional investments.

In addition to investment costs, DSM also helps reduce production and emission costs by up to 12.5% and 10% respectively. These reductions occur because DSM not only smoothes demand but also promotes energy efficiency throughout the system. By reducing peak demand and balancing energy use, power plants can operate more efficiently, reducing the amount of fuel needed and minimising wear and tear on equipment. This results in lower production costs.

DSM also contributes to lower emissions by reducing overall energy demand, particularly during periods of high demand, which less efficient, higher-emitting power plants often meet. Power plants that might otherwise be used during peak periods are often more polluting due to the need to ramp up production quickly, so reducing reliance on these plants results in lower overall emissions.
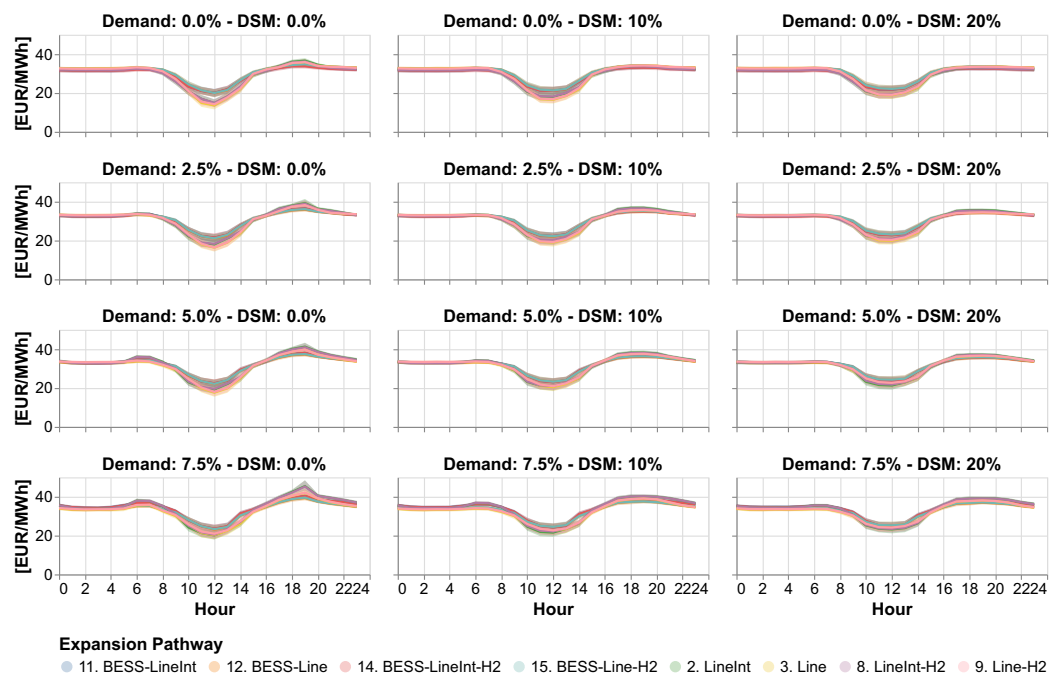
Fig. 4.14.: KPI-9: Marginal electricity cost per expansion pathway, hour of the day (average one) and demand growth and DSM rate. [Source: Author's own illustration]

Similarly, Figure 4.14 shows the Short-Term Marginal Cost (STMC) of electricity over different hours of the day, taking into account different levels of demand growth and DSM rates. Each subplot shows average values at the European system level, providing a comprehensive overview of how these factors affect the STMC over different time periods.

- *Impact of demand growth on marginal costs:* The results indicate a significant impact of demand growth rates on the marginal cost of electricity. At a lower demand growth rate (0%), marginal costs remain relatively stable throughout the day, with a slight decrease observed at midday when demand is expected to be lower. This stability is due to the balance between supply and demand, with the existing capacity of the system sufficiently meeting demand without significant stress.

  However, as the demand growth rate increases to 7.5%, marginal costs show more pronounced fluctuations throughout the day. In particular, peak marginal costs are observed in the early morning (between 6:00 and 8:00, reaching an average of 40 EUR/MWh) and in the late evening (between 18:00 and 20:00, peaking at 50 EUR/MWh). This pattern suggests that the grid is more congested during these hours, mainly due to increased electricity demand pushing the system closer to its operational limits. As a result, more expensive generation resources are likely to be dispatched, increasing the STMC.

- *Role of demand-side management in modulating marginal costs:* The introduction of DSM, with participation rates ranging from 0% to 20%, shows a moderating effect on marginal costs throughout the day. In scenarios without DSM (0% participation),

the variation in marginal costs is more pronounced, especially at higher demand growth rates. For example, at a demand growth rate of 7.5%, the absence of DSM results in sharp cost peaks, reflecting the inability of the system to evenly distribute the electricity demand.

Conversely, the implementation of DSM (with a participation rate of 20%) leads to a smoother marginal cost curve throughout the day. Specifically, the morning peak cost is reduced from 40 EUR/MWh to 37 EUR/MWh and the evening peak cost is reduced from 50 EUR/MWh to 40 EUR/MWh. This flattening effect indicates that DSM effectively mitigates peak prices by redistributing net demand more evenly, reducing the reliance on expensive generation during high-demand periods.

However, the analysis also shows that DSM can lead to a slight increase in STMC during the trough hours (10:00 to 14:00) with a demand growth rate of 7.5%, with costs increasing from 20-27 EUR/MWh to 22-30 EUR/MWh. This increase is attributed to the shift of demand from peak to off-peak hours due to DSM strategies. While DSM reduces peak demand, it can slightly increase off-peak demand, requiring the use of additional generation resources during these typically lower-cost periods.

Economic value of BESS and H2 subsystems

This section assesses the economic value of the BESS and H2 subsystems using KPIs 10 and 11. These KPIs are calculated in a similar way to KPIs 6 and 7 (see Table 4.4) by comparing the differences between the expansion pathways with and without the assessed ESS relative to their respective investment costs.

KPI 10 measures the cost-effectiveness of introducing BESS or H2 subsystems. For H2 subsystems, it is derived by dividing the difference in total system costs between pathways 15 (which includes all lines, BESS and H2 subsystems) and 12 (which includes all lines and BESS) by the difference in total investment costs between these pathways. This KPI quantifies the reduction in total system cost per unit of additional investment due to the inclusion of H2 subsystems.

A similar method is used to calculate the KPI for BESS, comparing pathways 15 and 9 (the latter including all lines and H2 subsystems but excluding BESS). For these calculations, paths 9, 12 and 15 include both national and international lines. Alternatively, paths 8, 11 and 14 can be used to assess scenarios that only consider international lines.

Figure 4.15 illustrates KPI-10 in million euros (MEUR) per MEUR (p.u. terms) for different demand growth and DSM rates. The figure includes scenarios with only international lines and scenarios with both national and international lines. The key findings are as follows:

- *Performance of BESS considering only international lines:* BESS shows significantly greater reductions in KPI-10 compared to H2 subsystems, with reductions ranging from 2.5 to 8.3 times higher. This can be attributed to the flexibility and rapid response capabilities of BESS, which are critical for managing network stability and cost-effectiveness in scenarios with complex cross-border interactions.
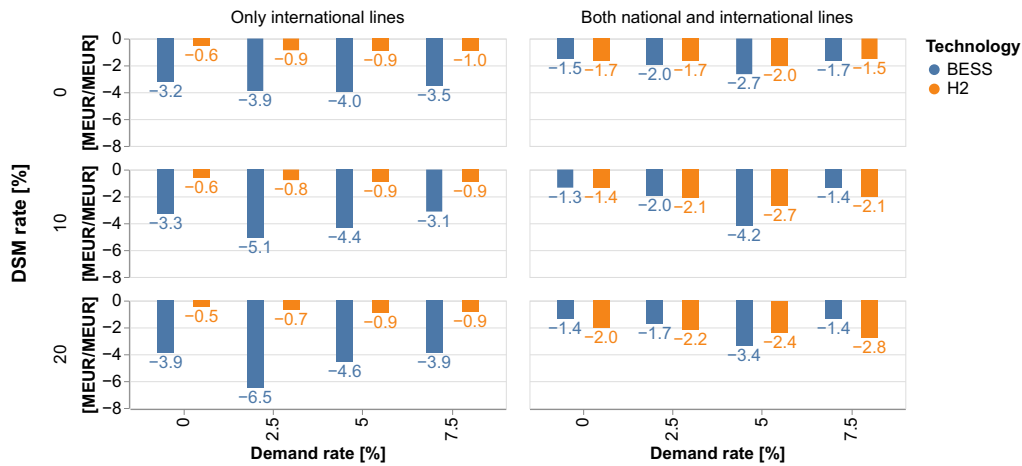
Fig. 4.15.: KPI-10: Reduction in the total system cost per incremental investment cost using pathways with and without BESS or H2 subsystems. [Source: Author's own illustration]

An upward trend in BESS is observed as DSM rates increase. For a 2.5% demand growth rate, the KPI-10 values for BESS increase from 3.9 p.u. to 6.5 p.u. as DSM rates increase from 0% to 20%. This trend indicates that BESS is more effective when peak demand is managed by DSM strategies that optimise storage and discharge cycles. However, this upward trend in KPI-10 with increasing DSM rates generally decreases at higher demand growth rates.

- *Performance of BESS and H2 subsystems considering both national and international lines:* The reductions in KPI-10 for BESS and H2 subsystems become more comparable. Excluding scenarios with a 5% demand growth rate, H2 subsystems provide greater reductions, ranging from 7% to 100% greater than BESS at DSM rates above 0%. This is because the system benefits from a more integrated network configuration, which improves the performance of the H2 subsystems.

  H2 subsystems are particularly effective at higher DSM rates due to their ability to provide long-term storage, which supports grid adequacy over longer periods. This capability is particularly beneficial in reduced peak demand scenarios managed by DSM, as it aligns well with the need for sustained energy supply over longer periods.

On the other hand, Figure 4.16 shows the incremental Internal Rate of Return (IRR), a key metric for assessing the financial impact of additional investment and operational cost savings in scenarios with and without BESS or H2 subsystems. For BESS, the IRR is calculated by comparing expansion paths 15 (which includes all lines plus BESS and H2 subsystems) and 9 (which includes all lines plus H2 subsystems), focusing on international lines. For H2 subsystems, the IRR is derived by comparing paths 15 and 12 (which includes all lines plus BESS). When considering both national and international lines, paths 8, 11 and 14 are analysed instead of 9, 12 and 15.
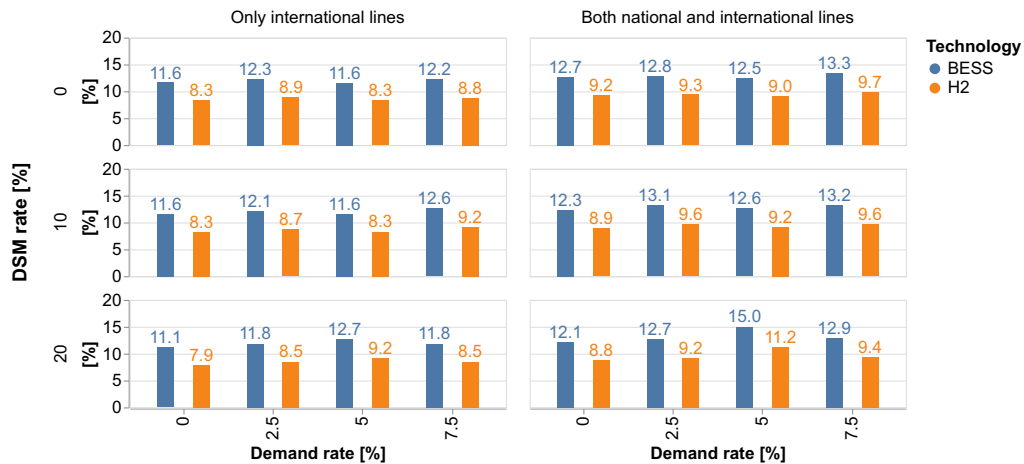
Fig. 4.16.: KPI-11: Incremental system rate of return on investments computed considering pathways with and without BESS or H2 subsystems. [Source: Author's own illustration]

This incremental IRR provides a measure of the financial return on additional investment in BESS or H2 subsystems by taking into account the cost savings achieved through their integration into the energy system. A higher IRR indicates that investment in a particular storage system - whether BESS or H2 - will deliver greater savings relative to its cost, making it a more attractive option. In all scenarios, the IRR is higher when both national and international lines are considered, compared to only considering international lines. For BESS, this increase ranges from 4% to 18%, while for H2 subsystems, it ranges from 4% to 22%. When only international lines are considered for grid strengthening, the IRR for BESS is notably higher, ranging from 37% to 41%, compared to the IRR for H2 subsystems. However, when both national and international lines are included, the IRR for BESS decreases slightly, ranging from 34% to 39%.

The main findings are summarised below:

- *Improved IRR with national and international lines:* The increase in IRR when both national and international lines are considered can be attributed to the larger scope of the investment, which likely results in greater operational efficiencies and cost savings. Integrating both types of lines might provide more opportunities to optimise the energy grid, enhancing the financial returns on the investment.

- *Comparative performance of BESS and H2 subsystems:* The IRR for BESS is consistently higher than for H2 subsystems when only international lines are considered. This could be due to BESS being more efficient or cost-effective in scenarios where the infrastructure is limited to international lines. However, when both national and international lines are included, the IRR for BESS decreases slightly. This reduction might indicate that the relative advantage of BESS diminishes when the system is expanded, possibly because the benefits of H2 subsystems become more pronounced in a larger, more interconnected grid.
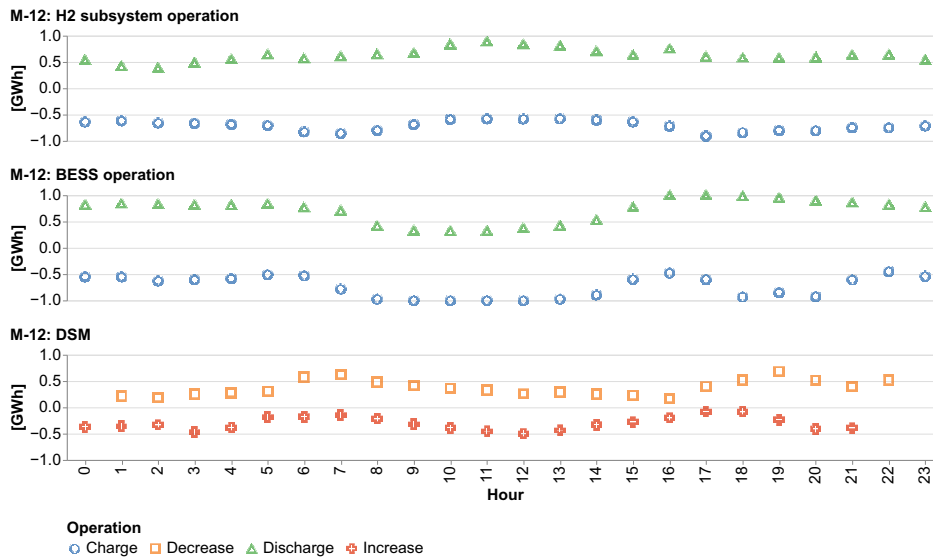
Fig. 4.17.: M-12: Hourly distribution of average electricity charge/consumption and discharge/generation for the BESS and H2 subsystems, together with the reduction/increase in electricity consumption due to DSM, shown as points for each type across the whole system. [Source: Author's own illustration]

Functional performance of the BESS, H2 subsystems and DSM

Here I aim to identify the function of BESS, H2 subsystems and DSM in the system operation using M-12. This metric shows the charging and discharging operations, as well as the increases and decreases in consumption controlled by DSM, to try to identify their typical timing throughout the day and week. This provides some insight into the operating patterns and efficient operation of the system.

Figure 4.17 illustrates the metric M-12 showing the hourly operating patterns of the H2 subsystems, BESS and DSM in terms of energy production and consumption (in GWh) over a typical day for the whole European system. The figure provides an insight into how these technologies interact with the energy system throughout the day.

The values shown are hourly averages across all sites and scenarios, capturing simultaneous charging and discharging activities. This simultaneous appearance is due to the averaging process: while the original time series show discrete zero values during periods when neither charging nor discharging occurs, the aggregation of non-zero values results in overlapping averages for charging and discharging within the same hour. This approach highlights broader operational trends over the 24-hour cycle rather than individual events.

In addition, simultaneous charging during peak hours can be explained by regional variations in generation. For example, in areas with significant wind or hydro generation, surplus energy during peak hours can be stored in BESS or H2 subsystems to alleviate local transmission congestion. This storage capability enables better utilisation of renewable energy and increases grid flexibility, ensuring that these technologies contribute effectively to system stability even during periods of high demand.

- *H2 subsystem performance:* The H2 subsystem shows a consistent and stable operating pattern throughout the day, with energy consumption and production generally fluctuating within a narrow range of -1 GWh to +1 GWh. This smoothness is evident at all hours, indicating that the H2 subsystem does not significantly alter its operation in response to short-term fluctuations in electricity demand or supply. Specific hours such as early morning (0 to 6 hours) and late night (20 to 23 hours) do not show significant deviations from the overall stable trend, reinforcing the role of the H2 subsystem as a long-term balancing tool rather than a short-term reactive component.

- *BESS performance:* The operation of BESS shows considerable variability, with charging and discharging values ranging from approximately -1 GWh to +1 GWh. This variability is more pronounced during certain hours of the day. For example, during the late morning (9 to 11 hours) and early afternoon (12 to 15 hours), there is a noticeable increase in BESS discharge activity (green triangles), which is likely to correspond to periods of higher electricity demand or the need to balance solar generation peaks. Conversely, the early morning hours (0 to 5 hours) and the late evening hours (18 to 23 hours) show increased charging activity (blue circles), indicating that BESS is absorbing excess energy, possibly from lower demand or surplus generation during these times.

  This pattern suggests that BESS is highly responsive to the diurnal cycle of electricity demand and supply, playing a critical role in providing immediate balance. The ability of BESS to dynamically switch between charge and discharge modes highlights its role in managing the variability and RES intermittency and matching energy availability to consumption patterns.

- *DSM performance:* DSM show moderate variability, with net electricity consumption adjustments ranging from -1 GWh to +1 GWh. The variability of DSM is characterised by a distinct pattern of hourly increases (red crosses) and decreases (orange squares), reflecting its active role in adjusting demand. Certain hours, such as the early morning (0 to 5 hours), show a tendency towards increased consumption (red crosses), possibly to take advantage of lower energy prices or surplus generation. During midday to early afternoon (12 to 15 hours), DSM shows a more balanced operation with both increases and decreases, suggesting a more reactive role in managing peak demand or shifting consumption to match supply availability.

  In particular, DSM is less reactive than BESS during periods of quick change in demand but plays a complementary role in smoothing out minor discrepancies in demand, thus contributing to demand-supply balance. The relatively predictable pattern of DSM adjustments highlights its effectiveness in mitigating smaller, more regular fluctuations rather than responding to large, sudden shifts in demand or supply.

These hourly trends highlight the complementary nature of these technologies: the H2 subsystems provide a stable backdrop by managing long-term supply variability, BESS provides rapid and flexible adjustments to short-term variability, and DSM ensures that demand-side adjustments are fine-tuned to system conditions. Together, these systems
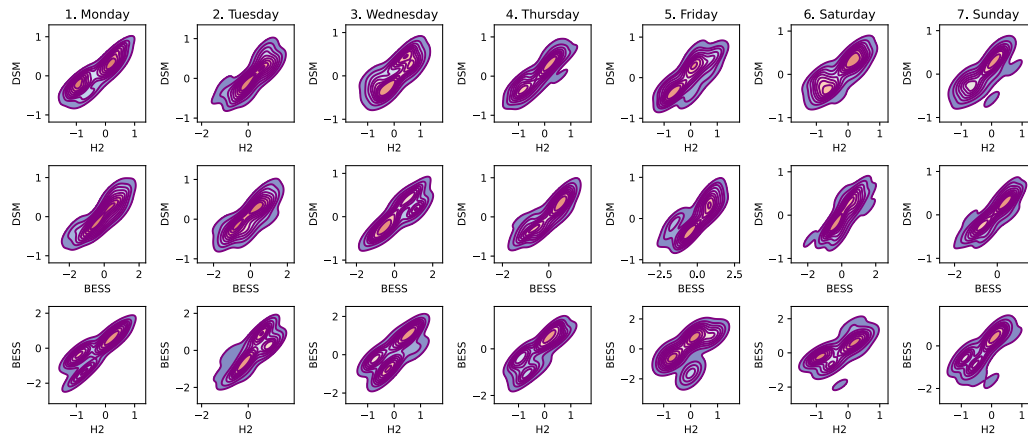
Fig. 4.18.: M-12: Kernel Density Estimation of BESS and H2 subsystem charge/discharge decisions and DSM electricity consumption increase/decrease. [Source: Author's own illustration].

improve the flexibility of the system by leveraging their specific operational strengths at different times of the day.

To complement this analysis, it is important to analyse the interactions between the DSM, BESS and H2 subsystems to optimise the overall performance of the system. Kernel Density Estimate (KDE) plots help us to explore these interactions by showing the underlying distributions and relationships between variables without assuming linearity. They provide a detailed view of the distribution of data, allowing the identification of multiple modes of operation and the analysis of daily variations.

Figure 4.18 shows a series of KDE contour plots visualising the relationships between DSM, H2 subsystems and BESS over the days of the typical week. The plots are arranged in rows representing different pairwise comparisons of these variables: DSM vs. H2, DSM vs. BESS, and BESS vs. H2. Each column corresponds to a different day, from Monday to Sunday. This analysis provides insights into the temporal variability and underlying operation modes that characterise the interactions between these critical components of the energy system. These insights are as follows for pairwise comparison:

- *DSM vs H2 subsystems:* The first row of plots shows the relationship between DSM and hydrogen for each day of the week. The contour shapes in these plots show a predominantly linear and strong relationship, characterised by elongated density distributions that consistently extend along a diagonal axis. However, there are notable instances of multimodal distributions on certain days, such as Tuesday and Friday, where multiple peaks are observed within the density contours. These multimodal patterns suggest that the DSM-hydrogen relationship is influenced by different modes or states of operation that vary from day to day.
  For example, the presence of multiple modes on Tuesdays and Fridays indicates different variations in electricity production or consumption by H2 subsystems that differ from other days. These variations are due to external factors such as fluctuating energy prices or varying levels of renewable generation.

- *DSM vs. BESS:* The second row of plots explores the relationship between DSM and BESS. Similar to the DSM-H2 relationship, the plots exhibit a generally linear pattern, though with a slightly wider spread, indicating greater variability. Multimodal distributions are evident on certain days, particularly Tuesday and Saturday, where distinct peaks suggest the existence of multiple operational scenarios or behaviours within the DSM-BESS interactions.

  The wider spread of contours and the presence of multimodal distributions on these days suggest that the relationship between DSM and BESS is more complex. This complexity might be due to the dynamic nature of battery charge and discharge cycles, which are closely tied to short-term balancing needs, demand peaks, and renewable energy availability. The variability across different days implies that the system's reliance on BESS support may shift in response to weekly demand patterns.

- *BESS vs H2 subsystem:* The last row shows the contours for the BESS vs. H2 relationship, which shows the most complex and variable patterns of the three comparisons. The plots for this relationship often show non-linear and multimodal distributions, with notable variations in shape and density throughout the week. For example, on Friday and Sunday, there are several distinct peaks, suggesting that the BESS and H2 subsystems operate under different regimes.

  The complexity and multimodality observed in the BESS-H2 relationship suggest that these systems are subject to a variety of operational constraints and external influences. These could include changes in RES generation profiles, shifts in grid demand, or strategic decisions related to energy storage and dispatch.

The multimodal distributions observed in the KDE plots indicate that the relationships between DSM, BESS, and H2 subsystems are not uniform across all days. Instead, these relationships exhibit distinct modes that correspond to different operational scenarios or states. The presence of multiple peaks within the density distributions suggests that the system operates under a range of conditions that vary by day, reflecting the dynamic nature of electricity demand, storage, and production.

4.5 Conclusions on the Role of Different Utility-Scale Storage and DSM Flexibility Solutions

The comprehensive analyses presented in this chapter demonstrate the significant economic and operational benefits of integrating DSM, BESS and H2 subsystems into the power system. By evaluating KPIs such as the share of RES in the energy mix, IRR on investments and total system cost reductions, it is clear that these technologies are essential for increasing system flexibility and economic efficiency.

The results highlight the key role of DSM in reducing the need for storage solutions and minimising the impact on additional grid capacity requirements while maximising the integration of renewable generation. The effective use of DSM, in conjunction with new national and international transmission lines, is essential for a resilient and sustainable

energy system in Europe. The findings underline the need for a coordinated approach to demand management and grid infrastructure development to meet future energy challenges. Higher DSM participation and lower demand growth correlate with higher renewable energy shares, demonstrating the importance of DSM in the integration of renewables. However, DSM alone cannot fully address the challenges of static renewable capacity amid growing demand, underlining the need for continued investment in both storage solutions and grid infrastructure. In addition, the economic benefits of DSM, reflected in significant system cost reductions, underline its value in smoothing demand, reducing peak loads, improving energy efficiency and meeting long-term sustainability goal.

The analysis also highlights the critical role of the BESS and H2 subsystems. BESS deployment can reduce the need for additional grid capacity by up to 30%, highlighting its importance in grid reinforcement strategies and it is . The combined investment in energy storage and grid infrastructure significantly optimises the use of renewable energy by minimising curtailment and improving energy distribution. While H2 subsystems are more effective at reducing renewable curtailment than minimising grid capacity requirements since it is installed in specific places close to renewable production, and they serve as a complementary technology in future energy systems.

The key advantage of BESS is its ability to respond to short-term variations in net demand, making it ideal for providing short-term flexibility. The analysis shows that BESS deployment results in significant system cost reductions per unit of investment, especially when combined with international transmission lines. The incremental IRR of BESS investments ranges from 11.1% to 13.3%, exceeding that of H2 subsystems, making BESS a more attractive option for economic returns. Conversely, H2 subsystems offer longer-term flexibility with more stable operating patterns and provide economic benefits under varying demand and DSM rates, particularly when both national and international lines are in place. Although the IRR for H2 subsystem investments is slightly lower (up to 9.7%), the overall system cost reductions remain significant despite of the reduced amount installed in comparison to BESS, particularly when combined with network investments, demonstrating their value in reducing overall operating costs.

On the other hand, the results computed show the role of BESS and H2 subsystems. The deployment of storage systems, particularly BESS and H2 subsystems, significantly reduces the need for additional grid capacity. This reduction can be as high as 30% with the inclusion of BESS, underscoring its critical role in grid reinforcement strategies. But, combining ESS with grid infrastructure investments generally yields substantial benefits. This synergy maximizes RES utilization by reducing curtailment and optimising energy distribution. While H2 subsystems are more effective in reducing RES curtailment than minimizing grid capacity requirements, indicating that this technology plays a complementary role in future energy systems.

The operational dynamics between the DSM, BESS and H2 subsystems show different modes of interaction on different days, reflecting their complementary roles in the energy system. The DSM-H2 relationship shows a strong linear pattern with occasional multimodal distributions, while the DSM-BESS relationship is more complex, reflecting the role of BESS

in short-term system balancing. And, the BESS-H2 relationship is the most complex, with non-linear and multimodal patterns, suggesting that these systems do not have a strong correlation and operate under various regimes influenced. In addition, the integration of new national and international lines, especially in key areas such as Central Europe, the Iberian Peninsula, Italy, Sweden and the UK, enhances the economic benefits of both BESS and H2 subsystems. Strategic grid reinforcements, particularly on international routes such as France-UK, Poland-Sweden and Norway-UK, are critical to ensuring reliable energy supplies and maximising the value of storage and renewables across Europe. These reinforcements, together with strategic storage deployments, can significantly improve economic returns and overall system efficiency by optimising total investment and operational cost savings.

Conclusions

<div style="text-align: right; font-size: 2em;">5</div>

This thesis provides a comprehensive study and several advances in addressing the TEP problem. It includes the development of an advanced network planning model that better reflects the complexity of modern power systems. An enhanced generation representation is introduced to optimise the use of renewable energy sources and improve system operation. For the same purpose, the energy storage model is developed adequately to efficiently represent the management of energy supply and energy storage. In addition, the role of local flexibility in accommodating fluctuating energy demand and generation patterns is explored. By incorporating utility-scale storage solutions, the thesis addresses the challenges of balancing supply and demand to ensure a more resilient and sustainable energy infrastructure.

5.1 Key Takeaways

In summary, this thesis provides a detailed analysis and innovative solutions to optimise TEP models, ultimately contributing to the advancement of their computational performance and their practical representation of the system functioning. In this work, I make use of different case studies to address the research questions. The main findings of this thesis are summarised and described in detail below:

1. **System Operation Representation (RQ-1):**

   a) **Network representation:** This thesis presents an innovative approach to represent power flows using an AC-OPF model based on the Branch Flow model within the TEP problem, incorporating cycle constraints. These cycle constraints are classified according to whether they refer to dynamic or static cycles, where the operation of the dynamic cycles depends on the investment in lines that complete the respective cycles. Accurately identifying and classifying these cycles is essential, as is the implementation of appropriate constraints linking line investments to cycle operations and power flows. The strategies for identification and classification, as well as the effective cycle representation within the proposed TEP formulation, are critical. Developing and implementing these strategies represents a significant improvement over previous TEP formulations using AC-OPF, due to the linear nature of all constraints. For instance, the proposed formulation has been tested using the RTS-GMLC system over 8736 hours and several case studies, and shows a significant improvement in computational efficiency of up to 23%, while preserving the solution quality and extending the application boundaries to deal with larger scale optimisation problems.

b) **Energy storage:** Similarly, the representation of energy storage operation focuses on computational efficiency and is addressed by relaxing the binary variable used to define the charge and discharge states, which reduces the computational burden while maintaining the quality of the design solution. This relaxation is crucial, given the consideration of different storage types, from batteries to hydro reservoirs, which would typically introduce numerous binary variables. The proposed approach successfully addresses this challenge by, instead, using continuous variables and constraints to define the several modes of usage of storage devices. This strategy is fundamental to accurately representing the operation of generation and storage units within the planning problem, although not in a way as detailed as in power system operation or generation unit scheduling problems.

2. **Local flexibility through DERs (RQ-2):** Within the work in this thesis, I have investigated the computation of the value and impact of the local flexibility in TEP. I have done this by considering several case studies of TSO-DSO coordination and no coordination. The case studies defined consider the single area RTS-96 for the transmission system, the standard 33-bus system for the distribution systems, and several microgrids. Local flexibility is, then, provided by microgrids that feature electricity demand together with other DERs, such as rooftop solar generation and residential BESS. The integration of the management of several DERs at specific distribution nodes enables effective energy management, reduces peak loads and reduces overall system costs by up to 21%, including the reduction or full avoidance of the need for new transmission infrastructure. In addition, the case studies are also employed to assess the value of two primary flexibility services: the baseline service (FS-B) and the capacity limitation service (FS-C), which drives microgrids to adjust the local electricity consumption and, therefore, contribute to system balance and efficiency. In particular, in these case studies, FS-C may manage to reduce total system costs by up to 10%. In these case studies, FS-C turns out to be more efficient than FS-B, demonstrating how the economic and operational benefits of local flexibility can be increased.

3. **Strategic deployment of utility-scale storage (RQ-3):** Within this thesis project, I also evaluate the use of DSM, BESS and H2 subsystems as centralised flexibility sources in a European scale system for several scenarios and expansion pathways. A TEP formulation has been developed to efficiently represent the economic management of BESS and H2 subsystems, providing expansion plans, as well as the system operation decisions and costs of different types (investment, operation, total) used in the assessment I carry out. DSM increases grid flexibility by shifting demand away from peak periods. As results showed, it could be deemed as an effective solution to complement the flexibility provided by BESS, increasing the amount of energy that can be shifted. The operation cost reductions achieved through the combined mobilization of the flexibility provided by DSM and BESS are up to 66%. BESS provide short-term flexibility since its output can quickly adapt to address imbalances, while H2 subsystems, which include hydrogen production, storage and its use to produce electricity, address medium- and long-term flexibility needs. Moreover, the

results computed show that the integration of DSM, BESS and H2 subsystems creates significant economic and operational benefits for power systems. DSM is crucial to reduce the additional storage capacity needed, as well as the grid capacity expansion needs, while increasing the amount of renewable energy that is integrated into the system. However, DSM alone cannot fully cover the growing system demand and balance the output of static renewable generation. This highlights the need to invest in some new storage and grid capacity. BESSs, with its ability to handle short-term demand fluctuations, reduce the need for new grid capacity by up to 30%, and provide higher economic returns than H2 subsystems (IRR of 11.1% to 13.3%). H2 subsystems, while offering slightly lower returns than BESS (up to 9.7%), provide long-term flexibility and cost savings, especially when combined with transmission grid reinforcements. The interplay between DSM, BESS and H2 subsystems reflects their complementary roles in enhancing system flexibility and stability. Strategic grid reinforcements, especially along key international lines, further enhance the value of these technologies by allowing them to further increase the use of renewable energy when it has the largest value, minimising curtailments and increasing the economic returns of investments in these technologies. This highlights the importance of coordinating the investments in storage and grid infrastructure for a sustainable energy transition in Europe.

Achieving the scalability of the modelling and optimisation developments produced is also a main focus of this thesis. The expansion planning problems, especially TEP, are notoriously known for being combinatorial. Failure to represent a problem in a compact enough way in any dimension - whether temporal, spatial, or technological - can turn a solvable problem into an intractable one, or result in prohibitively huge computation times. This problem persists regardless of the size of the test system, the technologies modelled, or the number of time steps considered. In this thesis, the scalability of the planning approaches developed by significantly increasing the size of the problems addressed while keeping CPU times within reasonable limits. The scalability improvements to the TEP formulations proposed here are related to one of several strategic lines of research developed in this thesis:

First, **search space reduction** is achieved through the enforcement of strategic constraints. Specifically, cycle constraints and tight bounds on voltage magnitudes and angles are employed. These constraints effectively constrain the feasible solution space, making the optimisation process more manageable and efficient.

Secondly, **rigorous control over the number of binary variables** is exerted. This is achieved following several approaches:

- **Imposing constraints among binary variables:** These constraints link the binary variables representing the belonging of branches to cycles to those other binary variables defined for the transmission lines in these branches. In this way, the decisions made on a small set of binary variables condition the value of a large set of them.

- **Relaxation of variables referring to the charge and discharge states:** This technique relaxes the binary nature of the charge/discharge operation decisions, further reducing the complexity of the problem.

Thirdly, **careful implementation** of the modelling approaches developed: this avoids the creation of superfluous constrains/variables and enables the natural scaling of the optimisation problem. This includes the extensive use of subsets to define only those variables and constraints that are necessary, in order to keep the model as lean as possible. In addition, the selection of an appropriate power base is critical to keeping the parameters within the same order of magnitude on the decimal scale and to avoid having to deal with too small or large values of the problem variables and parameters, as this directly affects the efficiency of the optimisation process. Analysing statistical data on the problem size also helps to refine the model to improve its performance.

Finally, the **preparation of case studies** in terms of the system representation in them is crucial to appropriately evaluating the trade-offs to be struck between the accuracy and compactness of the representation made of the problem in the temporal, spatial, and technological dimensions. In this thesis, case studies have been developed based on the RTS-GMLC, RTS24 and European scale systems ranging from 24 to 96 nodes. The studies addressed consider representative days, weeks, and the 8736 consecutive hours of the annual system operation while representing the functioning of different technologies for power generation and storage. If the representation made of the problem in one of the dimensions is more accurate, then the representation of the problem in the other two dimensions will typically need to consider a lower level of detail. Therefore, the modeller must carefully determine the appropriate level of detail in the representation of the system's functioning in each dimension to compute sufficiently accurate solutions as per the study's demands within reasonable computation times.

5.2 Future Research Directions

Future research efforts related to some of the above developments within my thesis project are described below:

- **Network representation:** This thesis has not addressed two important aspects for future transmission networks: topology optimisation (or line switching) and the integration of Flexible AC Transmission Systems (FACTS) for power flow control. Significant modelling developments are needed to adapt the current AC Optimal Power Flow (AC-OPF) with cycle constraints to effectively consider these two aspects of the functioning of the system.
  Topology optimisation has enormous potential for configuring critical network operation topologies capable of effectively addressing stressful operational situations resulting from the changes that occur in demand and generation. It can determine which lines should be connected or disconnected along the time to reduce the system operation costs. In addition, topology optimisation may significantly reduce network reinforcement costs, ensuring that the infrastructure dynamically adapts to changing

operation conditions. However, changing the grid topology would require changing the classification of cycle sets and adding additional constraints to the current formulation related to the connection or disconnection status of lines.

Apart from this, considering FACTS requires making changes to the formulation of the grid constraints due to the unique impact of these devices on cycle constraints. FACTS devices can change the electrical distances between nodes and alter the parameters of transmission lines, affecting the overall network configuration. What is more, the integration of FACTs poses additional challenges, such as determining the optimal locations for installing FACTS devices, and selecting the appropriate types of FACTS to be installed.

Both topology optimisation and FACTS integration in the network pose relevant modelling challenges but also have the potential to increase the system's ability to adapt to fluctuating demand and generation patterns, ultimately leading to a more resilient and cost-effective network.

- **Power generation and energy storage:** In this work careful consideration has been given to the representation of electricity generation and storage. However, considering several climate years and exploring sector coupling through the use of power-to-x technologies are two aspects of the planning of the system operation and expansion that I have not addressed in this work. In this thesis work, I consider a high temporal granularity to represent the system. However, I only consider one possible scenario and target year (horizon) and, therefore, adopt a deterministic, static, planning approach. This approach leaves aside the question of how to efficiently deal with multiple years and scenarios, which can affect investment decisions. In addressing this, one would face a significant computational challenge. Therefore, new methods would have to be developed to address these two aspects of planning. Additionally, considering the possibility of coupling the functioning of several sectors within the TEP is becoming increasingly important, since considering this could increase the efficiency and adequacy of the system but also increase the electricity demand. Considering an appropriate model of power-to-x technologies can provide important insight for planning network development.

  Moreover, the role of the DSM and H2 subsystems is investigated in this thesis. However, DSM modelling could be improved by considering different types of DSM, each with different management timeframes, consumer participation ratios, and proportions of DSM types per node. In the same way, hydrogen demand can also be considered in sectors beyond the electricity one. This broader scope could make investments in H2 subsystems more attractive by demonstrating their versatility and a wider range of their potential economic benefits.

- **TSO-DSO coordination:** This thesis examines TSO-DSO coordination within the TEP problem, with a particular focus on its impact on transmission investment decisions. Understanding how coordination affects investments is critical to optimising both transmission and distribution networks. The case study explored in this thesis, although relatively small compared to real-world systems, provides valuable information and demonstrates the potential impact and value of considering the interactions that take place between transmission and distribution networks.

However, as noted above, the approach adopted in this thesis raises critical questions about the potential expansion of distribution networks in conjunction with the expansion of the transmission network. Such an expansion may require new investments to connect distribution networks directly to the transmission network. This scenario is particularly interesting from the perspective of identifying new interconnections between the networks of TSOs and DSOs, but also from the perspective of determining who should pay for these interconnections.

- **Local flexibility provision through DERs:** In this thesis, the interplay between microgrids with DERs and DSO grids has been modelled using a bilevel approach to determine the impact and value of local flexibility within the TEP problem. This modelling framework effectively captures the complex interactions and potential conflicts arising from the integration of DERs into the grid. However, a significant enhancement of the model proposed in this thesis could involve considering the connection of electric vehicles (EVs) to microgrids.

  Considering EVs within microgrids will require modifying the bilevel formulation proposed, since considering the dynamic and stochastic nature of EV charging and discharging patterns would add another layer of complexity to the system. Such changes are expected to increase the conflicts arising between the microgrids and the distribution system operators, primarily due to the additional demand and storage capacity featured by EVs. The increases in interactions between these two resulting from the consideration of EVs within the microgrids would require the implementation of more sophisticated management strategies and could provide new insights into optimal grid operation.

  In addition, this work can be extended by representing, instead of microgrids, broader energy communities. The energy communities leverage collective resources and optimise the use of energy across multiple system stakeholders, including residential, commercial and industrial ones. By considering sector coupling within these communities- concerning energy carriers such as electricity, heat and gas - a model could address how the integration of the uses of different forms of energy within communities affects transmission investments. Understanding this interaction is critical because this could help quantifying the contribution of energy communities to reducing the additional transmission infrastructure needs.

  In addition, adopting this extended framework would allows us to assess the interactions taking place among TSOs, DSOs and energy communities. This could increase the efficiency and resilience within the energy system, but would also require additional coordination efforts among these different actors. By assessing these interactions, research can provide valuable insights into the development of policy and investment strategies that facilitate a more integrated and sustainable energy system.

- **Security and grid connection criteria** In addition to the previous directions, another critical aspect of TEP is the integration of enhanced reliability criteria into the design framework. Beyond the commonly used N-1 reliability criterion, which ensures that the system can withstand the loss of a single element (e.g. transmission line or generator), there is a need to further explore more stringent conditions such as N-k contingencies and probabilistic reliability measures. Incorporating these criteria will

allow for a more robust representation of system resilience under extreme events, including cascading failures and cyber-physical threats. Another promising avenue is to investigate how evolving grid connection criteria - such as more stringent technical requirements for renewable energy systems (e.g. voltage and frequency support, inertia contribution) - affect TEP outcomes. This is particularly relevant for systems transitioning to high levels of variable renewable energy. In addition, the integration of ESS, including utility-scale batteries and hybrid configurations (e.g. H2 storage), provides an opportunity to enhance grid flexibility and resilience while meeting security requirements. Research should focus on co-optimising the use of ESS with TEP to ensure that storage systems not only provide operational benefits but also contribute to system-wide reliability under different contingencies.

- **Scalability of the TEP problem:** Determining the appropriate level of detail to be considered in the representation of the system in a case study requires striking a balance among the level of detail represented for the several dimensions of the system functioning (spatial, temporal, uncertainty) and the size/complexity of the resulting problem, all this with the aim to achieve the objectives of the analysis.

  Further advances in determining an appropriate balance remain promising for future research. One possible way to proceed is to identify optimal scalability ratios, which can be framed in terms of the problem size and the resulting computational time, and the required level of detail deemed relevant in the spatial-technological, temporal, and uncertainty dimensions. Establishing optimal ranges for these ratios is crucial for modellers. Determining the acceptable level of these ratios can provide insights into the computational resources required and help estimate the time needed to solve a particular case study. Following this approach, one could, for example, determine the appropriate number of time steps to be considered within the temporal dimension, given the number of nodes to be represented, the number of different technologies per node, and the representation to be made of uncertainty. Each aspect of the system's functioning should be represented with a level of detail that is commensurate with its importance to achieve the goals of the analysis at hand. Having a fine time granularity may be critical to appropriately represent the functioning of generation and storage devices. In addition, following this approach, one could determine the increase in problem size and computing time involved in refining the granularity considered in a certain dimension, which is essential for efficient modelling.

  Another potential avenue for increasing the efficiency of the problem formulation involves identifying the variables and constraints that the solver removes before starting the optimisation process. Knowing which variables and constraints are relevant and which are non-relevant could allow one to develop tighter formulations and systematically determine the role played by each variable and constraint within the formulation. This is essential to elucidate the interplay between different problem components, leading to more robust and efficient optimisation models.

  Therefore, a more efficient and effective TEP formulation can be developed by evaluating the scalability of the one adopted and refining the identification of relevant variables and constraints. This identification can be further improved by using machine learning techniques focused on decision variables.

Through these comprehensive research avenues, researchers and practitioners can contribute to the development of a more resilient, reliable and sustainable transmission network capable of supporting the achievement of long-term climate goals and accommodating future technological advances. Besides, researchers can better understand the limits of TEP formulations to handle large case studies.

Bibliography

[1] Erik F Alvarez, Juan Camilo López, Luis Olmos, and Andres Ramos. "An optimal expansion planning of power systems considering cycle-based AC optimal power flow". In: *Sustainable Energy, Grids and Networks* (2024), p. 101413 (cit. on p. 7).

[2] Erik F. Alvarez, Luis Olmos, Andrés Ramos, et al. "Values and impacts of incorporating local flexibility services in transmission expansion planning". In: *Electric Power Systems Research* 212 (2022) (cit. on p. 7).

[3] Erik F. Alvarez, Pedro Sánchez-Martín, and Andrés Ramos. "Self-Scheduling for a Hydrogen-Based Virtual Power Plant in Day-Ahead Energy and Reserve Electricity Markets". In: *2024 20th International Conference on the European Energy Market (EEM)*. 2024, pp. 1–6 (cit. on p. 7).

[4] Dilayne Santos Oliveira, Sara Lumbreras, Erik F Alvarez, Andrés Ramos, and Luis Olmos. "Model-based energy planning: A methodology to choose and combine models to support policy decisions". In: *International Journal of Electrical Power & Energy Systems* 159 (2024), p. 110048 (cit. on p. 7).

[5] Andrés Ramos, Erik Quispe, and Sara Lumbreras. "OpenTEPES: Open-source Transmission and Generation Expansion Planning". In: *SoftwareX* 18 (2022) (cit. on pp. 7, 19, 39, 60, 72).

[6] Sara Lumbreras, Jesús David Gómez, Erik Francisco Alvarez, and Sebastien Huclin. "The Human Factor in Transmission Network Expansion Planning: The Grid That a Sustainable Energy System Needs". In: *Sustainability (Switzerland)* 14 (11 2022) (cit. on p. 8).

[7] Daniel Huppmann, Matthew J. Gidden, Zebedee Nicholls, et al. "pyam: Analysis and visualisation of integrated assessment and macro-energy scenarios". In: *Open Research Europe* 1 (2021) (cit. on p. 8).

[8] Lawrence E. Jones. *Renewable Energy Integration: Practical Management of Variability, Uncertainty, and Flexibility in Power Grids: Second Edition*. 2017 (cit. on p. 11).

[9] Md Mahmud Ul Tarik Chowdhury, Sukumar Kamalasadan, and Sumit Paudyal. "A Second-Order Cone Programming (SOCP) Based Optimal Power Flow (OPF) Model with Cyclic Constraints for Power Transmission Systems". In: *IEEE Transactions on Power Systems* (2023) (cit. on pp. 12, 23, 24).

[10] Fabian Neumann and Tom Brown. "Transmission Expansion Planning Using Cycle Flows". In: *e-Energy 2020 - Proceedings of the 11th ACM International Conference on Future Energy Systems* (2020) (cit. on pp. 12, 23).

[11] C. W. Lee, Simon K.K. Ng, J. Zhong, and Felix F. Wu. "Transmission expansion planning from past to future". In: 2006 (cit. on p. 14).

[12] R. Villasana, S. J. Salon, and L. L. Garver. "Transmission network planning using linear programming". In: *IEEE Transactions on Power Apparatus and Systems* PAS-104 (2 1985) (cit. on p. 14).

[13] Len L. Garver. "Transmission Network Estimation Using Linear Programming". In: *IEEE Transactions on Power Apparatus and Systems* PAS-89 (7 1970) (cit. on p. 14).

[14] Laura Bahiense, Gerson C. Oliveira, Mario Pereira, and Sergio Granville. "A mixed integer disjunctive model for transmission network expansion". In: *IEEE Transactions on Power Systems* 16 (3 2001) (cit. on p. 14).

[15] Daniela Quiroga, Enzo Sauma, and David Pozo. "Power system expansion planning under global and local emission mitigation policies". In: *Applied Energy* 239 (2019) (cit. on p. 14).

[16] Mojtaba Moradi-Sepahvand and Turaj Amraee. "Integrated expansion planning of electric energy generation, transmission, and storage for handling high shares of wind and solar power generation". In: *Applied Energy* 298 (2021) (cit. on p. 15).

[17] Natalia Alguacil, Alexis L. Motto, and Antonio J. Conejo. "Transmission expansion planning: A mixed-integer LP approach". In: *IEEE Transactions on Power Systems* 18 (3 2003) (cit. on p. 15).

[18] Sara Lumbreras and Andrés Ramos. *The new challenges to transmission expansion planning. Survey of recent practice and literature review*. 2016 (cit. on p. 15).

[19] Bose Subhonmesh, Steven H. Low, and K. Mani Chandy. "Equivalence of branch flow and bus injection models". In: 2012 (cit. on p. 19).

[20] Masoud Farivar and Steven H. Low. "Branch flow model: Relaxations and convexification-Part I". In: *IEEE Transactions on Power Systems* (2013) (cit. on pp. 19, 54).

[21] Leonardo H. Macedo, Cristiam V. Montes, John F. Franco, Marcos J. Rider, and Rubén Romero. "MILP branch flow model for concurrent AC multistage transmission expansion and reactive power planning with security constraints". In: *IET Generation, Transmission and Distribution* (2016) (cit. on pp. 20, 21, 44).

[22] Siyuan Wang, Guangchao Geng, Qy Jiang, and Rui Bo. "Generation Expansion Planning Considering Discrete Storage Model and Renewable Energy Uncertainty: A Bi-Interval Optimization Approach". In: *IEEE Transactions on Industrial Informatics* (2022) (cit. on pp. 28, 75).

[23] German Morales-Espana, Andres Ramos, and Javier Garcia-Gonzalez. "An MIP Formulation for Joint Market-Clearing of Energy and Reserves Based on Ramp Scheduling". In: *IEEE Transactions on Power Systems* 29 (1 Jan. 2014), pp. 476–488 (cit. on p. 29).

[24] Diego A. Tejada-Arango, Sara Lumbreras, Pedro Sanchez-Martin, and Andres Ramos. "Which Unit-Commitment Formulation is Best? A Comparison Framework". In: *IEEE Transactions on Power Systems* 35 (4 2020) (cit. on p. 29).

[25] Pelin Damcı-Kurt, Simge Küçükyavuz, Deepak Rajan, and Alper Atamtürk. "A polyhedral study of production ramping". In: *Mathematical Programming* 158 (1-2 2016) (cit. on p. 29).

[26]Deepak Rajan and Samer Takriti. *Minimum up/down polytopes of the unit commitment problem with start-up costs*. 2005 (cit. on p. 29).

[27]Carleton Coffrin, Hassan L. Hijazi, and Pascal Van Hentenryck. "Strengthening convex relaxations with bound tightening for power network optimization". In: *Lecture Notes in Computer Science (including subseries Lecture Notes in Artificial Intelligence and Lecture Notes in Bioinformatics)* 9255 (2015) (cit. on p. 31).

[28]Burak Kocuk et al. "Strong SOCP relaxations for the optimal power flow problem". In: *Operations Research* 64.6 (2016), pp. 1177–1196. arXiv: 1504.06770 (cit. on p. 31).

[29]Laura Vimmerstedt, Tyler Stehly, Sertac Akar, et al. *2022 Annual Technology Baseline (ATB) Cost and Performance Data for Electricity Generation Technologies*. June 2022 (cit. on pp. 36, 38).

[30]ENTSO-E. *European Resource Adequacy Assessment - ERAA - Downloads*. Accessed: 17.03.2023. 2022 (cit. on pp. 37, 38).

[31]Anil Ari, Nicolas Arregui, Simon Black, et al. *Surging energy prices in europe in the aftermath of the war: How to support the vulnerable and speed up the transition away from fossil fuels*. Accessed: 17.03.2023. 2022 (cit. on p. 37).

[32]Clayton Barrows, Eugene Preston, Andrea Staid, et al. "The IEEE Reliability Test System: A Proposed 2019 Update". In: *IEEE Transactions on Power Systems* 35 (1 2020) (cit. on pp. 37, 38, 43, 60).

[33]*NREL: System Advisor Model*. Accessed: 17.03.2023. 2022 (cit. on p. 38).

[34]Arthur Gonçalves Givisiez, Kyriacos Petrou, and Luis F. Ochoa. "A Review on TSO-DSO Coordination Models and Solution Techniques". In: *Electric Power Systems Research* 189 (2020) (cit. on p. 50).

[35]Anthony Papavasiliou and Ilyes Mezghani. "Coordination Schemes for the Integration of Transmission and Distribution System Operations". In: 2018 (cit. on p. 50).

[36]Martin Bolfek and Tomislav Capuder. "An analysis of optimal power flow based formulations regarding DSO-TSO flexibility provision". In: *International Journal of Electrical Power and Energy Systems* 131 (2021) (cit. on p. 50).

[37]Mohammed A. El-Meligy, Mohamed Sharaf, and Ahmed T. Soliman. "A coordinated scheme for transmission and distribution expansion planning: A Tri-level approach". In: *Electric Power Systems Research* 196 (2021) (cit. on p. 50).

[38]Charalampos Ziras, Jalal Kazempour, Emre Can Kara, et al. "A mid-term DSO market for capacity limits: How to estimate opportunity costs of aggregators?" In: *IEEE Transactions on Smart Grid* 11 (1 2020) (cit. on p. 51).

[39]Mahdi Pourakbari-Kasmaei, Miguel Asensio, Matti Lehtonen, and Javier Contreras. "Trilateral Planning Model for Integrated Community Energy Systems and PV-Based Prosumers-A Bilevel Stochastic Programming Approach". In: *IEEE Transactions on Power Systems* 35 (1 2020) (cit. on p. 51).

[40]Arslan Ahmad Bashir, Andreas Lund, Mahdi Pourakbari-Kasmaei, and Matti Lehtonen. "Minimizing Wind Power Curtailment and Carbon Emissions by Power to Heat Sector Coupling - A Stackelberg Game Approach". In: *IEEE Access* 8 (2020) (cit. on p. 51).

[41] Nur Mohammad and Yateendra Mishra. "Coordination of wind generation and demand response to minimise operation cost in dayahead electricity markets using bi-level optimisation framework". In: *IET Generation, Transmission and Distribution* 12 (16 2018) (cit. on p. 51).

[42] J. von Appen and M. Braun. "Strategic decision making of distribution network operators and investors in residential photovoltaic battery storage systems". In: *Applied Energy* 230 (2018) (cit. on p. 51).

[43] Xiaoyu Cao, Jianxue Wang, and Bo Zeng. "A Study on the Strong Duality of Second-Order Conic Relaxation of AC Optimal Power Flow in Radial Networks". In: *IEEE Transactions on Power Systems* 37 (1 2022) (cit. on p. 51).

[44] Alvaro Jose Gonzalez-Castellanos, David Pozo, and Aldo Bischi. "Non-Ideal Linear Operation Model for Li-Ion Batteries". In: *IEEE Transactions on Power Systems* 35 (2020) (cit. on pp. 56, 57).

[45] Mesut E. Baran and Felix F. Wu. "Network reconfiguration in distribution systems for loss reduction and load balancing". In: *IEEE Transactions on Power Delivery* 4 (2 1989) (cit. on p. 60).

[46] Catalina Alexandra Sima, Mihai Octavian Popescu, Claudia Laurenta Popescu, and Gheorghe Lazaroiu. "Integrating Energy Storage Systems and Transmission Expansion Planning in Renewable Energy Sources Power Systems". In: 2019 (cit. on p. 60).

[47] Kyriaki Antoniadou-Plytaria, Ankur Srivastava, Mohammad Ali Fotouhi Ghazvini, et al. "Chalmers Campus as a Testbed for Intelligent Grids and Local Energy Systems". In: 2019 (cit. on p. 60).

[48] P. Aristidou and T. Van Cutsem. "A parallel processing approach to dynamic simulations of combined transmission and distribution systems". In: *International Journal of Electrical Power and Energy Systems* 72 (2015) (cit. on p. 60).

[49] E.ON. *E.ON's switch flexibility market*. URL: https://www.eon.se/foeretag/elnaet/switch/marknader-produkter. (accessed: 10.07.2021) (cit. on p. 60).

[50] Xuan Zhang and Antonio J. Conejo. "Robust Transmission Expansion Planning Representing Long- and Short-Term Uncertainty". In: *IEEE Transactions on Power Systems* 33 (2 2018) (cit. on p. 69).

[51] Muhammad Numan, Donghan Feng, Farukh Abbas, Usama Rahman, and Waqas Ahmad Wattoo. "Impact assessment of a co-optimized dynamic line rating and transmission switching topology on network expansion planning". In: *International Transactions on Electrical Energy Systems* 30 (8 2020) (cit. on p. 69).

[52] Md Masud Rana, Moslem Uddin, Md Rasel Sarkar, et al. *Applications of energy storage systems in power grids with and without renewable energy integration — A comprehensive review*. 2023 (cit. on p. 70).

[53] Teresa Freire-Barceló, Francisco Martín-Martínez, Álvaro Sánchez-Miralles, et al. "Storage and demand response contribution to firm capacity: Analysis of the Spanish electricity system". In: *Energy Reports* 8 (2022) (cit. on pp. 70, 80, 86).

[54] Chico Hermanu Brillianto Apribowo, Sasongko Pramono Hadi, Franscisco Danang Wijaya, Mokhammad Isnaeni Bambang Setyonegoro, et al. "Optimal sizing and placement of battery energy storage system for maximum variable renewable energy penetration considering demand response flexibility: A case in Lombok power system, Indonesia". In: *Energy Conversion and Management: X* (2024), p. 100620 (cit. on p. 70).

[55] Christoph Loschan, Hans Auer, and Georg Lettner. "Synergies and competition: Examining flexibility options in the European electricity market". In: *International Journal of Electrical Power & Energy Systems* 159 (2024), p. 109992 (cit. on pp. 70, 71, 80).

[56] Carlos Bustos, Enzo Sauma, Sebastián Torre, et al. "Energy storage and transmission expansion planning: substitutes or complements?" In: *IET Generation, Transmission and Distribution* 12 (8 Apr. 2018), pp. 1738–1746 (cit. on p. 71).

[57] Eric L Miller, Simon T Thompson, Katie Randolph, et al. "US Department of Energy hydrogen and fuel cell technologies perspectives". In: *Mrs Bulletin* 45.1 (2020), pp. 57–64 (cit. on p. 78).

[58] S. Lumbreras, A. Ramos, and P. Sánchez. "Automatic selection of candidate investments for Transmission Expansion Planning". In: *International Journal of Electrical Power and Energy Systems* 59 (2014) (cit. on pp. 81, 82).

[59] Konstantin Löffler, Karlo Hainsch, Thorsten Burandt, et al. "Designing a model for the global energy system—GENeSYS-MOD: an application of the open-source energy modeling system (OSeMOSYS)". In: *Energies* 10.10 (2017), p. 1468 (cit. on pp. 83, 85).

List of Figures

List of Tables

Appendix

A.1 Additional Figures on the Impact of Utility-Scale Storage in Transmission Expansion Planning

Fig. A.1.: M-2: Total additional capacity in AC national and international networks. [Source: Author's own illustration]
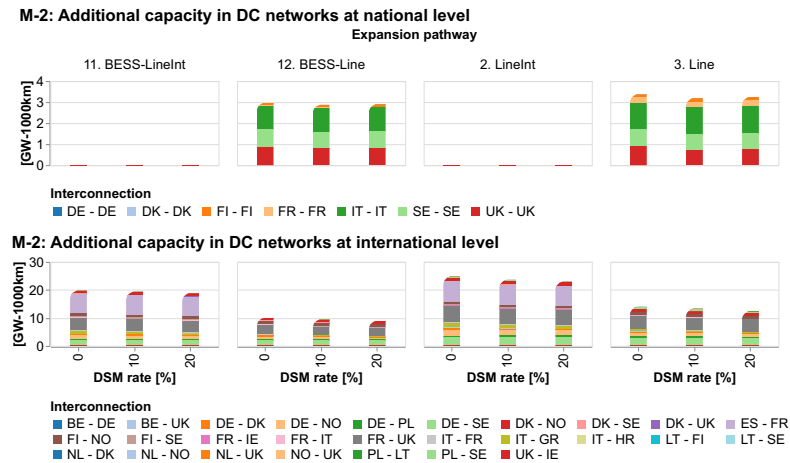
Fig. A.2.: M-2: Total additional capacity in DC national and international networks. [Source: Author's own illustration]